# Medicines for All Institute

# Process Development Report on the Cost-effective Synthesis of Fragment B of Lenacapavir

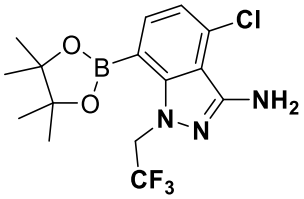


Report Prepared by:

Dr. Limei Jin
Dr. Naeem Asad
Michael Lyons
Dr. Shirley Muniz Machado Rodrigues
Dr. Justina M. Burns

Contact: m4all@vcu.edu

July 2024

Virginia Commonwealth University
College of Engineering
Department of Chemical and Life Science Engineering
Biotech 8, 737 N. 5th St
Richmond, VA 23219

## Executive Summary

This process development report (PDR) describes the results of synthetic route scouting (SRS) and scale-up optimization (OPT) efforts at Medicines for All Institute (M4ALL) to develop new, cost-effective synthetic strategies to make one of the key intermediates and cost-drivers in the synthesis of lenacapavir: 4-chloro-7-(4,4,5,5-tetramethyl-1,3,2-dioxaborolan-2-yl)-1-(2,2,2-trifluoroethyl)-1H-indazol-3-amine (**Frag B**). Lenacapavir is a first-in-class drug that targets the HIV capsid protein. It was developed by Gilead Sciences Inc. and approved by the FDA in 2022. The current baseline route to **Frag B** is a three-step process that commences from an expensive, densely functionalized starting material (Scheme 1.2.1, p.9) and culminates with a Pd-catalyzed borylation.[i] The densely substituted and heterogeneously halogenated starting material, 3-bromo-6-chloro-2-fluorobenzonitrile, and palladium in the Miyaura borylation introduce significant costs to Frag B manufacture. Herein, we report a 5-step synthesis of **Frag B** from inexpensive 2,6-dichlorobenzonitrile. Key steps include regioselective bromination, regioselective pyrazole formation and Grignard-mediated borylation. The process produces **Frag B** in a ~12% overall yield without column purification, and has been demonstrated end-to-end on 100-gram scale. Techno-economic (TE) cost analysis suggests that, compared to the incumbent process from 3-bromo-6-chloro-2-fluorobenzonitrile, this route offers a reduction of 45-55% in overall raw material cost (RMC) of **Frag B**.

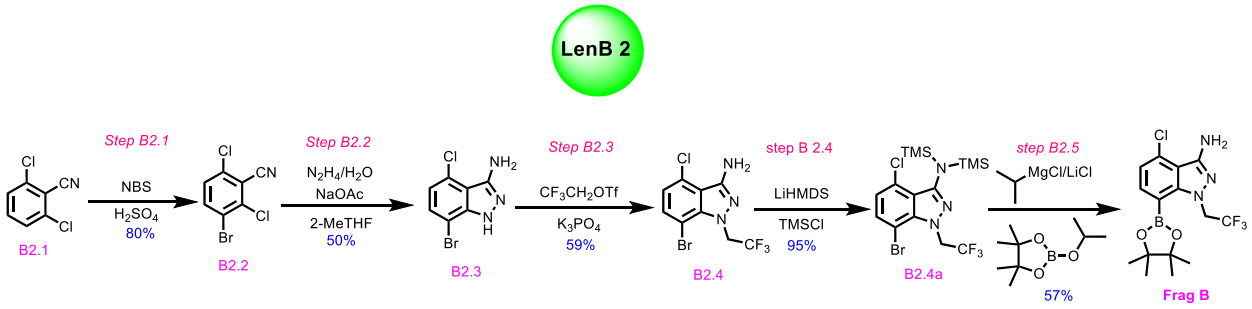


[i] An intermediate intramolecular nucleophilic aromatic substitution ($S_NAr$) step produces HF as a stoichiometric byproduct, which requires materials compatibility and safe-handling interventions in manufacturing.

www.medicines4all.vcu.edu

**Medicines for All – Contributors to the Research and Report**

| Contributor | Title / Role |
|---|---|
| Dr. Ryan Littich | Head of R&D [ii] |
| Dr. Limei Jin | Sr Scientist (Project Lead) |
| Dr. Naeem Asad | Postdoctoral Researcher |
| Dr. Shirley Muniz Machado Rodrigues | Postdoctoral Researcher |
| Michael Lyons | Graduate Student |
| Dr. Justina M. Burns | Associate Director of Analytical Chemistry |
| Dr. Michel Nuckols | Sr. Scientist [ii] |
| Janie Wierzbicki | Project Manager |

With research support provided by WuXi Apptec (China)

[ii] PDR review, revisions, additions

# Contents

# 1. Introduction

Human immunodeficiency virus (HIV), the virus that causes AIDS (acquired immunodeficiency syndrome), is one of the world's most serious health and development challenges. Approximately 39 million people are currently living with HIV, and tens of millions of people have died of AIDS-related causes since the beginning of the epidemic.[1] In 2020, there were approximately 20 million people on antiretroviral therapy (ART), a number which was expected to reach 24 million by 2024. Approved HIV treatment regimens currently fall into seven drug classes, based on their distinct mechanism of action. Today, approximately 22 million individuals are on a dolutegravir-based regimen: the "gold-standard" treatment comprises the combination of two nucleoside reverse transcriptase inhibitors (NRTIs), tenofovir disoproxil and lamivudine, and the integrase strand transfer inhibitor dolutegravir.[2]

Lenacapavir (Sunlenca®) is a high-potency HIV treatment in development by Gilead Sciences. The drug is a first-in-class HIV-1 capsid protein inhibitor that displays picomolar activity, extended pharmacokinetics, and little to no cross-resistance with clinically used antiretroviral agents.[3,4] Lenacapavir achieves its revolutionary anti-HIV-1 activity by blocking the viral replication of the HIV-1 virus, which is closely related to many processes of the viral lifecycle: uptake, assembly, and release.[5] Because of this classification, the FDA has designated lenacapavir as a breakthrough drug. The novel therapy has already gained approval from both the European Commission and the FDA in 2022 as a treatment for multidrug-resistant HIV (MDR HIV) infections.[6–8]

As of reporting, lenacapavir is in Phase 2/3 clinical trials with interim results showing viral suppression in the treatment of MDR HIV. Top-line results from Phase 3 clinical trials, reported June 2024, showed that lenacapavir was safe and 100% effective as a long-acting HIV pre-exposure prophylaxis (PrEP) among cisgender women. Lenacapavir will be provided in both oral and injectable forms in a multi-drug regimen, possibly requiring only two doses per year. In 2023, in the United States, the cost for HIV-indicated injections and tablets (wholesale; not for PrEP)

was $42,450 per patient per year.[9–11] In order to ensure patient's access to lenacapavir-for-PrEP globally, significantly lower annual costs must be realized.[10,iii]

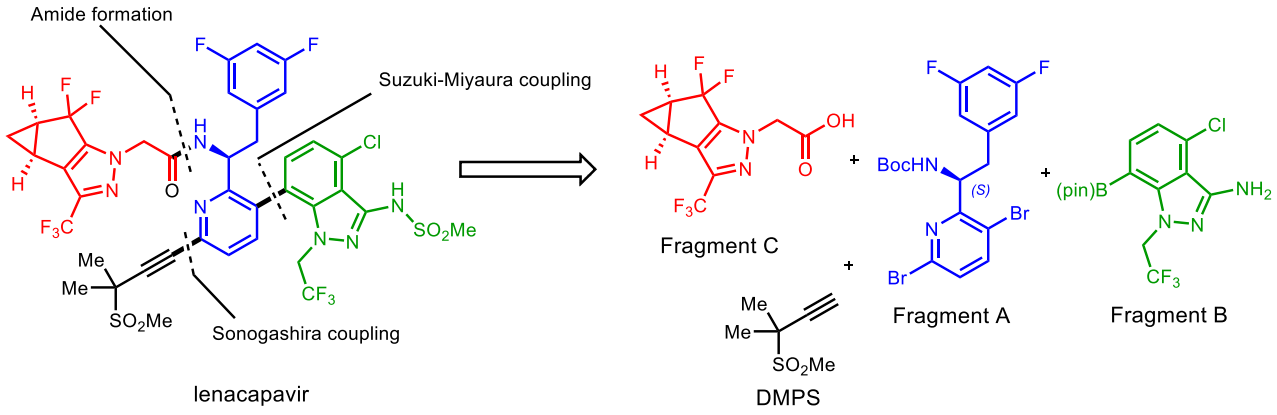


Figure 1.1.1. Retrosynthetic disconnections in lenacapavir.

## 1.1 Background: Lenacapavir Fragment B (**Frag B**)

Structurally speaking, lenacapavir is an extremely complex active pharmaceutical ingredient (API), with three chiral $sp^3$-hybridized carbon centers and 10 fluorine atoms in 4 different functional environments. Lenacapavir consists of three fragments - Fragment A, Fragment B (**Frag B)**, and Fragment C - as shown in Figure 1.1. Gilead has published several patents related to the initial synthesis and optimization of this molecule with several approaches to each fragment being demonstrated.[12–15] These routes utilize expensive starting materials and reagents and rely on expensive chiral separation techniques that are not amenable to scaleup.[5,16]

With support from the Bill and Melinda Gates Foundation (BMGF), Medicines for All (M4ALL) has been tasked with lowering the overall cost of this complex molecule.[5,16,17] The Gilead synthesis of **Frag B** requires a heterogeneously tris-halogenated aromatic compound as a starting material and a Pd-catalyzed borylation. TE analysis indicates that **Frag B**'s relatively high raw material costs (RMC) are driven primarily by this densely substituted, polyhalogenated aromatic starting material and the precious metal catalyst. Thus, modifications or improvements

[iii] For example, "PrEP medications would need to cost <$54 a year per patient for South Africa to afford them."[10]

to these and other aspects of Frag B's construction may have significant impacts on the overall cost of the molecule. This is the focus of this PDR report.

## 1.2 Synthetic strategy for lenacapavir Fragment B

Gilead's incumbent **Frag B** synthesis has been demonstrated on a kilo scale (Scheme 1.2.1).[16] The synthetic route begins with cyanation of 1-bromo-4-chloro-2-fluorobenzene (**1.1**) to afford 3-bromo-6-chloro-2-fluorobenzonitrile (**1.2**) and subsequent cyclization with hydrazine to give indazol-3-amine **1.3**.[18] Alkylation with $CF_3CH_2OTf$, results in **1.4** which is borylated under homogeneous Pd catalysis to generate **Frag B**. This synthesis is concise and efficient, however there are several drawbacks: 1) the starting material 1-bromo-4-chloro-2-fluorobenzene (**1.1**) is expensive;[iv] 2) the homogeneous Pd catalyst is expensive and unrecyclable; 3) the nitrile addition-$S_NAr$ reaction cascade of **1.2** with hydrazine evolves HF, which introduces safety and glass etching concerns.[19]A two-step Grignard-based borylation from **1.4** was also disclosed in Gilead's patent. This latter approach provides a promising method to reduce the cost of **Frag B** synthesis, but the small scale and undisclosed details leave much to be understood.

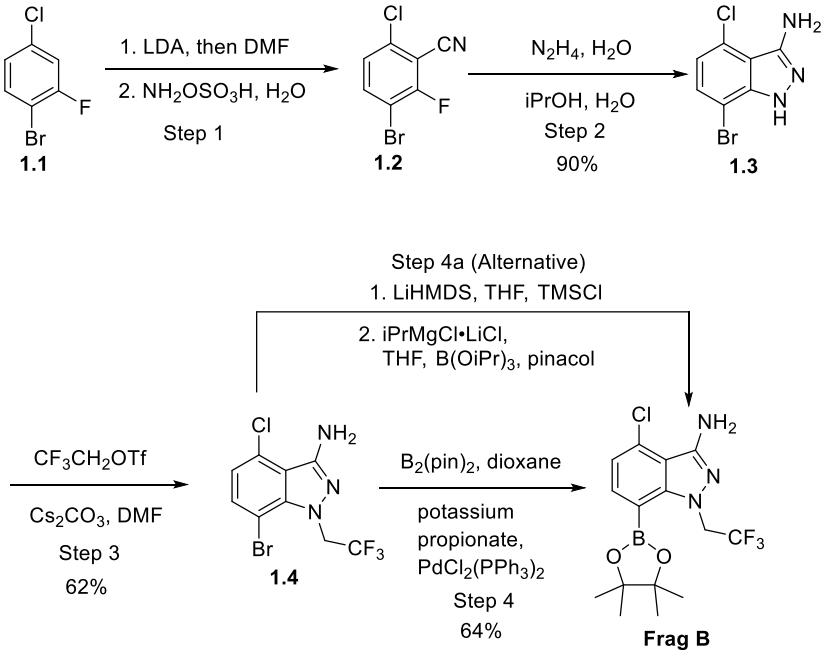


Scheme 1.2.1. Gilead-reported approach to **Frag B**.

[iv] $460/kg (0.1 mT; Zauba, 2014)

M4ALL enacted an iterative regioselective aromatic substitution strategy - electrophilic and nucleophilic additions - to drive down **Frag B** raw material costs. The approach leverages the commodity 2,6-dichlorobenzonitrile (**B2.1**, $13/kg) as starting material. (Scheme 1.2.2). The 5-step sequence is characterized by key regioselective electrophilic bromination (Step B2.1), regioselective pyrazole formation (Step B2.2), and Grignard-mediated borylation (Step B2.5) steps. The process produces **Frag B** in a ~12% overall yield without column purification. The use of low-cost 2,6-dichlorobenzonitrile and Grignard-mediated borylation enables significant cost saving in the synthesis of **Frag B**. Additionally, nucleophilic aromatic substitution ($S_NAr$) of **B2.1** with hydrazine hydrate eliminates the formation of HF which mitigates EHS and materials compatibility concerns.

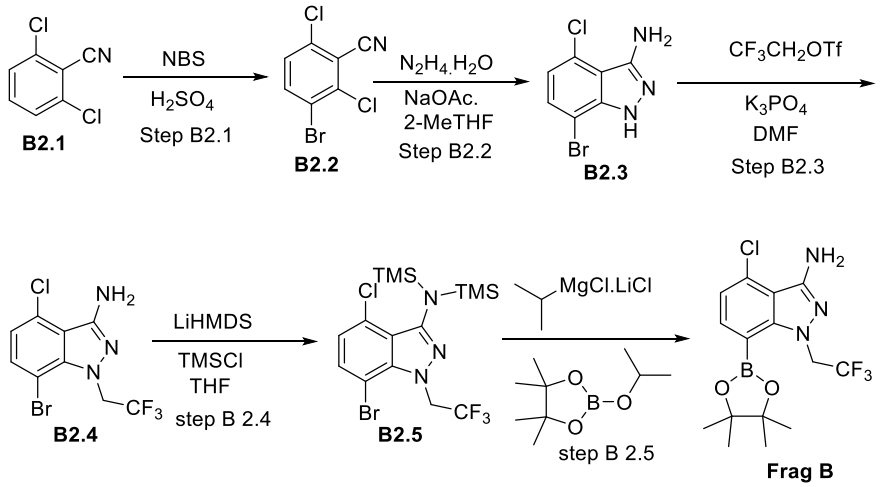


Scheme 1.2.2. M4ALL approach to **Frag B** (LenB 2)

# 2. Results & Discussion

## 2.1 Bromination of B2.1

### 2.1.1 Optimization of bromination of B2.1

Initial efforts for bromination of 2,6-dichlorobenzonitrile (**B2.1**) followed the method of Song et al., who reported 60% yield after treating **B2.1** with potassium bromate and sulfuric acid.[20] Poor conversion and substantial side product generation was observed when the reported conditions were enacted in M4ALL laboratories. Doubling the equivalents of reagents and

lowering the temperature did not improve the outcome. The authors also noted that this bromination method was highly exothermic, and thus exhibited potential safety issues.

With the reported potassium bromate procedure not yielding sufficient results, other brominating reagents (e.g., *N*-bromosuccinimide, bromine) were examined at different temperatures (25, 60, and 100 °C). As shown in Table 2.1.1, *N*-bromosuccinimide at 25 °C afforded the desired product in the greatest yield and was therefore chosen as the brominating agent moving forward (entry 6).

Table 2.1.1. Bromination of 2,6-dichlorobenzonitrile **B2.1**

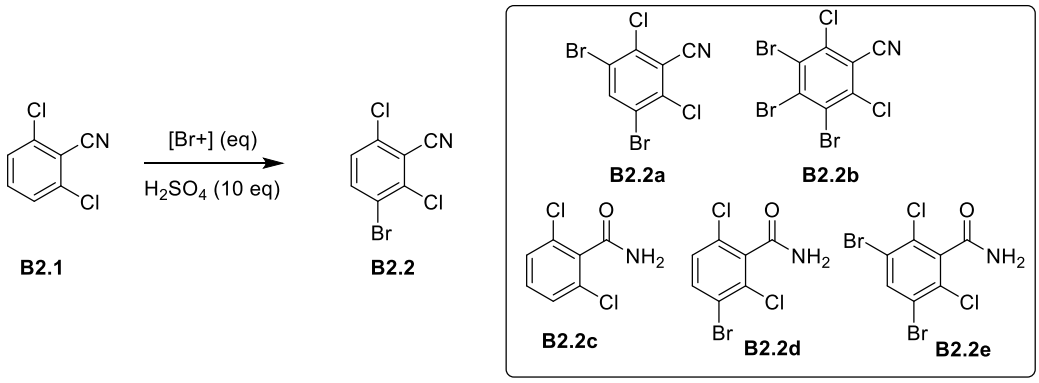


| #[a] | [Br+] (eq) | T (°C) | B2.1 (A%) | B2.2 (A%) | B2.2a (A%) | B2.2b (A%) | B2.2c (A%) | B2.2d (A%) | B2.2e (A%) |
|---|---|---|---|---|---|---|---|---|---|
| 1 | $KBrO_3$ (3) | **25** | 63 | 21 | 10 | 0.4 | 4 | 1 | - |
| 2[b] | $KBrO_3$ (3) | **60** | 34 | 19 | 23 | 2 | 19 | 2 | - |
| 3[b] | $KBrO_3$ (6) | 25 | 38 | 19 | 19 | 8 | 10 | 4 | 2 |
| 4 | $KBrO_3$ (3) | 60 | 28 | 32 | 20 | 6 | 6 | 4 | 2 |
| 5 | $KBrO_3$ (3) | 100 | 17 | 4 | 2 | - | 28 | 31 | 17 |
| **6** | **NBS (1.2)** | **25** | **2** | **67** | **21** | **-** | **-** | **8** | **2** |
| 7 | NBS (1.2) | 60 | 0.5 | 0.5 | 5 | - | 0.2 | 66 | 28 |
| 8 | NBS (1.2) | 100 | 0.7 | 0.6 | 4 | - | 2 | 61 | 33 |
| 9 | $Br_2$ (2) | 25 | 72 | - | - | - | 28 | - | - |
| 10 | $Br_2$ (2) | 60 | 4 | - | - | - | 96 | - | - |

| | | | | | | | | | |
|---|---|---|---|---|---|---|---|---|---|
| 11 | $Br_2$ (2) | 100 | 3 | - | - | - | 97 | - | - |

[a]All reactions were performed with 2,6-dichlorobenzonitrile (100 mg) under the conditions shown in the table for 18 h unless otherwise stated, all data were IPC of crude reaction mixtures obtained by GC-MS total ion chromatogram (TIC) and reported as A%. [b] 5g of 2,6-dichlorobenzonitrile.

Next, the importance of acid was screened in the bromination with NBS. Sulfuric acid (96%), aq. sulfuric acid (60%), aq. hydrochloric acid (37%), acetic acid, and trifluoroacetic acid were investigated - as was one control experiment, which did not include acid. Only the sulfuric acid conditions yielded the desired product. Investigation of equivalents and concentration of $H_2SO_4$ were further conducted, as summarized in Table 2.1.2. The results indicated that 10 equivalents of 96% $H_2SO_4$ was the optimal choice for bromination, yielding 98 A% (entry 5; TIC GC-MS) **B2.2**. Preferred scale-up conditions for the bromination were thus identified: NBS (1.07 eq), 96% $H_2SO_4$ (10 eq), 25 °C, 18h.

Table 2.1.2. Concentration of $H_2SO_4$ screening in bromination of **B2.1** with NBS

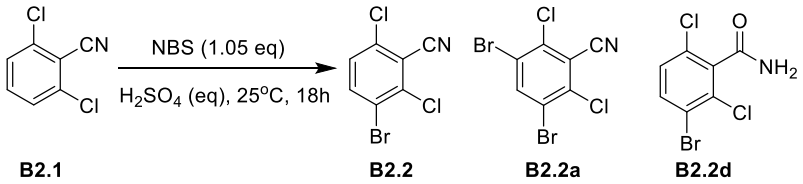


**B2.1** **B2.2** **B2.2a** **B2.2d**

| #[a] | Sulfuric Acid (eq (conc)) | **B2.1 (A%)** | **B2.2 (A%)** | **B2.2a (A%)** | **B2.2d (A%)** |
|---|---|---|---|---|---|
| 1 | 3 (96 %) | 39 | 50 | 11 | - |
| 2 | 5 (96 %) | 21 | 70 | 9 | 0.1 |
| 3 | 7 (96 %) | 17 | 76 | 7 | 0.2 |
| 4 | 9 (96 %) | 3 | 96 | 2 | 0.2 |
| 5 | 10 (96%) | 2 | 98 | - | - |
| 6 | 9 (70 %) | 29 | 70 | 1 | - |
| 7 | 9 (80 %) | 14 | 66 | 20 | 0.3 |

[a]All reactions were performed with 2,6-dichlorobenzonitrile (2 g) with NBS (1.05 eq), at 25°C, 18 h unless otherwise stated, all data were IPC of crude reaction mixtures obtained by GC-MS total ion chromatogram (TIC) and reported as A%.

With optimized reaction conditions, our focus shifted to purifying **B2.2** to >96 wt%. Initially, varying ratios of three binary solvent solutions, methanol:water, ethanol:water and heptanes:ethanol were screened for recrystallization (Table 2.1.3.). In each condition, the worked-up crude was dissolved with minimal solvent volumes at 80 °C. Once dissolved, the solution was held at 80 °C for 30 minutes with mechanical stirring before allowing the medium to cool to room temperature overnight, after which the precipitates were collected. Recrystallization screening results are summarized in Table 2.1.3. Both the methanol:water and ethanol:water conditions resulted in high purity and yield. The ethanol:water conditions were further pursued as they required fewer solvent volumes for dissolution, making them more practical at scale. Specifically, the 90:10 ethanol:water condition was chosen for further development (entry 4).

Table 2.1.3. Recrystallization screening for purification of **B2.2**

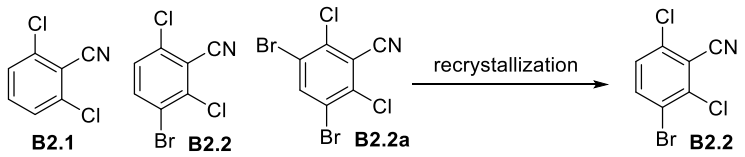


| #[a] | Solvent (Ratio) | Solvent Volumes | **B2.1** (A%) | **B2.2** (A%) | **B2.2a** (A%) | Recovery Yield (%)[b] |
|---|---|---|---|---|---|---|
| 1 | Methanol:Water (90:10) | 13 | 0.6 | 98.5 | 0.9 | 82 |
| 2 | Methanol:Water (80:20) | 26 | 0.1 | 99.6 | 0.3 | 88 |
| 3 | Methanol:Water (70:30) | 34 | - | 99.5 | 0.5 | 84 |
| 4 | Ethanol:Water (90:10) | 9 | 0.2 | 99.6 | 0.3 | 76 |
| 5 | Ethanol:Water (80:20) | 18 | 0.1 | 99.7 | 0.2 | 78 |
| 6 | Ethanol:Water (70:30) | 26 | - | 99.6 | 0.3 | 72 |

| | | | | | | |
|---|---|---|---|---|---|---|
| 7 | Heptanes:Ethanol (90:10) | 10 | 0.3 | 99.3 | 0.4 | 78 |
| 8 | Heptanes:Ethanol (90:10) | 10 | 2.8 | 94.4 | 2.8 | 80 |
| 9 | Heptanes:Ethanol (90:10) | 8 | 2 | 97.1 | 0.9 | 76 |

[a]All crystallizations utilized 500 mg crude reaction product. Binary solvent systems containing the crude were warmed to 80 °C and then allowed to cool to room temperature overnight to obtain precipitates of the desired compound unless otherwise stated. A% results were obtained by GCMS-TIC. [b]Isolated yields from recrystallization.

It was found that the volume of ethanol:water (90:10 v/v) could be lowered to 6 volumes for the purification. Six volumes of solvent do not completely dissolve the crude **B2.2** and instead forms a slurry. Impurities are reliably purged via slurring, giving the desired **B2.2** in 81% isolated yield with 97% purity (QNMR) (Table 2.1.4, entry 1). While beginning bromination scale-up, we observed that **B2.2** was very hygroscopic solid. Accordingly, after filtering the precipitate during work-up, crude **B2.2** was washed with ethyl acetate (3V) to remove trace moisture. Ethyl acetate washing afforded **B2.2** in 91% isolated yield and 96% purity (QNMR) (Table 2.1.4, entry 2). The ethyl acetate method was prioritized for scale-up, as it provided higher isolated yield and a simpler process to access **B2.2**. As a result, the finalized procedure from the optimization phase of the bromination of **B2.1** was to use NBS (1.05 eq), sulfuric acid (96%, 10 eq), room temperature, and a 20 h reaction, followed by purification via ethyl acetate (3V) washing.

Table 2.1.4. 5g scale bromination and purification

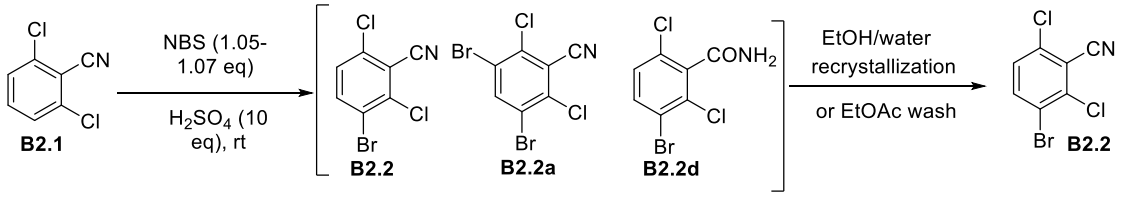


| #[a] | Sample | B2.1 (%)[d] | B2.2 (%)[d] | B2.2a (%)[d] | B2.2d (%)[d] | Isolated Yield (%) |
|---|---|---|---|---|---|---|
| 1[b] | Crude | 5 | 89 | 1 | 5 | - |
| | Ethanol:water (90:10) recrystallization | 1 | 97 | 1 | 2 | 81 |
| 2[c] | Crude | 2 | 89 | 2 | 7 | - |

| | | | | | | |
|---|---|---|---|---|---|---|
| | EtOAc Wash | 2 | 96 | 1 | 1 | 91 |

[a]All reactions were performed with 2,6-dichlorobenzonitrile (5 g) with NBS (1.05 eq), at 25°C, 18h unless otherwise stated. [b]Crystallization from ethanol:water (90:10, 6V), at 80 °C to 25 °C, 12h. [c]The crude was washed with ethyl acetate (3V). [d]Results are shown as relative qNMR %.

### 2.1.3 Scale-up of bromination of **B2.1**

Optimized conditions were demonstrated up to 300 grams in a ChemRxnHub reactor (Figure 2.1.1). This process generated the bromide with an overall isolated yield of 77-82%, and purity of up to 97% by qNMR. The results are summarized in Table 2.1.5, showing robust reproducibility of the developed bromination procedure. The purification was straightforward as depicted on small scale: after completion of the reaction, the crude product mixture was poured into 15 volumes of ice-cold water and the resulting precipitate was collected by filtration. The filter cake was washed with 3 volumes of ethyl acetate to obtain the desired 3-aminoindazole **B2.2**.

Figure 2.1.3.1. 2L reactor for bromination at 290 g scale

Table 2.1.5. Scale-up of bromination of **B2.1** with NBS

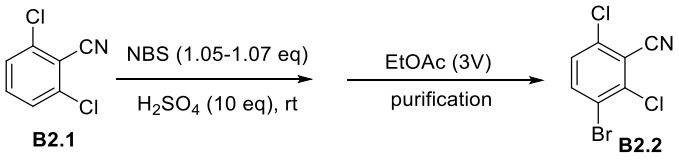

| # | Scale (g) | qNMR Purity (%) | Isolated Yield (%) |
|---|---|---|---|
| 1 | 25 | 96 | 82 |
| 2 | 50 | 97 | 82 |
| 3 | 125 | 95 | 80 |
| 4 | 125 | 95 | 77 |
| 5 | 125 | 96 | 81 |
| 6 | 290 | 95 | 80 |

[a]All reactions were performed with 2,6-dichlorobenzonitrile with NBS (1.05 -1.07 eq), at 25 °C, 18 h unless otherwise stated, the crude was washed with ethyl acetate (3V).

## 2.2 Cyclization of B2.2

### 2.2.1 Optimization of cyclization of B2.2

We investigated a suitable condition for the cyclization of **B2.2** with hydrazine hydrate.[19,21] Our aim was to achieve a regioselective cyclization in which the chlorine atom in the 2-position (proximal to the bromine) undergoes $S_NAr$ displacement by hydrazine or its nitrile addition adduct. Though the 2-chlorine atom is activated via the σ-withdrawing effect of bromine, bromine also introduces steric hindrance. Finding suitable conditions for this regioselective displacement was the main challenge for this strategy. Reaction parameters screened included solvent, temperature, hydrazine equivalents, as well as additives such as bases, Lewis acids and salts.

A variety of solvents – polar aprotic solvents, protic solvents, alkaline solvents, and other organic media – were screened in the cyclization chemistry (Table 2.2.1). Cyclization in polar aprotic solvents such as NMP and DMSO[v] (60 °C, 2 eq hydrazine hydrate, 1.2 eq NaOAc)[21] resulted in non-selective reaction of the **B2.2** chloro substituents with ~50:50 ratio of **B2.3** and **B2.3a** (Table 2.2.1, entries 1-2). The ratio of **B2.3**:**B2.3a** improved to 65:35 when switching the solvent to ethanol and further improved to 70:30 with IPA as a solvent (Table 2.2.1, entries 3-4). To achieve >95% conversion, an elevated reaction temperature (95 °C) and excess hydrazine hydrate was needed. The reactions were carried out in heavy wall pressure vessels. These promising results spurred further solvent screening for better regioselectivity. Among the other solvents screened, DIPEA and 2-MeTHF afforded the highest ratio of desired regioisomer (Table

[v] Yang and coworkers assessed weak bases on the thermal decomposition behavior of DMSO. A mixture comprising 73 wt % DMSO and 27 wt % $K_2CO_3$ was analyzed for thermal stability by DSC. An exothermic event with an onset temperature of 257 °C was recorded. *Org. Process Res. Dev.* **2020**, *24*, 916–939.

2.2.1, entries 5-9). Considered a greener solvent, 2-MeTHF was selected. Hydrazine equivalents were investigated to obtain an optimal condition for this transformation. It was found that 4 equivalents of hydrazine hydrate afforded >98% conversion of compound **B2.2**. (Table 2.2.1, entries 10-11). Reactions with hydrazine hydrate less than 4 equivalents gave incompletion.[vi] Additionally, screening showed 5 V of 2-MeTHF afforded >99% conversion with 70:30 ratio of **B2.3**:**B2.3a** (Table 2.2.1, entry 12). Testing revealed that a minimum of 4 equivalents of hydrazine hydrate were required for reaction completion in solvents like ethanol, THF and 2-MeTHF.

Table 2.2.1. Optimization of cyclization of **B2.2**

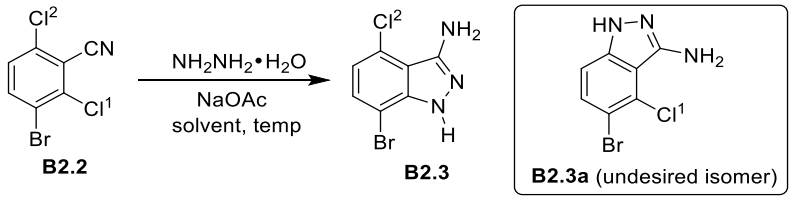


| Entry[a] | Solvent | Temp (°C) | Eq of $NH_2NH_2•H_2O$ | Conversion (%)[b] | Ratio[c] **B2.3:B2.3a** |
|---|---|---|---|---|---|
| 1 | NMP | 60 | 2 | 100 | ~50:50 |
| 2 | DMSO | 60 | 2 | 100 | ~50:50 |
| 3 | EtOH | 95 | 10 | 100 | 65:35 |
| 4 | IPA | 95 | 10 | 100 | 70:30 |
| 5 | DIPEA | 95 | 10 | 100 | 75:25 |
| 6 | Pyridine | 95 | 10 | 100 | 68:32 |
| 7 | THF | 95 | 10 | 100 | 70:30 |
| 8 | Diglyme | 95 | 10 | 100 | 70:30 |
| 9 | 2-MeTHF | 95 | 10 | 100 | 73:27 |
| 10 | 2-MeTHF | 95 | 8 | 100 | 70:30 |
| 11 | 2-MeTHF | 95 | 4 | 98 | 70:30 |

[vi] The reaction of **B2.2** with 3 equivalents of hydrazine hydrate afforded 65% conversion with 10:3:7 ratio of **B2.3**:**B2.3a** :**B2.2**.

| | | | | | |
|---|---|---|---|---|---|
| 12[c] | 2-MeTHF | 95 | 4 | 99 | 70:30 |

[a]All reactions were performed in heavy wall pressure vessels with **B2.2** (0.5 g) in the presence of NaOAc (1.2 eq), under the conditions shown in the table (18 h, 10 V solvent) unless otherwise stated. [b]Conversion was determined by GCMS-TIC A%. [c]Ratio of the crude was obtained by GCMS TIC A %.

Next, our effort focused on purging the unwanted regioisomer (**B2.3a**) to achieve **B2.3** purity >99% by recrystallization. Owing to the greater solubility of the undesired regioisomer in binary solutions of polar solvents and water, the crude solid was dissolved in binary solvent systems of ethanol, IPA and methanol with water as the anti-solvent at reflux conditions. Methanol-water systems proved to be the solvent media of choice for crystallization. The crude product was dissolved in 20 volumes of 80:20 methanol:water at reflux and **B2.3** precipitated upon cooling in 70% recovery yield with 96-98% purity (qNMR). Serendipitously, it was found that cooling the crude reaction mixture (2-MeTHF (4V)) at -25 °C for two hours afforded **B2.3** in almost 100 GCMS TIC A% purity with 49-53% isolated yield, rejecting all undesired **B2.3a**.

The optimized cyclization conditions for scale up were (hydrazine hydrate (4 eq), NaOAc (1.2 eq), 2-MeTHF (5 V), 95 °C) with purification by recrystallization using 80:20 methanol:water.

### 2.2.2 Scale-up of cyclization of B2.2

Kruger and coworkers found that the addition of sodium acetate was needed to mitigate safety concerns regarding the utilization of hydrazine hydrate on scale.[21] The sodium acetate quenches the resulting HCl during the cyclization, which suppresses the possible formation of highly energetic hydrazine HCl conjugates. After safety assessment[19,21] on scale,[vii] the optimized protocol was successfully demonstrated in 20-80 gram reactions. Cyclization in 2-MeTHF needs an internal temperature of >90 °C to obtain a full conversion, therefore a pressure reactor was

[vii] Based on Kruger and coworkers paper about the safety assessment of the cyclization with hydrazine hydrate, it was found that the run-away temperature of the cyclization increased to >300 °C by adding NaOAc (1 eq) and using a low-boiling-point solvent. Thus, our cyclization was carried out by adding NaOAc (1.2 eq) and maintaining the reaction temperature below 100 °C in a Parr reactor with a blast shield.

utilized for scale-up.[viii] All reactions were performed in round-bottom pressure flasks (Ace Glassware) with thermowells (Figure 2.2.1a) or a Parr reactor (Figure 2.2.1b).

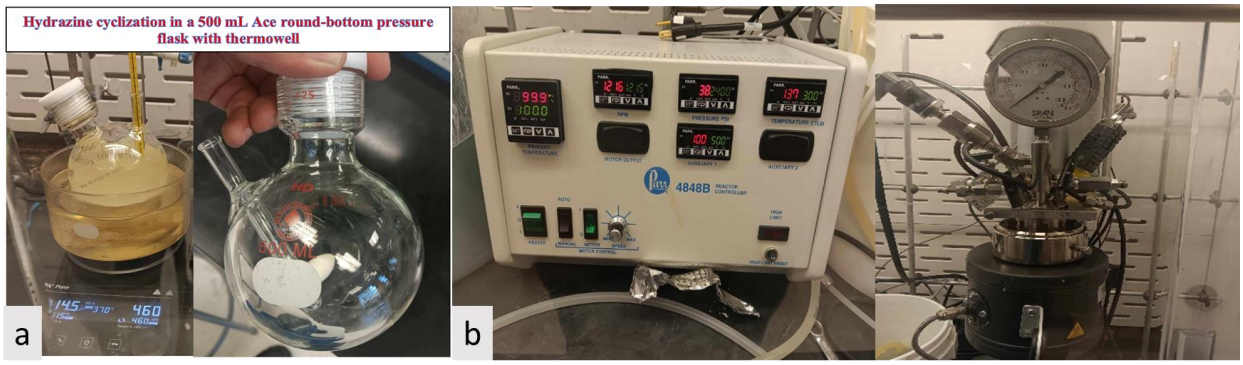


Figure 2.2.1. (a) Ace heavy wall pressure flask and (b) Parr reactor with controller for cyclization with hydrazine.

As shown in Table 2.2.2.2, the reaction of **B2.2**, hydrazine hydrate (4 eq) and NaOAc (1.2 eq) in 2-MeTHF (5 V) at 95 °C afforded the crude of regioisomers (molar ratio of **B2.3**:**B2.3a**: 70:30 by GC-MS TIC A%) in quantitative yield. After recrystallization from 20 volumes of 80:20 methanol:water (or the reaction mixture temperature was immediately decreased to -25 °C) **B2.3** was obtained in 46-56% isolated yield with 91-98 wt% purity (qNMR). GC-MS A% of these products was 97-100%, suggesting organic impurities in the final product were negligible.

NOTE - key failure mode observed in Step B2.2: Rigorous cleaning procedures must be observed for reactors intended for use in the herein reported process. In particular, trace palladium residues - and presumably other trace metals – can create significant pressure excursions (e.g., up to 160 psig observed in Parr batches). Normal operating pressures, absent trace metal contaminants, remained between 40-50 psig.

Table 2.2.2. Synthesis and purification of 7-bromo-4-chloro-1H-indazol-3-amine (**B2.3**)

[viii] To mitigate the disadvantage of using the pressure reactor for scale up; we tried the reaction in diglyme and a similar ratio of regioselectivity with a full conversion was obtained. But more solvent screen is needed to identify a proper high boiling solvent for scale up.

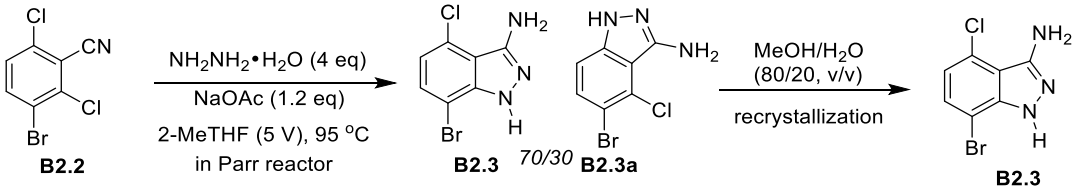


| #[a] | scale (g) | Purity | | | KF/%[d] | Yield (%)[e] | output (g) |
|---|---|---|---|---|---|---|---|
| | | A% GCMS-TIC | Wt% (qNMR) | Wt. % (GCMS) | | | |
| 1[b,f] | 55 | - | 96 | - | - | 53 | 30 |
| 2[b,f] | 50 | - | 97 | - | - | 49 | 25 |
| 3[b,g] | 40 | 97 | 98 | - | - | 56 | 21 |
| 4[b,g] | 80 | 100 | 96 | - | - | 46 | 38 |
| 5[b,g] | 40 | 100 | 95 | 94.7 ± 1.7% | 0.24 | 53 | 22 |
| 6[b,g] | 40 | 100 | 91 | 92.2 ± 4.9% | 0.27 | 55 | 24 |
| 7[c,g] | 40 | 100 | 95 | - | - | 53 | 22 |
| 8[c,g] | 20 | 100 | 97 | 93.7 ± 3.5% | 0.32 | 54 | 11 |

[a]All reactions were performed in a Parr reactor or Ace Glassware heavy wall pressure flask with **B2.2** (20-80 g), hydrazine hydrate (4 eq), NaOAc (1.2 eq), 2-MeTHF (5 V), 95 °C (internal temperature), 18 h, and GCMS showed the crude mixtures to be 70:30 **B2.3:B2.3a**. [b]Carried out in a Parr reactor. [c]Carried out in Ace heavy wall pressure flask. [d]Karl-Fischer titration. [e]Corrected isolated yield based on qNMR wt% purity. [f]Purification via recrystallization in methanol:water (80:20). [g]Purification by cooling the crude reaction to -25 °C.

Steric and electronic distinctions of **B2.2**'s two chlorine substituents are hypothesized to play a decisive role in the regioselective cyclization with hydrazine hydrate. The detailed mechanistic basis of the regioselectivity is, however, unclear at this time. The condensation reaction between 2,6-dichlorobenzonitrile and hydrazine hydrate may have progressed by two possible pathways: 1) $S_NAr$ occurred first followed by intramolecular nitrile addition (Scheme 2.2.1, Path 1); or 2) nitrile addition occurred first followed by an intramolecular $S_NAr$ reaction (Scheme 2.2.1, Path 2).[19,21] Our experimental results indicated that the regioselective cyclization was solvent dependent.[ix]

[ix] In silico calculations of transition state energies along Paths 1 and 2 have not been undertaken, as of the time of this writing. The authors do not offer, here, hypotheses regarding the operable mechanism or mechanism-as-a-function-of-solvent-medium (see Table 2.2.1.1).

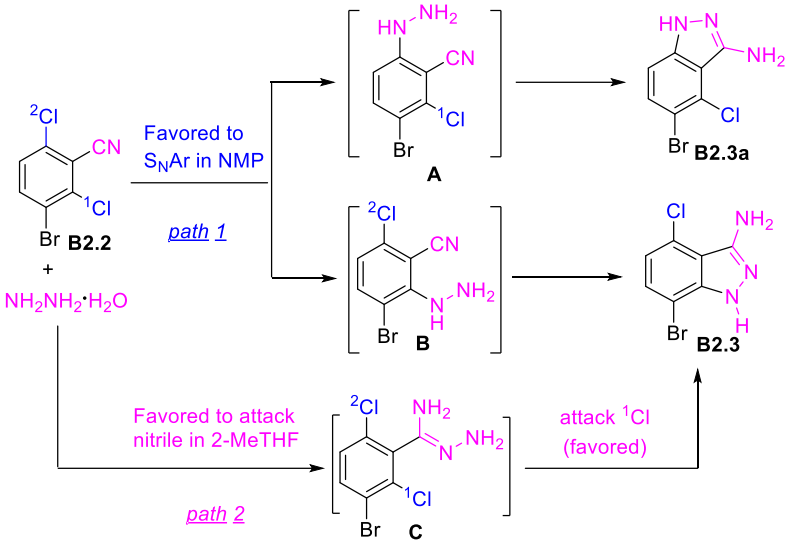


Scheme 2.2.1. A plausible pathway for the formation of indazole

## 2.3 Alkylation of B2.3

### 2.3.1 Optimization of alkylation of B2.3

The synthesis of **B2.4** has been reported by Gilead Sciences, Inc.[5,16] Alkylation of **B2.3** with 2,2,2-trifluoroethyl trifluoromethanesulfonate ($CF_3CH_2OTf$, triflate) in the presence of $Cs_2CO_3$ afforded **B2.4** in 60-70% yield. Initially, we prepared **B2.4** according to the reported protocol and observed a significant amount of undesired regioisomer **B2.4a** (Table 2.3.1, entry 1). To improve the yield and lower the cost of the transformation, we investigated minimizing the formation of the undesired isomer by switching the alkylating reagent. *N*-Alkylation of **B2.3** with either 2,2,2-trifluoroethyl methanesulfonate ($CF_3CH_2OMs$, mesylate) or 2,2,2-trifluoroethyl 4-methylbenzenesulfonate ($CF_3CH_2OTs$, tosylate) minimized the formation of the undesired **B2.4a**; **B2.4** was formed almost exclusively (Table 2.3.1, entries 2-3). Although isolated yield was low, high regioselectivities encouraged further evaluation. $CF_3CH_2OMs$ was the focal point of further optimization, considering its ready availability and potential atom economy gains relative to the incumbent triflate. Multiple conditions were screened, including bases, reaction temperatures, solvents, $CF_3CH_2OMs$ equivalents and base equivalents. Results are summarized in Table 2.3.1; ultimately, low in-solution purity and downstream isolated yield of **B2.4** was observed. Column purification – undesirable in the manufacturing setting – was required to purge impurities from

**B2.4**.[x] Negating our hypotheses for net more-economical alkylation, we revisited *N*-alkylation by $CF_3CH_2OTf$.

Table 2.3.1. Initial condition screen of alkylation of **B2.3**

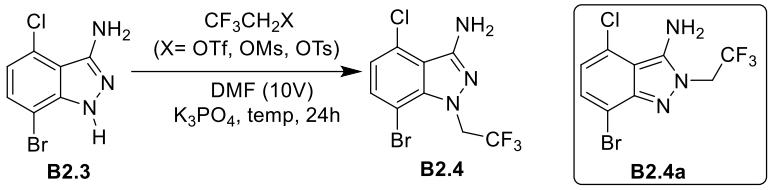


| #[a] | Reagent (eq)[d] | T/°C | **B2.3**[e] (A%) | IPC ratio[e] **B2.4/B2.4a** | **B2.4** (A%)[e] | **Isolated yield (%)** |
|---|---|---|---|---|---|---|
| 1[b] | OTf (1.2) / $Cs_2CO_3$ (2.0) | 25 | 0.4 | 60:39 | 60 | 62 |
| 2 | OMs (1.2) / $K_3PO_4$ (1.5) | 80 | - | >99:1 | - | 27 |
| 3 | OTs (1.2) / $K_3PO_4$ (1.5) | 80 | - | >97:2 | - | 11 |
| 4 | OMs (1.1) / $K_3PO_4$ (1.2) | 80 | 43 | 50/5 | - | - |
| 5 | OTs (1.1) / $K_3PO_4$ (1.2) | 80 | 26 | 64/5 | - | - |
| 6 | OMs (1.2) / $K_3PO_4$ (2.0) | 90 | | >99:1 | 37 | - |
| 7 | OMs (1.2) / $K_3PO_4$ (2.0) | 80 | - | >99:1 | 56 | - |
| 8 | OMs (1.2) / $K_3PO_4$ (2.0) | 70 | 5 | >99:1 | 50 | - |
| 9 | OMs (1.2) / $K_3PO_4$ (1.5) | 100 | 37 | >99:1 | 35 | - |
| 10 | OMs (1.2) / $K_3PO_4$ (2.0) | 100 | - | >99:1 | 59 | - |
| 11 | OMs (1.5) / $K_3PO_4$ (2.5) | 100 | -- | >99:1 | 56 | - |
| 12[c] | OMs (1.7) / $K_3PO_4$ (2.0) | 80 | - | >99:1 | 43 | 34 |

[a]All reactions were performed with **B2.3** (0.5-1 g), alkylating reagent, base and conditions as described in the table in DMF (10V) for 24h unless otherwise stated. [b]1-2h. [c]10 g scale. [d]$CF_3CH_2OTf$: OTf; $CF_3CH_2OTs$: OTs; $CF_3CH_2OMs$: OMs. [e]A% and IPC ratio were obtained by GC-MS TIC.

In revisiting *N*-alkylation of **B2.3** with $CF_3CH_2OTf$, we aimed to reveal cost savings via additional process intensification.[xi] Standard conditions were used with $CF_3CH_2OTf$ (1.2 eq) and

[x] High regioselectivity was observed in all screened conditions. Notably, **B2.3** decomposes under alkaline conditions at 80-100°C, as observed by NMR analysis of the crude. We hypothesize that decomposition is responsible for the low isolated yield of alkylation with mesylate and tosylate.
[xi] $CF_3CH_2OTf$-based alkylation was previously developed, demonstrated on kilogram scale.[16]

$Cs_2CO_3$ (2.0 eq) in DMF (10V) at 25 °C. The reaction under this condition proceeded smoothly and **B2.4** was obtained in 60% isolated yield after aqueous workup. We examined other readily available bases and fine-tuned the equivalents of $CF_3CH_2OTf$ (Table 2.3.2). Complete conversion was achieved with 1.6 eq of $K_3PO_4$ and 1.05 eq $CF_3CH_2OTf$. It was determined that 10 V of DMF was optimal as lower volumes increased the exotherm. For example, with 5V DMF, the exotherm is difficult to control during the addition of $CF_3CH_2OTf$. No reaction occurred with $Na_2CO_3$ or $K_2CO_3$ as a base. Optimized alkylation conditions comprise $CF_3CH_2OTf$ (1.05 eq), $K_3PO_4$ (1.6 eq), DMF (10V) at 25 °C. [Critical Process Parameter: To minimize undesired side reactions, it is imperative to add $CF_3CH_2OTf$ slowly, to maintain internal temperature below 45 °C; **B2.3** decomposition is observed under alkaline conditions, above this temperature.] Under optimal conditions, the ratio of **B2.4:B2.4a** is observed in the range of 70:30 to 60:40. Upon reaction completion, **B2.4** was precipitated by adding 10 volumes of water to the reaction at room temperature. **B2.4** was obtained by filtration with the undesired **B2.4a** remaining in the aqueous layer.

Table 2.3.2. Optimization of alkylation with $CF_3CH_2OTf$

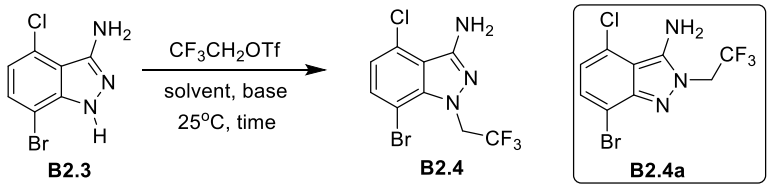


| #[a] | Scale (g) | Base (eq) | $CF_3CH_2OTf$ (eq) | Time/h | Ratio[b] **B2.4/B2.4a** | Isolated Yield (%) |
|---|---|---|---|---|---|---|
| 1 | 2 | $Cs_2CO_3$ (2) | 1.2 | 1.5 | 60:40 | 59 |
| 2 | 18 | $Cs_2CO_3$ (2) | 1.2 | 1.5 | 60:40 | 60 |
| 3 | 0.5 | $K_3PO_4$ (1.6) | 1.05 | 2 | 71:29 | 63 |
| 4 | 0.5 | $K_3PO_4$ (1.6) | 1.1 | 2 | 70:30 | 61 |
| 5 | 18 | $K_3PO_4$ (1.6) | 1.1 | 2 | 70:30 | 63 |

[a]All reactions were performed with **B2.3**, $CF_3CH_2OTf$ and conditions as described in the table in DMF (10V) for 1.5-2 h unless otherwise stated. [b]Ratio was obtained by GC-MS TIC A%.

### 2.3.2 Scale up of alkylation of B2.3

Preparation of **B2.4** was performed on an 18-45 g scale using optimized conditions ($CF_3CH_2OTf$ (1.05 eq), $K_3PO_4$ (1.6 eq), DMF (10V) at 25 °C, 2h). Aqueous workup purged the undesired alkylation regioisomer **B2.4a** completely, affording **B2.4** in 55-62% yield and 96-99 wt% purity (qNMR). The details of these reactions are summarized in Table 2.3.3.

Table 2.3.3. Scale up of the alkylation of **B2.3** with $CF_3CH_2OTf$

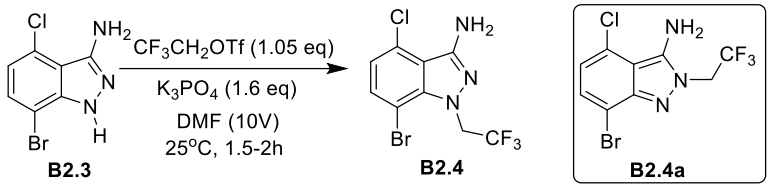


| # | Scale (g) | IPC Ratio **B2.4:B2.4a** | Yield[b] (%) | Output (g) | Purity A% (GCMS-TIC) | Purity wt% (qNMR) | Purity wt% (GCMS) | KF (%)[c] |
|---|---|---|---|---|---|---|---|---|
| 1 | 45 | 70:30 | 62 | 36 | 96 | 99 | 94 | 0.42 |
| 2 | 40 | 70:30 | 59 | 32 | 100 | 98 | - | - |
| 3 | 30 | 70:30 | 55 | 23 | 94 | 96 | - | - |
| 4 | 22 | 70:30 | 57 | 17 | 98 | 98 | - | - |
| 5 | 18 | 70:30 | 60 | 15 | 95 | 96 | - | - |

[a]All reactions were performed with **B2.3**, $CF_3CH_2OTf$ (1.05 eq), $K_3PO_4$ (1.6 eq), DMF (10V), 1.5-2 h. [b]Corrected isolated yield based on qNMR wt% purity. [c]Karl-Fischer titration.

## 2.4 Borylation of B2.4

### 2.4.1 Optimization of borylation of B2.4

Miyaura borylation of **B2.4** to furnish **Frag B** is known in the literature.[16] To obtain **Frag B** as a reference standard for our process development, we used this Pd-borylation approach to make the **Frag B** (Table 2.4.1). The Pd-catalyzed borylation of **B2.4** with $B_2pin_2$ proceeded in the presence of 2.7 mol% $PdCl_2(PPh_3)_2$ in a binary solvent of DMF/toluene (3:1, v/v, 8V). Under these conditions, **Frag B** was obtained in 89 A% with 11 A% debrominated **B2.5a** forming concurrently. Isopropyl acetate:heptane (1:10, 6V) was identified as a practical recrystallization solvent system to afford **Frag B** in 74% isolated yield and purity >99 wt % (20 g scale).

Table 2.4.1. Synthesis of **Frag B** as reference standard by Pd-catalyzed borylation of **B2.4**

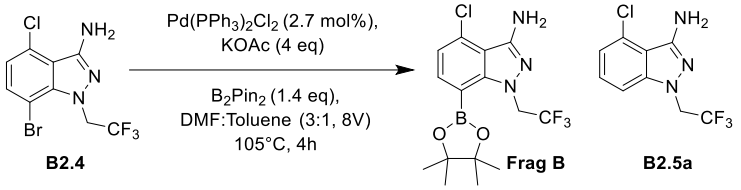


| # | Scale (g) | Yield[a] (%) | Output (g) | Purity[b] | | |
|---|---|---|---|---|---|---|
| | | | | GCMS (A%) | qNMR (wt%) | wt % |
| 1 | 20 | 74 | 17 | >99 | >95 | >99 |

[a]Isolated yield after recrystallization from isopropyl acetate/heptane (1/10, 6V). [b]A% and wt% were obtained by GCMS TIC A%.

To ameliorate cost impacts of Pd catalysis in **Frag B** manufacture, a deeper investigation of Gilead's metal-halogen exchange strategy for borylation was undertaken.[xii] Bis-*N*-TMS protected **B2.5** was prepared according to the literature[12], to avoid interference from the **B2.4**'s free amine in the metal-halogen exchange reactions.[xiii] As shown in Table 2.4.2 (entries 1-3), treatment of **B2.5** with LDA and various boron sources (i.e. *i*PrOBpin, $B(OMe)_3$ and $B(O\textit{i}Pr)_3$) resulted in no desired borylated product. The deshydrofluorinated compound **TMS-B2.5b** was detected by GCMS identified by mass alone. Switching LDA to Turbo Grignard (*i*PrMgCl·LiCl), neither **TMS-Frag B** nor **TMS-B2.5b** were detected. However, desbrominated **TMS-B2.5a** was observed when $B(OiPr)_3$ or $B(OMe)_3$ were used as the boron source (Table 2.4.2, entries 4-6). When *i*PrOBpin (2 eq) was used, the Grignard-mediated borylation (1.6 eq *i*PrMgCl·LiCl) at 25 °C delivered the desired **TMS-Frag B** in 26 A% (Table 2.4.2, entry 7). 38 A% of **TMS-Frag B** was achieved when the reaction was carried out at 0 °C (Table 2.4.2, entry 8). Full conversion required 3 eq of the Turbo Grignard reagent with up to 51 A% of **TMS-Frag B** (Table 2.4.2, entry 9). Excess Turbo Grignard ultimately resulted in a higher cost for this step than the incumbent process.

To achieve a more cost-effective Grignard-borylation, solvent volumes were screened. Full conversion of **B2.5** was achieved by decreasing solvent volumes, equivalents of iPrMgCl·LiCl and *i*PrOBpin. 7V of solvent delivered 81 A% **TMS-Frag B** on treatment of **B2.5** with 1.6 eq of

[xii] Borylation of **B2.4** mediated by less expensive metals such as $Fe(acac)_3$,[22] diethyl Zinc[23] and $NiCl_2Dppp$[24], was explored, as was pyridine-catalyzed radical borylation.[25] In all cases, products of debromination dominated.
[xiii] Experiments using LDA or LiHMDS gave, primarily, products of **B2.4** debromination rather than borylation.

*i*PrMgCl·LiCl and 1.2 eq of *i*PrOBpin. After quenching with 3 eq of aqueous HCl (1M), the same A% of **Frag B** was obtained (Table 2.4.2, entry 10). [Critical Process Parameter: Order of addition of iPrMgCl·LiCl and iPrOBpin is critical; magnesium-halogen exchange must be complete before adding iPrOBpin.] Mg-halogen exchange between **B2.5** and Turbo Grignard reagent was monitored by crude NMR, GCMS and TLC. After metal-halogen exchange was complete, addition of iPrOBpin enabled formation of **TMS-Frag B** with full conversion. Thus, optimized Grignard-mediated borylation conditions are as follows: iPrMgCl·LiCl (1.6 eq), iPrOBpin (1.2 eq), toluene (7V) at 0 °C, followed by TMS-deprotection with aq. HCl (1M, 3 eq).

Table 2.4.2. Optimization of metal-halogen exchange borylation of **B2.5**

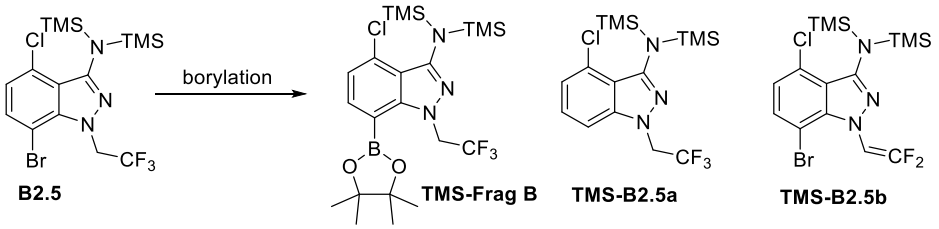


| #[a] | Solvent (V) | Base (eq) | [Boron] (eq) | T (°C) | IPC crude[c] | | | |
|---|---|---|---|---|---|---|---|---|
| | | | | | **B2.5** (A%) | **TMS-Frag B** (A%) | **TMS-B2.5a** (A%) | **TMS-B2.5b** (A%) |
| 1[b] | THF (10) | LDA (1.5) | Bpin-O*i*Pr (1.2) | -20 | 35 | 0 | 0 | 25 |
| 2 | THF (10) | LDA (1.5) | $B(OiPr)_3$ (1.2) | -20 | 60 | 0 | 0 | 34 |
| 3 | THF (10) | LDA (1.5) | $B(OMe)_3$ (1.2) | -20 | 67 | 0 | 0 | 33 |
| 4 | THF (10) | *i*PrMgCl·LiCl (4) | $B(OMe)_3$ (2) | 0 | 31 | 0 | 69 | 0 |
| 5 | Toluene (10) | *i*PrMgCl·LiCl (1.6) | $B(OMe)_3$ (2) | 0 | 90 | 0 | 9 | 0 |
| 6 | Toluene (10) | *i*PrMgCl·LiCl (1.6) | $B(OiPr)_3$ (2) | 0 | 71 | 0 | 25 | 0 |
| 7[b] | Toluene (15) | *i*PrMgCl·LiCl (1.6) | Bpin-O*i*Pr (2) | 25 | 30 | 26 | 2 | 13 |
| 8 | Toluene (15) | *i*PrMgCl·LiCl (1.6) | Bpin-O*i*Pr (1.2) | 0 | 35 | 38 | 19 | 0 |
| 9 | Toluene (10) | *i*PrMgCl·LiCl (3) | Bpin-O*i*Pr (2) | 0 | 0 | 51 | 40 | 0 |
| 10[c] | Toluene (7) | *i*PrMgCl·LiCl (1.6) | Bpin-O*i*Pr (1.2) | 0 | 0 | 81 | 15 | 0 |

[a]All reactions were performed with **B2.5** (1g) and conditions described in the table. For ease of analysis, the crude was sampled without TMS deprotection as the focus of the screen was to identify the best condition for borylation.

[b]Unknown impurities are present in the crude. [c]In-process analysis of the crude was obtained by GCMS TIC A%. [c]The same ratio of **Frag B:B2.5a** (81:15) was observed after TMS deprotection with 3 eq HCl (1M) for 2 h.

With the above optimized Grignard-mediated borylation conditions in place, attention turned to **Frag B** purification by recrystallization. Binary solvent systems EtOAc:heptanes and iPrOAc:heptanes were examined for recrystallization of crude **Frag B** (81% purity by qNMR). Both solvent systems afforded **Frag B** in 64-72% recovery yield and >99 purity by qNMR. iPrOAc:heptanes (1:9) was chosen for purification in scale-up.

Table 2.4.3. Condition screening of recrystallization of the crude **Frag B**[xiv]

| # | Scale (mg)[a] | Solvent (Ratio) | Solvent volume | Recrystallization[b] Yield (%) | Purity (%)[c] |
|---|---|---|---|---|---|
| 1 | 250 | EtOAc:Heptanes (1:4) | 8 | 64 | >99 |
| 2 | 250 | EtOAc:Heptanes (1:9) | 10 | 72 | >99 |
| 3 | 250 | *i*PrOAc:Heptanes (1:4) | 10 | 67 | >99 |
| 4 | 250 | *i*PrOAc:Heptanes (1:9) | 10 | 72 | >99 |

[a]Crude Frag B prior to recrystallization contained 81% (by qNMR) Frag B by GCMS TIC A%. The material was synthesized by reaction with *i*PrMgCl·LiCl (1.6 eq), *i*PrOBpin (1.2 eq), toluene (7V), 0 °C, and deprotected by aq. HCl (1M, 3 eq). [b]Crude was dissolved in the binary solvent by heating to 65 °C for 30 min then allowed cool to 25 °C and maintained at that temperature overnight. Precipitated solid was collected and analyzed. [c]Purity of the material after recrystallization was determined by qNMR.

### 2.4.3 Scale-up of borylation of B2.4

Grignard-mediated borylation to produce **B2.5** was demonstrated on decagram scale. First, **B2.4** was with treated with TMSCl (2.3 eq in THF (10V)) in the presence of LiHMDS (2.1 eq) at 0°C, to provide TMS-protected **B2.5** in 91-97% isolated yield (96-100% purity, qNMR). [Critical Process Parameter: Trace moisture (e.g., entrained in THF) must be eliminated from TMS protected **B2.5** before progressing to the metal-halogen exchange / borylation. Trace moisture was eliminated by azeotropic distillation with toluene.] The results are summarized in Table 2.4.4.

Table 2.4.4. Synthesis of **B2.5**

[xiv] The team will pursue competencies in rational DOE, exploiting the onsite Crystal16. We have discussed the gains available via quantitatively following nucleation events vs. time, temperature, etc.

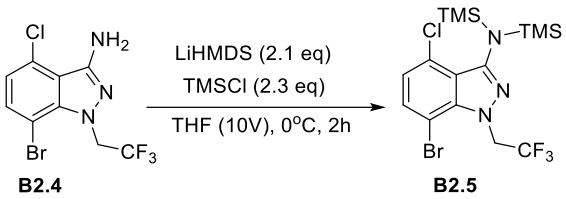


| #[a] | Scale (g) | Yield (%) | Output (g) | Purity | |
|---|---|---|---|---|---|
| | | | | GCMS (A%)[b] | qNMR (%) |
| 1 | 2 | 91 | 2.6 | 96 | 100 |
| 2 | 10 | 97 | 14.4 | - | 100 |
| 3 | 20 | 93 | 28 | - | 96 |
| 4 | 40 | 95 | 56.7 | - | 96 |

[a]All reactions were carried out with LiHMDS (2.1 eq), TMSCl (2.3 eq), THF (10V), under $N_2$. The crude was quenched with 0 °C $NH_4Cl$ (sat., 2.5V), extracted with toluene (15V), then azeotropically distilled. [b]A% was obtained by GCMS TIC.

With **B2.5** in hand, **Frag B** was prepared on 18-29g scales utilizing the optimized Grignard borylation process (Turbo Grignard reagent (1.5 eq), iPrOBpin (1.2 eq), Toluene (7V), 0°C). The ratio of **Frag B** and desbrominated **B2.5a** was between 80/15 and 86/13 by GCMS TIC A%, after acidic quench to remove TMS protecting groups. Recrystallization from iPrOAc/heptanes resulted in 51-57% **Frag B** yield with >96 wt% purity. Results are summarized in Table 2.4.5.

Table 2.4.5. Grignard-based borylation to synthesis of **Frag B**

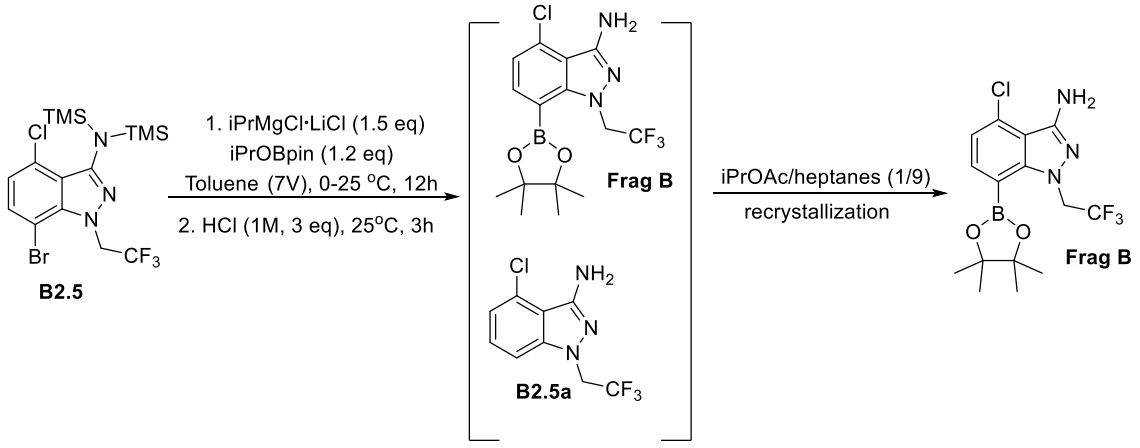


| #[a] | Scale (g) | Ratio of crude | Yield (%) | Output (g) | Purity[b] | KF (%)[c] |
|---|---|---|---|---|---|---|

| | | Frag B: B2.5a | | | GCMS (A%) | qNMR | wt % | |
|---|---|---|---|---|---|---|---|---|
| 1 | 20 | 84:16 | 52 | 8.5 | 100 | 99 | 95.6 ± 4.0% | 0.21 ± 0.01% |
| 2 | 29 | 91:9 | 57 | 13.2 | 100 | 99 | 99.9% ± 4.7% | 0.20% ± 0.01% |
| 3 | 18 | 87:13 | 51 | 7.55 | 100 | 99 | 101.6 ± 4.4% | 0.20 ± 0.02% |

[a]Reactions were conducted with Turbo Grignard reagent (1.5 eq), iPrOBpin (1.2 eq), Toluene (7V), 0-25°C; TMS protecting groups were removed via aq. HCl quench (1M, 3 eq). Crude was dissolved in iPrOAc/heptanes (1/9, 10V) by heating to 65°C for 30min, allowed to cool to 25°C and incubated overnight. Precipitates were collected and analyzed. [b]Purity was obtained by GCMS (TIC A%), qNMR and wt%. [c]Karl-Fischer titration.

# 3. Experimental sections

## 3.1 Analytical Report for Lenacapavir Frag B

Based on the five-step synthesis developed by M4All for lenacapavir **Frag B** (Scheme 3.1.1), the M4All analytical team developed GC-MS detection method for it, its intermediates and starting materials.

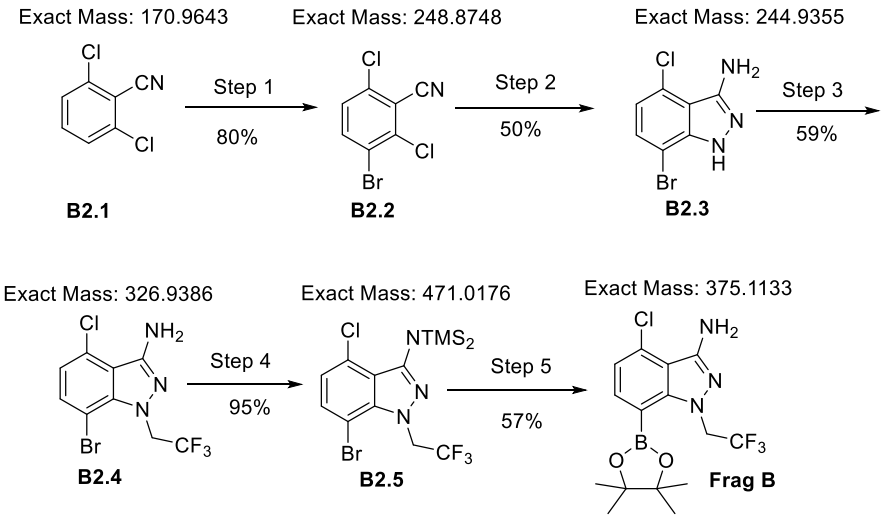


Scheme 3.1.1. Synthesis of lenacapavir **Frag B**

### 3.1.1 Pharmacopoeia Methods

Neither compendial methods nor monographs from the United States Pharmacopoeia and the European Pharmacopeia are available for lenacapavir **Frag B**.

## 3.1.2 Method Development

### *3.1.2.1 Chromatographic Conditions*

Initially method development work was performed using a LC-DAD. However, there were problems achieving baseline separation for **B2.3** desired and undesired isomers. As these isomers baseline separated readily on the GC-MS, this technique was utilized. The GC-MS method adopted utilized an Agilent J&W HP-5MS GC Column, 30 m, 0.25 mm, 0.25 µm with a split ratio of 100:1 (140 mL/min split flow) and an injection temperature of 250 °C. Column temperature was initially held at 50 °C for 3 minutes, ramped to 250 °C at 25 °C/min, held 3 minutes and then finally ramped to 300 °C at 25 °C/min and held for 3 minutes. The chromatogram below depicts the separation between the analytes (Figure 3.1.2.1).

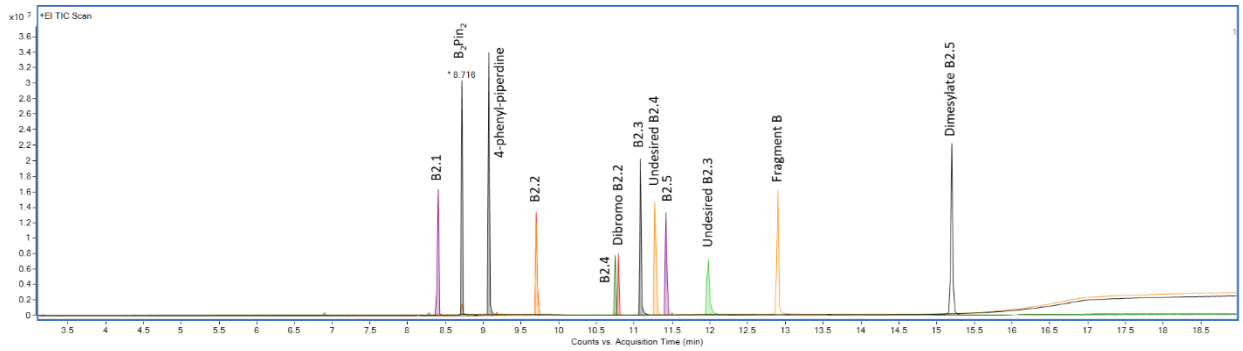


Figure 3.1.2.1. GC-MS chromatogram for all starting materials, intermediates and product in the synthesis of **Frag B**.

### *3.1.2.2 Relative Response Factors*

Response factors were not determined for lenacapavir **Frag B**.

### *3.1.2.3 MS Spectra*

MS spectra of each compound are found in Appendix 4.2.

### *3.1.2.4 Linearity*

**Frag B** linearity was tested over the range of 0.1 mg/mL to 1.1 mg/mL. For a 7-level curve over this range was the fit was quadratic with an $R^2 > 0.99$ (Figure 3.1.2.2). The choice of quadratic fit was confirmed on two separate instruments over multiple days.

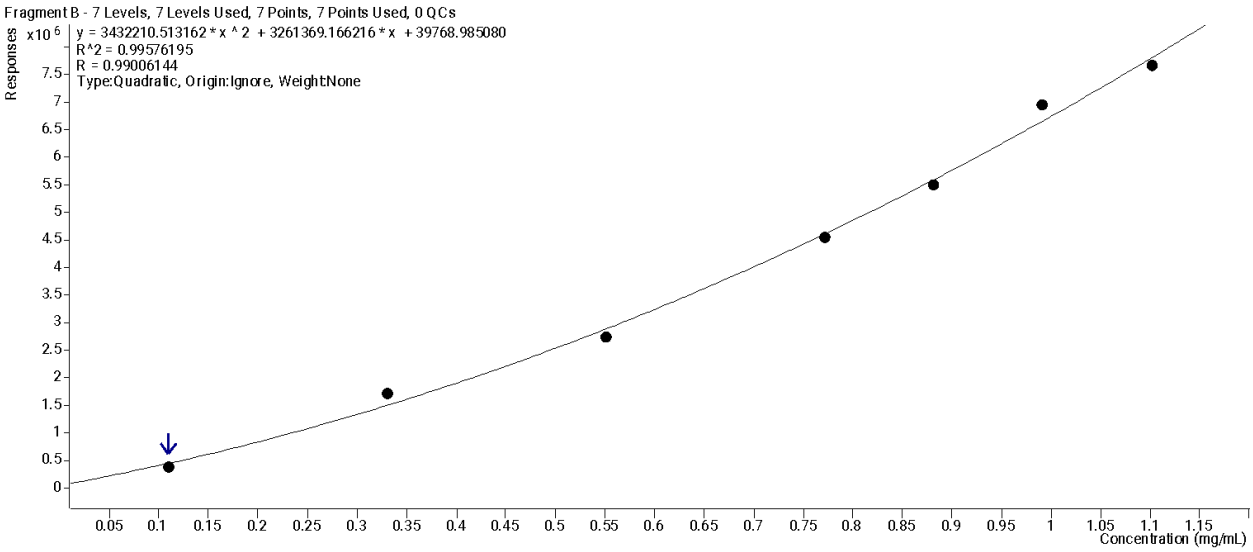


Figure 3.1.2.2. A 7-level calibration curve for **Frag B**.

#### *3.1.2.5 Limit of Detection (LOD) and Limit of Quantitation (LOQ)*

Limits were not determined for the starting materials, intermediates, impurities or product.

### 3.1.3 Impurities

#### *3.1.3.1 Starting Material Impurities*

Impurities were not specified nor determined for lenacapavir **Frag B** starting materials.

#### *3.1.3.2 Synthesis Impurities*

The undesired isomers of **B2.3** and **B2.4** were isolated and provided as standards. The developed GC-MS method baseline separated the undesired isomers from the desired products. No other impurities were isolated and characterized for lenacapavir **Frag B** or for the intermediates *en route* to lenacapavir **Frag B**.

### 3.1.4 Forced Degradation Studies

Forced degradation studies were not performed for lenacapavir **Frag B** nor its starting materials, intermediates and impurities.

### 3.1.5 Methods

Analytical methods used to support the synthesis of lenacapavir **Frag B** are appended to this report.

#### *3.1.5.1 Key Starting Materials*

**B2.1** is analyzed via GC-MS using the method “LenB 2” (attached).

#### 3.1.5.2 Reagent and Solvents

Residual solvents were not quantified for lenacapavir **Frag B**.

#### 3.1.5.3 Intermediates

The **B2.2**, **B2.3**, **B2.4** and **B2.5** are synthetic intermediates in this process. These intermediates as well as crude and isolated **Frag B** are analyzed using "LenB-1".

#### 3.1.5.4 In-Process Controls (IPC)

Requirements for IPCs were not set on this process. However, when IPC samples were collected, they were analyzed via GC-MS using the "LenB-1" method.

#### 3.1.5.5 Final Product Analysis

Isolated **Frag B** was assayed using the "LenB-1". This material was also subjected to KF titration of water content.

#### 3.1.5.6 Method Appropriateness

During development of the "LenB-1" certain performance characteristics were evaluated to select analytical conditions. These results are described above and include linearity. This method was not tested for specificity. Method validation was not performed.

## 3.2 Detailed experimental procedure

### 3.2.1 General Method

Reagents and solvents were obtained from commercial suppliers and used as received unless otherwise indicated. Reactions were monitored by TLC (precoated silica gel 60 F254 plates, EMD Chemicals), Agilent GCMS or crude $^{1}$H NMR. HRMS was recorded using Perkin Elmer Axion 2 ToF MS, ionization mode: positive with scan range: 100 - 1000 m/z, flight tube voltage: 8 kV, spray voltage: 3.5 kV, solvent: methanol. TLC was visualized with UV light. The proton ($^{1}$H NMR), carbon ($^{13}$C NMR) and 2-DNMR spectra of the compounds were recorded on Bruker Avance III HD Ascend 600 MHz spectrometer. The NMR solvents used were DMSO-$d_6$, $CDCl_3$ and $CD_3OD$. The chemical shifts were reported in parts per million (ppm). Coupling constants J are reported in hertz (Hz). The abbreviations used to designate signal multiplicity were: s, singlet; d, doublet; t, triplet; q, quartet, p, pentet; dd, doublet of doublets; ddd, doublet of doublet of doublets; dt, double of triplets; ddt, doublet of doublet of triplets; m, multiplet; br, broad.

### 3.2.2 Experimental procedure

**Preparation of 7-bromo-4-chloro-1H-indazol-3-amine (B2.3) as a standard based on literature method** [16]

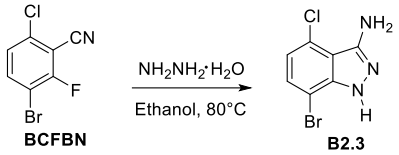


A mixture of 3-bromo-6-chloro-2-fluorobenzonitrile (BCFBN) (250 mg), ethanol (2.0 mL) and hydrazine hydrate (0.35 mL; 5 eq) was stirred at 80 °C for 1 h. After completion, the solution was allowed to cool to 45 °C and water was added slowly to produce a white precipitate. Following the addition of water, the mixture was stirred for 30 minutes. The solids were isolated via filtration. The solids were washed with water and then dried under vacuum at 45 °C to afford the desired compound 7-bromo-4-chloro-lH-indazol-3-amine (**B2.3,** 229 mg) in 87% yield and 99.8% A% (GCMS TIC). $^{1}$H NMR (600 MHz, DMSO-d6) δ 12.23 (s, 1H), 7.41 (d, J = 7.9 Hz, 1H), 6.85 (d, J = 7.9 Hz, 1H), 5.33 (s, 2H). $^{13}$C NMR (151 MHz, DMSO-d6) δ 149.1, 141.1, 129.5, 125.2, 119.1, 111.9, 101.0. MS-EI (*m/z*): 245 and 247.

**Preparation of 3-bromo-2,6-dichlorobenzonitrile (B2.2)**

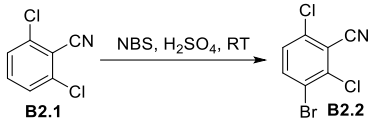


To a 2 L ChemRxnHub reactor at room temperature, 2,6-dichlorobenzonitrile (290.0 g, 1.68 mol) was added followed by addition of 96% sulfuric acid (10 eq, 0.92 L, 16.8 mol) with stirring at 25°C. After addition of sulfuric acid, the reaction mixture was stirred for 15 minutes to obtain a clear yellowish solution. The mixture was cooled to 0°C and *N*-bromosuccinimide (321 g, 1.07 eq, 1.8 mol) was added in portions over the course of 10 minutes at 0°C and a slightly exotherm was observed. The reaction mixture was stirred at 25 °C for 18h to afford a thick, pale yellowish orange slurry. After completion of the reaction (monitored by $^{1}$HNMR), the crude mixture was slowly

discharged to a work-up vessel containing chilled water (2.9 L, 10V, 0-5 °C). The slurry was stirred 45 minutes then the resulting precipitates collected by filtration. The filter cake was washed with water (500 mL (1.7V) ×5), dried under house vacuum and then washed with ethyl acetate (300 mL (1V) × 3). The solid was dried under vacuum to obtain the product (355 g, yield: 80%; purity by qNMR: 95%; A% by GCMS TIC: 97%, containing 2% of dibromodichlorobenzonitrile). $^{1}$H NMR (600 MHz, DMSO-d6) δ 8.11 (d, J = 8.8 Hz, 1H), 7.66 (d, J = 8.8 Hz, 1H). $^{13}$C NMR (151 MHz, DMSO-d6) δ 138.9, 137.3, 136.5, 129.8, 121.7, 114.5, 113.3. $^{13}$C NMR DEPT 135 (151 MHz, DMSO-d6) δ 138.9, 129.8. MS-EI (*m/z*): 251.

**Preparation of 7-bromo-4-chloro-1H-indol-3-amine (B2.3)**

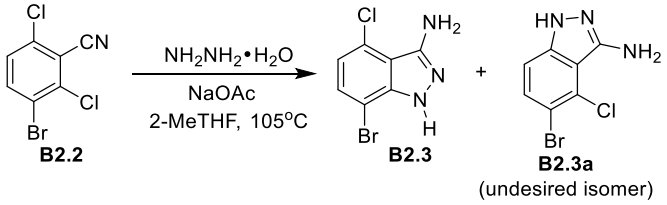


To a rigorously cleaned, nitrogen-purged 1L Parr reactor equipped with a stainless-steel stirrer shaft and turbine-type impeller was charged 3-bromo-2,6-dichlorobenzonitrile (80.0 g, 1 eq, 296 mmol), hydrazine hydrate (76 mL, 4 eq, 1.2 mol), sodium acetate (29.1, 1.2 eq, 355 mmol) and 2-MeTHF (5 V, 400 mL) at room temperature. The reaction mixture was warmed to 105 °C (45 psig) and held at this temperature for 18h. The reaction was monitored by NMR. Upon completion, the crude mixture was slowly cooled to -25°C. Pure **B2.3** precipitated and was filtered while the solution was still cold. The compound was washed with 10 volumes of water and dried (38.4g, yield: 49%; purity by qNMR: 96%; purity by wt% with comparison to a known standard: 94.7 ± 1.7%, GCMS TIC A%: 100%, Water content (KF): 0.24 ± 0.03%. $^{1}$H NMR (600 MHz, DMSO-d6) δ 12.23 (s, 1H), 7.41 (d, J = 7.9 Hz, 1H), 6.85 (d, J = 7.9 Hz, 1H), 5.33 (s, 2H). $^{13}$C NMR (151 MHz, DMSO-d6) δ 149.1, 141.1, 129.5, 125.2, 119.1, 111.9, 101.0. $^{13}$C NMR DEPT 135 (151 MHz, DMSO-d6) δ 129.5, 119.1. HRMS (*m/z*): $[M+H]^+$ calcd. for $C_7H_6BrClN_3^+$: 247.9413 amu; found: 247.9412 amu.

For comparison, the undesired isomer **B2.3a** was purified by column chromatography ($SiO_2$, ethyl acetate/heptanes = 10/90) to obtain the characterization data. Compound **B2.3a**: $^1$H NMR (600 MHz, DMSO-d6) δ 12.0 (s, 1H), 7.45 (d, J = 8.8 Hz, 1H), 7.19 (d, J = 8.8 Hz, 1H), 5.27 (s, 2H). $^{13}$C NMR (151 MHz, DMSO-d6) δ 148.5, 141.8, 131.1, 125.7, 112.3, 110.9, 110.3. HRMS (*m/z*): $[M+H]^+$ calcd for $C_7H_5BrClN_3 \cdot H^+$: 247.9413 amu; found: 247.9400 amu.

**Preparation of 7-bromo-4-chloro-1-(2,2,2-trifluoroethyl)-1H-indazol-3-amine (B2.4)**

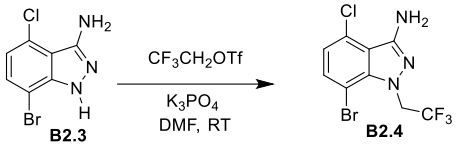


To a flask (1 L) equipped with an overhead mechanical stirrer was added 7-bromo-4-chloro-1H-indazol-3-amine (45 g, 1 eq), DMF (450 mL, 10V) and $K_3PO_4$ (56 g, 1.5 eq). The mixture was stirred at 25°C for 30 min. 2,2,2-Trifluoroethyl trifluoromethanesulfonate (43.4 g, 28.2 mL, 1.05 eq) was added slowly over the course of 15 minutes to maintain the temperature below 45°C. The mixture was then stirred at 25°C for 2 hours. Upon completion, the reaction was added to water (10 V, 450 mL) at room temperature then stirred for 20 min to precipitate solids. The precipitates were filtered and further washed with water (225 mL, 5V) then dried. The crude product was added to a binary solvent system comprising DMF:$H_2O$ (1:2, 4V). The resulting slurry was stirred for 30 min at room temperature. The slurry was filtered and then dried under vacuum at 50 °C for 12h to give the desired product (36 g, 62% yield; purity by qNMR: 99%; GCMS TIC A%: 100%, purity by wt% with comparison to a known standard: 94.1 ± 1.2%). $^1$H NMR (600 MHz, $CDCl_3$) δ 7.49 – 7.39 (m, 1H), 6.88 (d, J = 8.0 Hz, 1H), 5.21 (q, J = 8.1 Hz, 2H). $^{13}$C NMR (151 MHz, $CDCl_3$) δ 148.4, 139.9, 133.1, 126.7, 123.2 ($q^1_{CF3}$, J = 282.4 Hz), 121.2, 115.1, 100.9, 49.9 ($q^2_{CF3}$, J = 33.2 Hz). HRMS $[M+H]^+$ calcd for $C_9H_6BrClF_3N_3 \cdot H^+$: 327.9464 amu; found: 327.9462 amu.

**Preparation of 4-chloro-7-(4,4,5,5-tetramethyl-1,3,2-dioxaborolan-2-yl)-1-(2,2,2-trifluoroethyl)-N,N-bis(trimethylsilyl)-1H-indazol-3-amine (B2.5)**

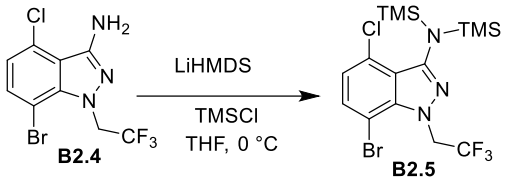


To a nitrogen-inerted three-necked flask (1 L) equipped with a J-Kem probe, and a magnetic stirbar were added 7-bromo-4-chloro-1-(2,2,2-trifluoroethyl)-1H-indazol-3-amine (40 g, 1 eq, 121.76 mmol) and THF (10 V, 400 mL). The mixture was cooled to 0 °C and chlorotrimethylsilane (30 g, 35.5 mL, 2.3 eq, 280.04 mmol) was added dropwise, followed by lithium bis(trimethylsilyl)amide (1.0 M, 42.8 g, 256 mL, 2.1 eq, 256 mmol) at 0°C under $N_2$ (keeping the internal temperature below 5.0°C). The resulting mixture was stirred at 0°C for 2 h. Upon completion (monitored by TLC) the reaction was quenched with ice-cold saturated aqueous $NH_4Cl$ (100 mL, 2V). The mixture was extracted with toluene (600 mL, 15V). The organic layer was washed with brine (200 mL, 5V) and then concentrated with azeotropic distillation to afford the product as a thick oil (56.7g, yield: 95%; purity by qNMR: 96%; GCMS TIC A%: 96%). $^1$H NMR (600 MHz, $CDCl_3$) δ 7.32 (t, J = 6.1 Hz, 1H), 6.84 (d, J = 8.0 Hz, 1H), 5.27 (q, J = 8.0 Hz, 2H), 0.00 (s, 18H). $^{13}$C NMR (151 MHz, $CDCl_3$) δ 148.5, 138.4, 130.9, 125.9, 121.9($q^1_{CF3}$, J = 282.8 Hz), 121.5, 120.4, 99.6, 48.8 ($q^2_{CF3}$, J = 34.2 Hz), 4.1. GCMS (*m/z*): 471.

**Preparation of 4-chloro-7-(4,4,5,5-tetramethyl-1,3,2-dioxaborolan-2-yl)-1-(2,2,2-trifluoroethyl)-1H-indazol-3-amine (Frag B)**

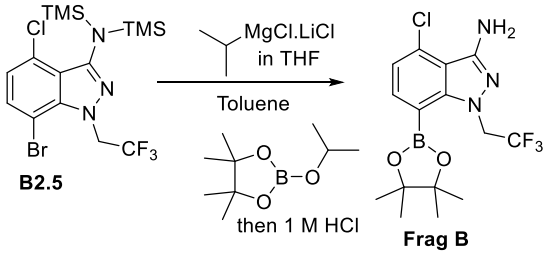


7-bromo-4-chloro-1-(2,2,2-trifluoroethyl)-N,N-bis(trimethylsilyl)-1H-indazol-3-amine (29.0 g, 1 eq, 61.3 mmol) was dissolved in anhydrous toluene (203 mL, 7V) and transferred to an oven dried flask under $N_2$. The flask was equipped with a magnetic stirrer and a J-Kem temperature probe for

measuring the internal temperature. The assembly was cooled at 0 °C and isopropylmagnesium chloride-lithium chloride complex in THF (1.3M, 13.36 g, 71 mL, 1.5 eq, 92 mmol) was added slowly to maintain the internal temperature below 10°C. The addition was completed in 15 min and the reaction was stirred at the same temperature for additional 1.5 h. After the completion of magnesium-halogen exchange (monitored by crude $^{1}$HNMR and TLC), 2-isopropoxy-4,4,5,5-tetramethyl-1,3,2-dioxaborolane (14 g, 15.3 mL, 1.2 eq, 73.6 mmol) was added slowly, maintaining the internal temperature below 5 °C. After addition, the resulting mixture was stirred at 0 °C for 3 h then warmed to 25 °C and stirred for additional 12 h. Upon completion, the reaction was quenched with water (116 mL, 4V, 25 °C, 5 min stirring). The aqueous phase was extracted with ethyl acetate (230 mL, 8V) and filtered over celite. The organic layer was separated, washed with brine, dried and then evaporated. The obtained residue was dissolved in THF:$CH_3CN$ (10:1, 230 mL, 8V) and then HCl (1M, 184 mL, 3 eq, 184 mmol) was added slowly, maintaining the temperature below 35 °C. The mixture was stirred for additional 2 h. After the deprotection was complete, the aqueous THF/$CH_3CN$ medium was extracted with ethyl acetate (290 mL, 10 V) and the solvent was evaporated. Heptanes:iPrOAc (9:1, 290 mL, 10 V) as per mass of crude isolated after deprotection was added and heated to 75 °C for 1 h then cooled to room temperature and stirred for an additional 6 h. The precipitate was filtered and dried under house vacuum at 25 °C for 2h to afford the desired product **Frag B** (13.2g, yield: 57%; purity by qNMR: 99%; GCMS TIC A%: 100%; by wt% with comparison to a known standard: 100%; KF: 0.20%) $^{1}$H NMR (600 MHz, $CDCl_3$) δ 7.83 (d, J = 7.6 Hz, 1H), 6.99 (d, J = 7.6 Hz, 1H), 5.41 (q, J = 8.6 Hz, 2H), 1.37 (s, 12H). $^{13}$C NMR (151 MHz, $CDCl_3$) δ148.5, 145.9, 138.7, 130.9, 124.4 ($q^{1}_{CF3}$, J = 282.4 Hz), 119.5, 113.0, 84.6, 50.6 ($q^{2}_{CF3}$, J = 33.9 Hz), 24.7. HRMS $[M+H]^+$ calcd for $C_{15}H_{18}BrClF_3N_3O_2 \cdot H^+$: 376.1205 amu; found: 376.1218 amu.

### 3.2.3 NMR Spectra

3-bromo-2,6-dichlorobenzonitrile (**B2.2**)

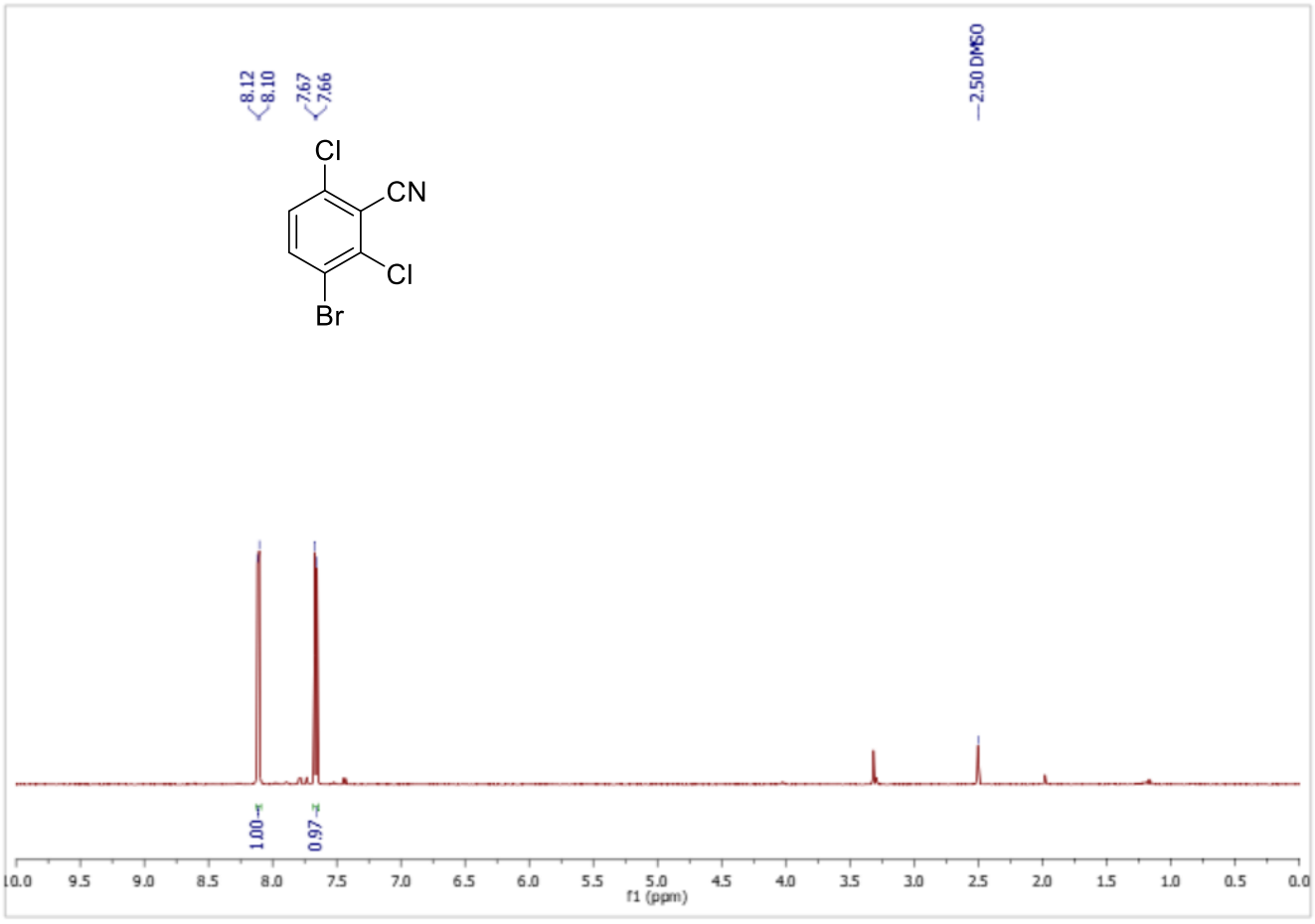


Figure 3.2.3.1 $^{1}$HNMR of 3-bromo-2,6-dichlorobenzonitrile (**B2.2**) in DMSO-d6.

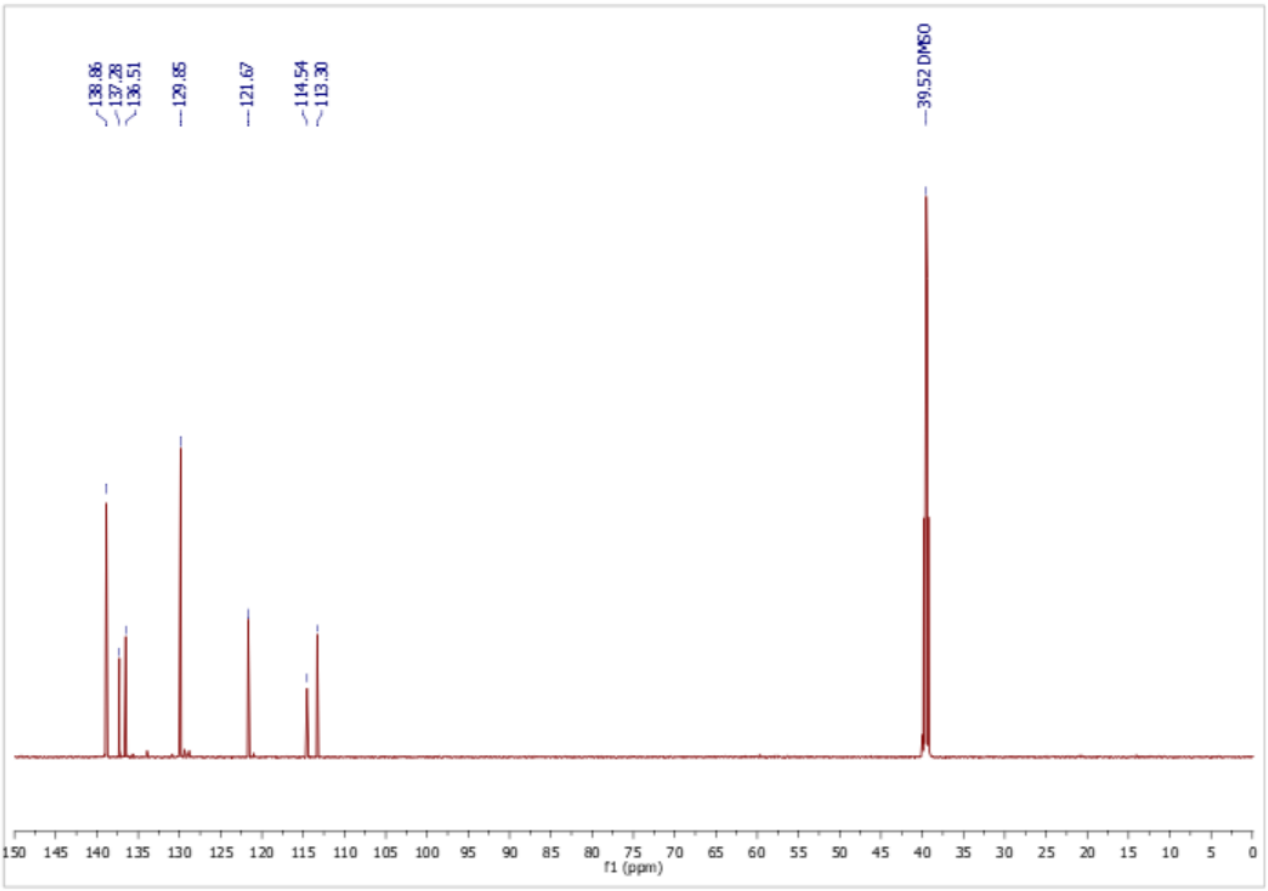


Figure 3.2.3.2 $^{13}$CNMR of 3-bromo-2,6-dichlorobenzonitrile (**B2.2**) in DMSO-d6.

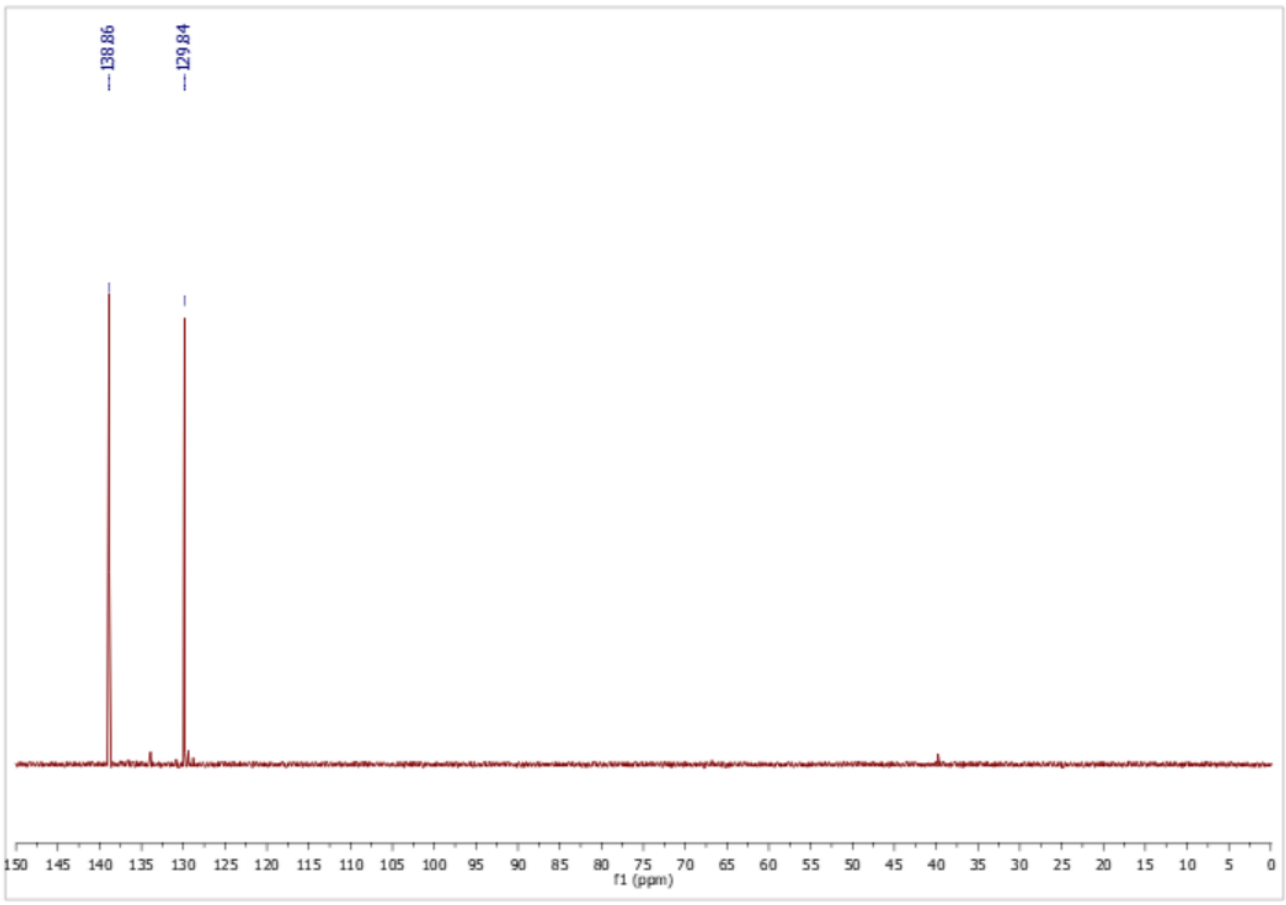


Figure 3.2.3.3 DEPT-135 of 3-bromo-2,6-dichlorobenzonitrile (**B2.2**) in DMSO-d6.

7-bromo-4-chloro-1H-indazol-3-amine (B2.3)

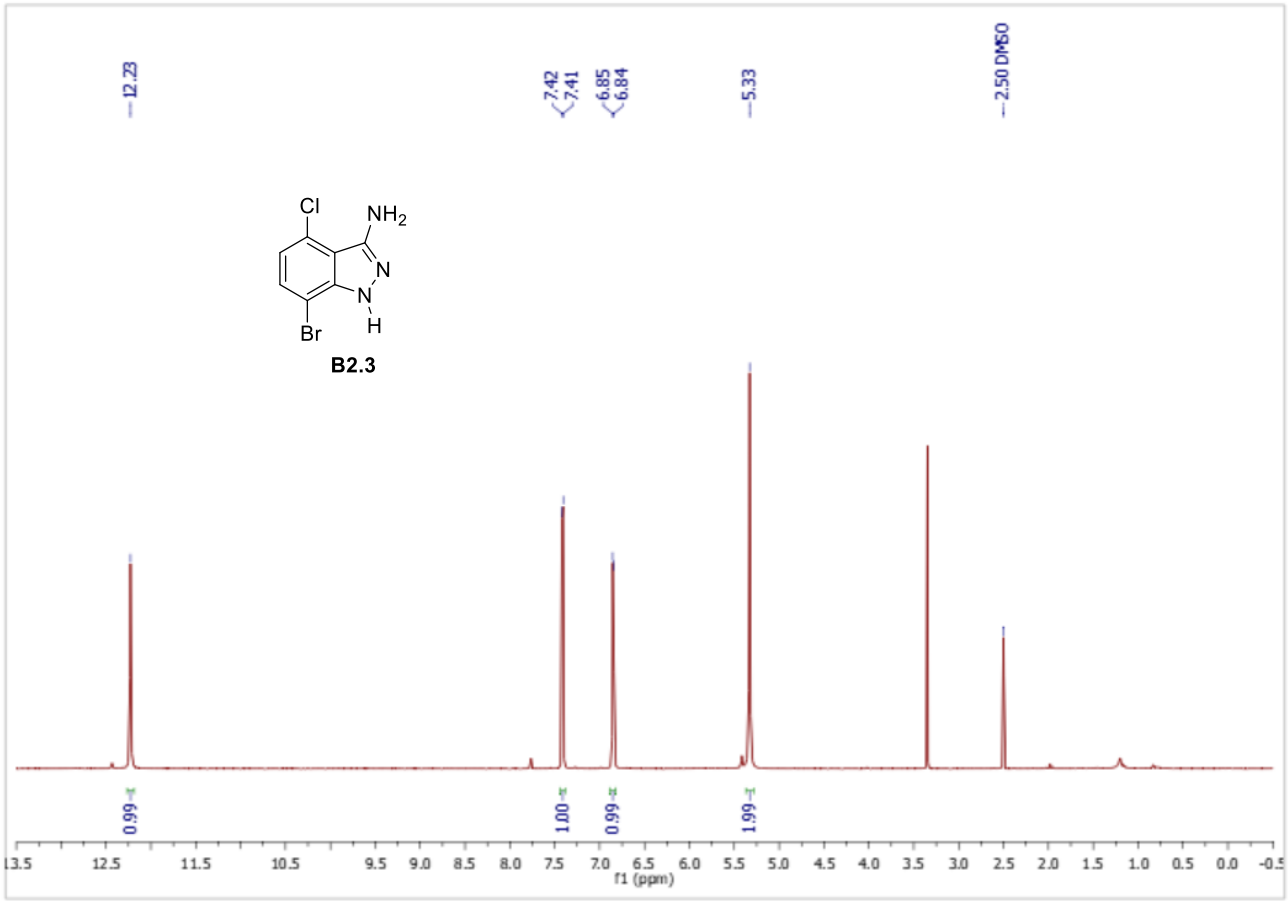


Figure 3.2.3.4 $^{1}$HNMR of 7-bromo-4-chloro-1H-indazole-3-amine (**B2.3**) in DMSO-d6.

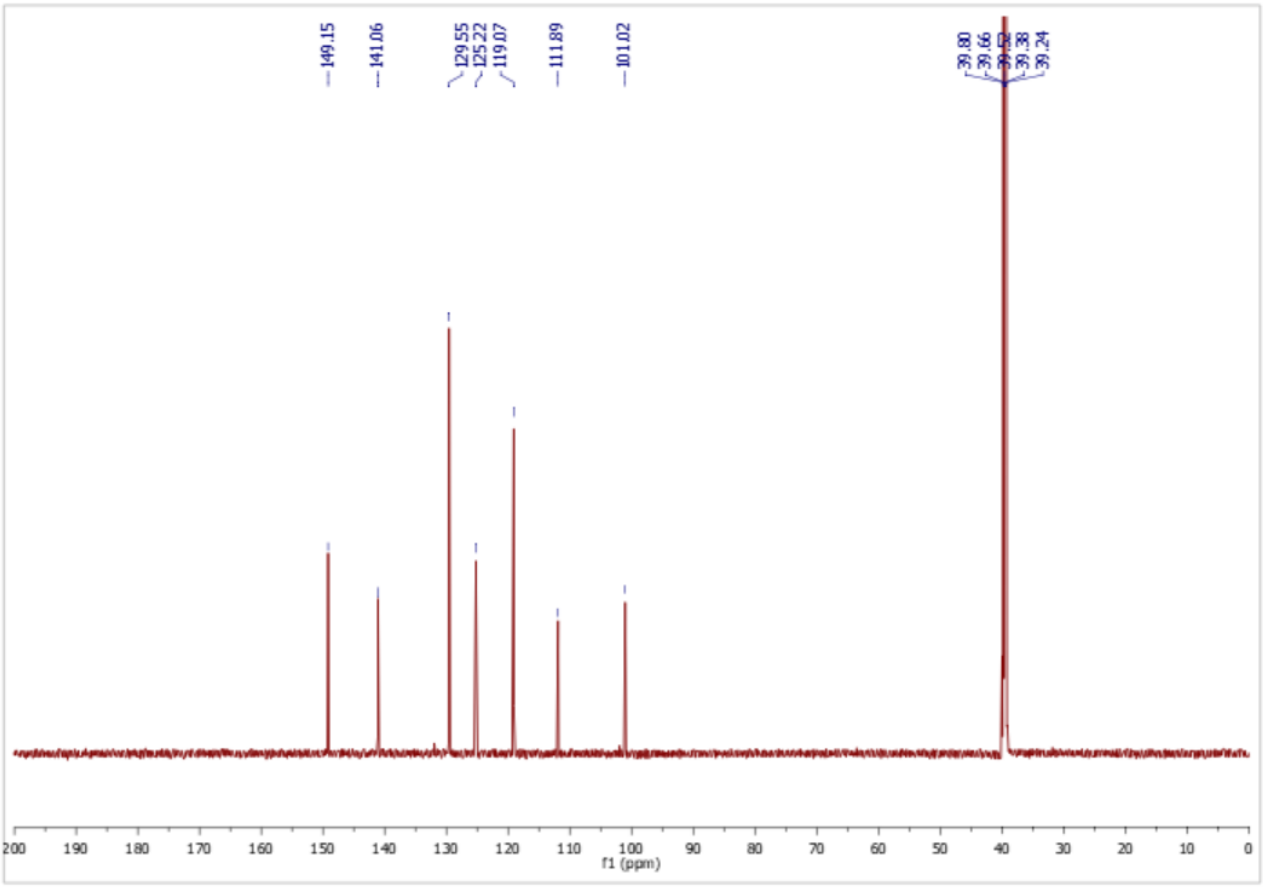


Figure 3.2.3.5 $^{13}$CNMR of 7-bromo-4-chloro-1H-indazole-3-amine (**B2.3**) in DMSO-d6.

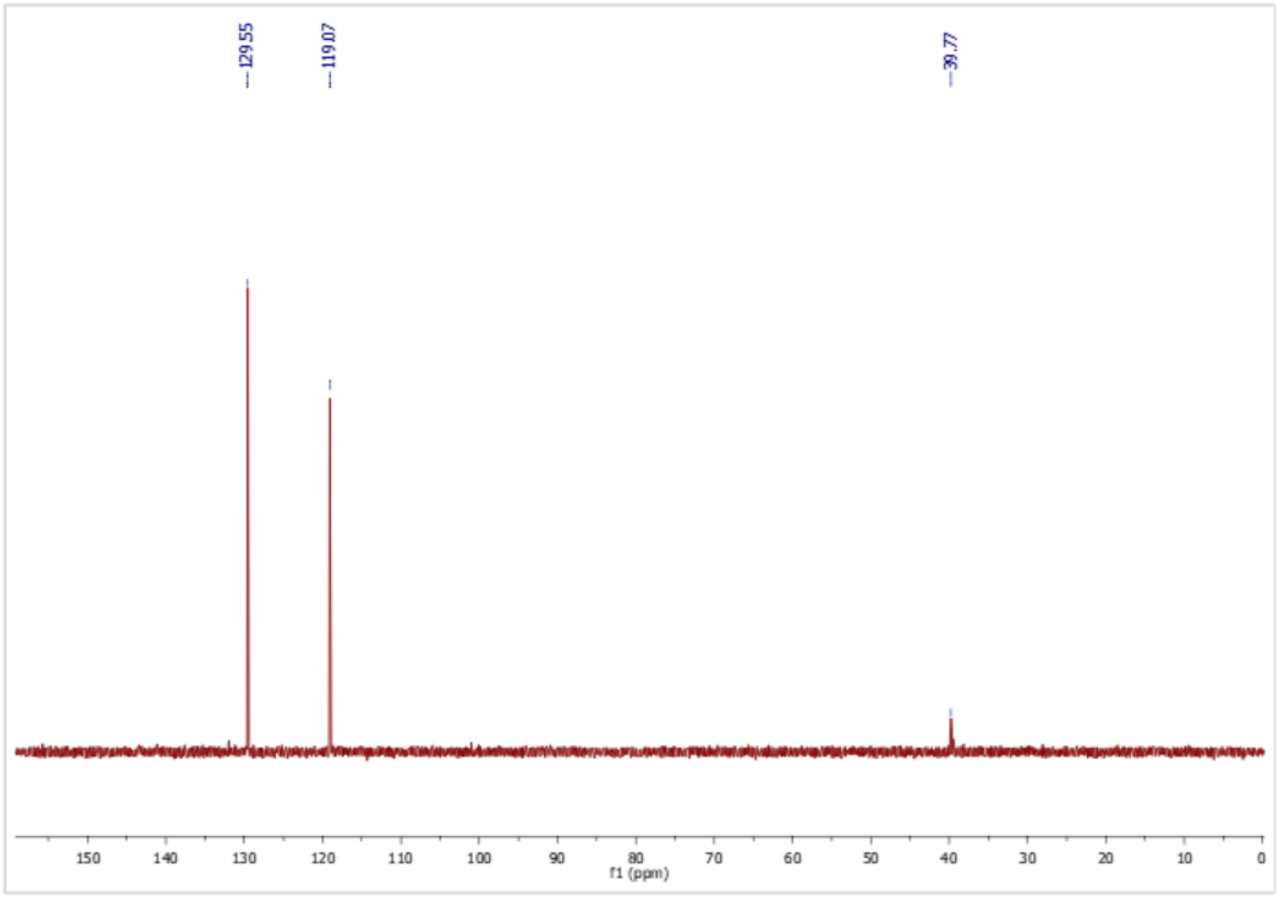


Figure 3.2.3.6 DEPT-135 of 7-bromo-4-chloro-1H-indazole-3-amine (**B2.3**) in DMSO-d6.

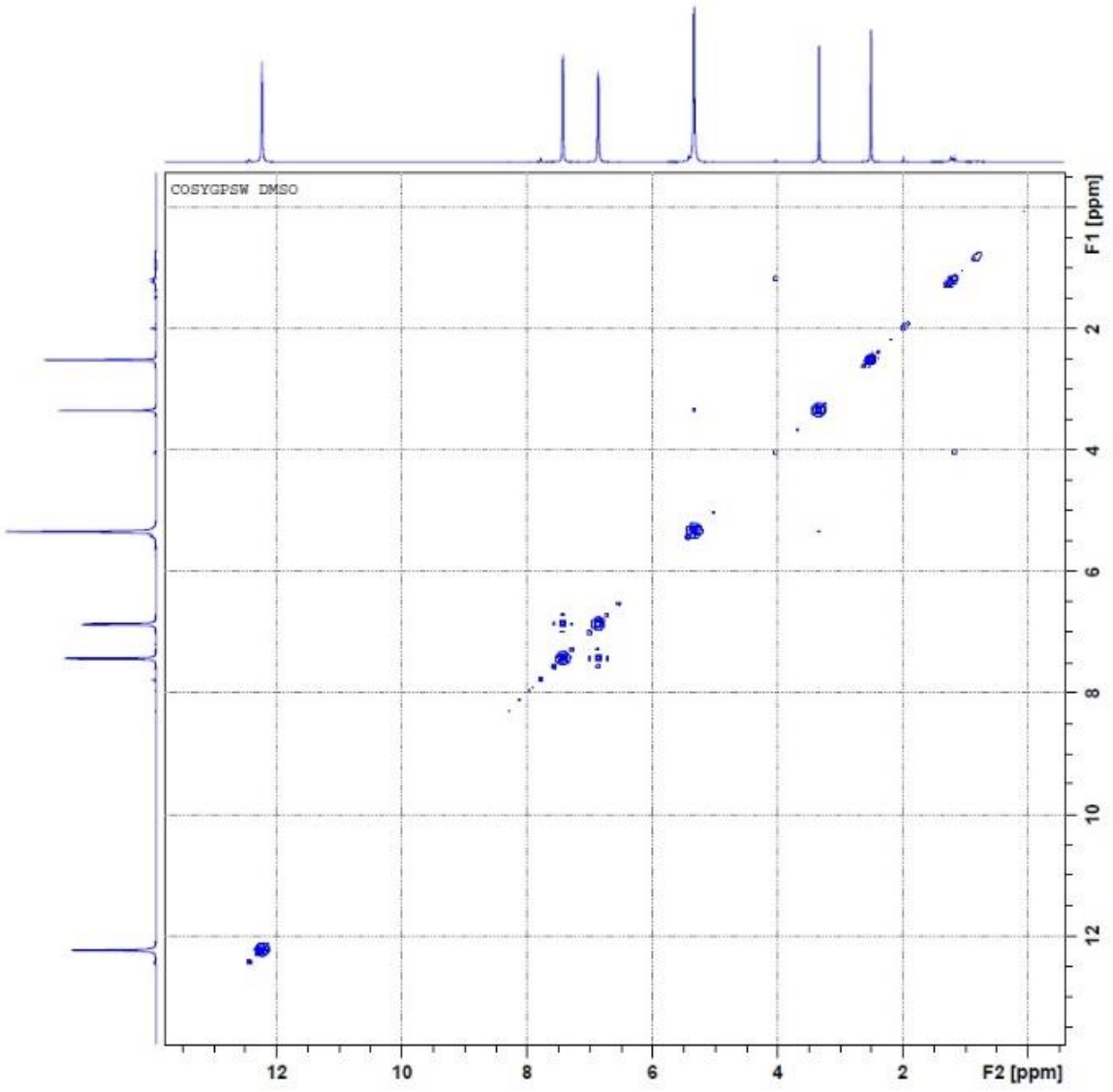


Figure 3.2.3.7 $^{1}$H-$^{1}$H COSY of 7-bromo-4-chloro-1H-indazole-3-amine (**B2.3**) in DMSO-d6.

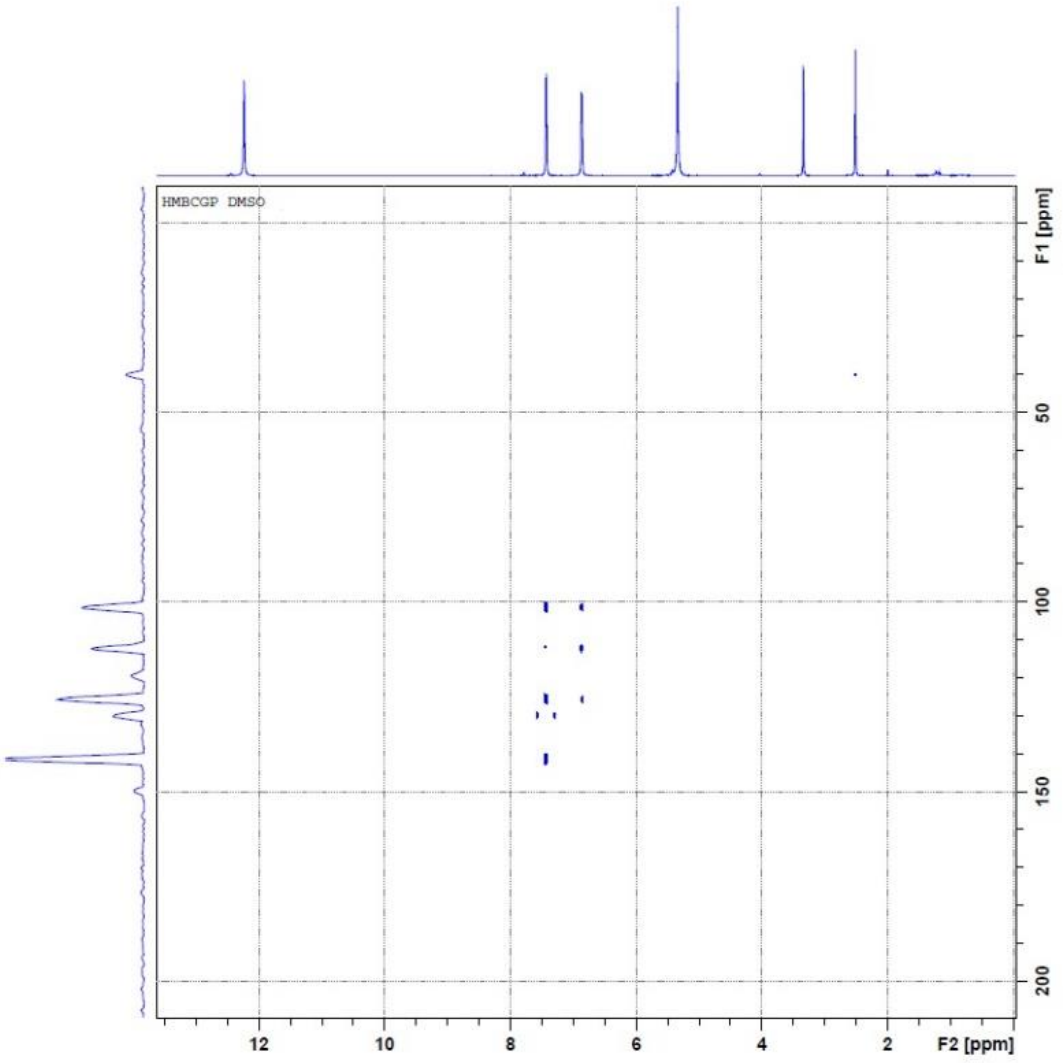


Figure 3.2.3.8 HMBC of 7-bromo-4-chloro-1H-indazole-3-amine (**B2.3**) in DMSO-d6.

7-bromo-4-chloro-1-(2,2,2-trifluoroethyl)-1H-indazol-3-amine (B2.4)

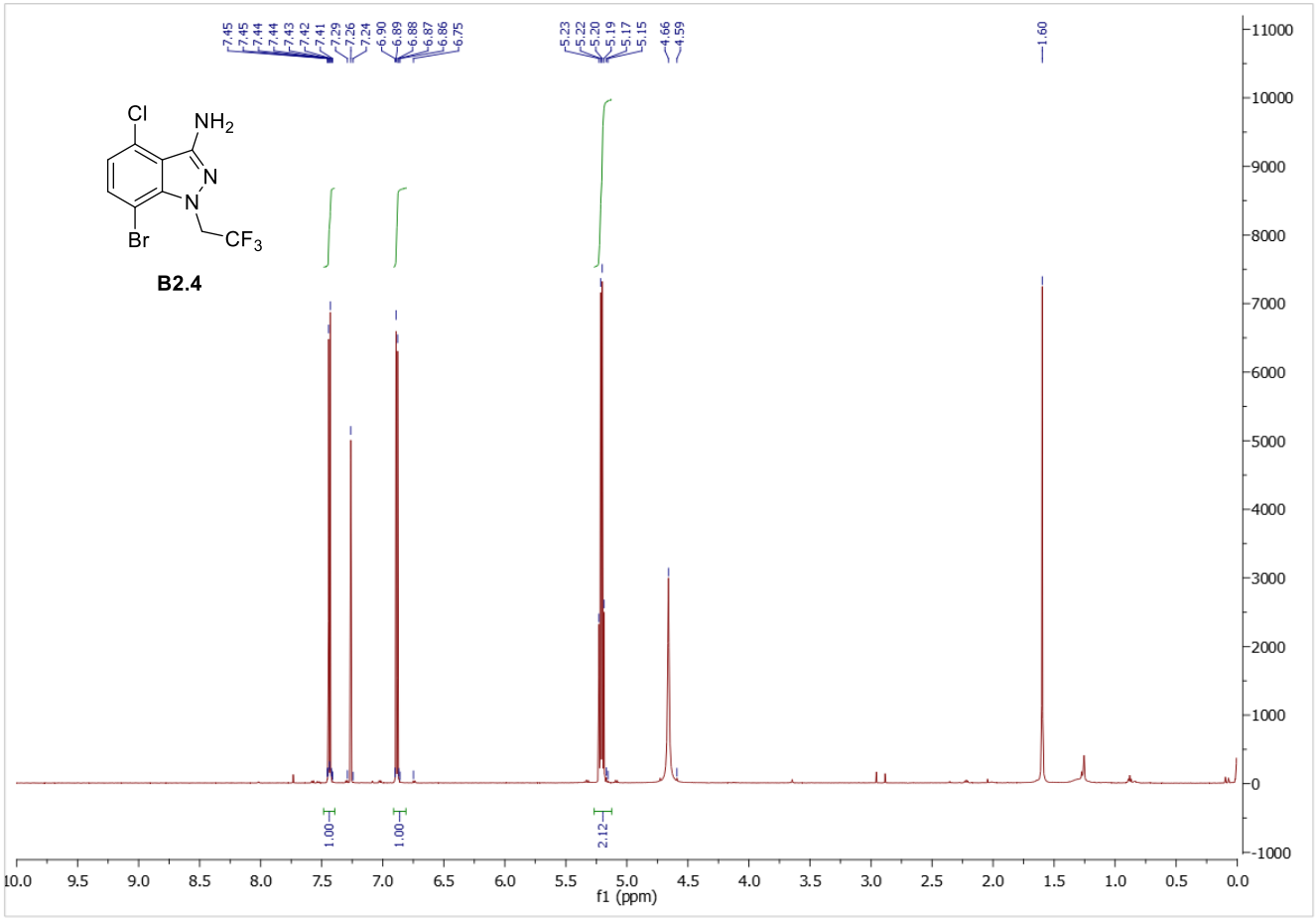


Figure 3.2.3.9 $^{1}$HNMR of 7-bromo-4-chloro-1-(2,2,2-trifluoroethyl)-1H-indazol-3-amine (**B2.4**) in $CDCl_3$

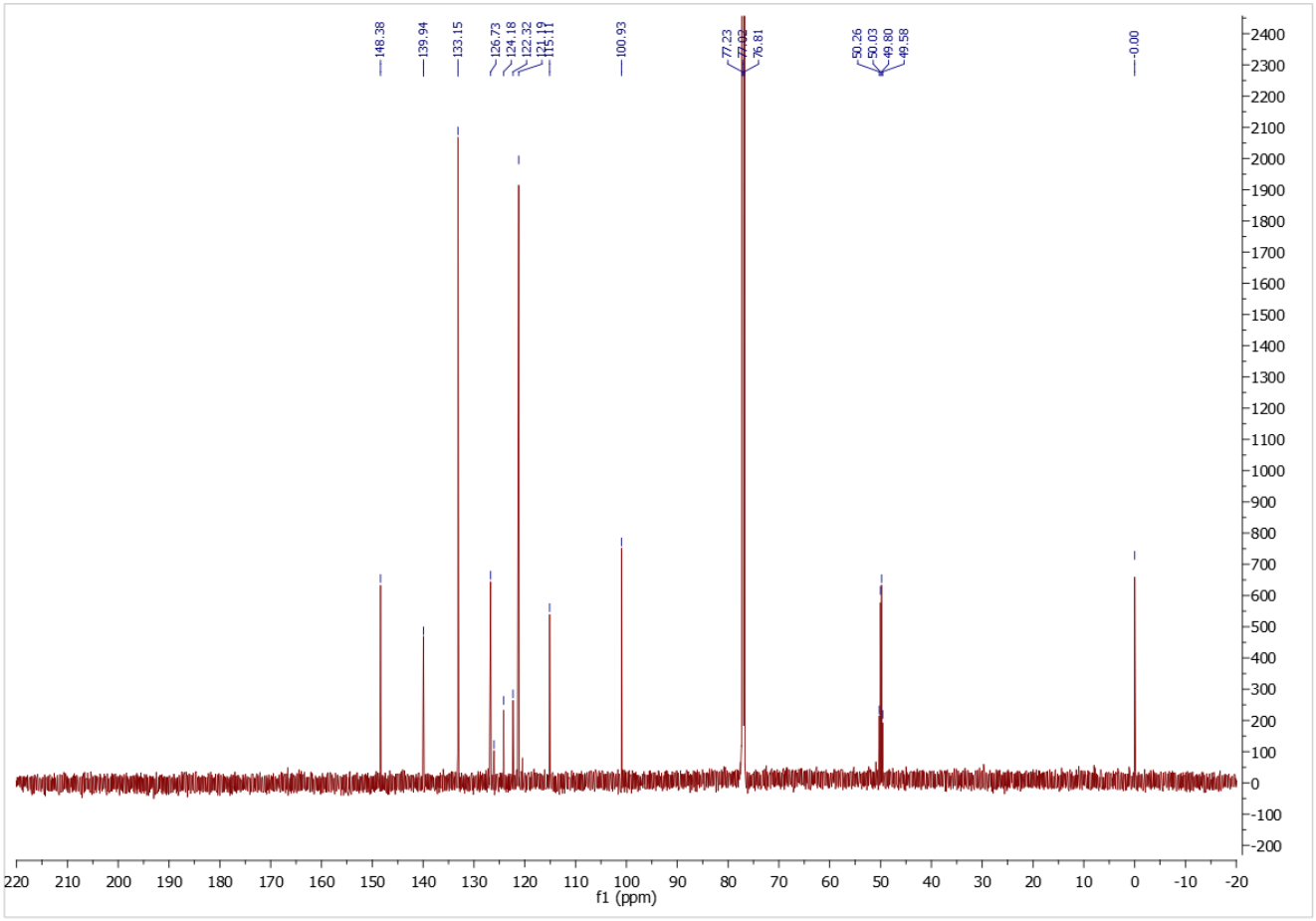


Figure 3.2.3.10 $^{13}$CNMR of 7-bromo-4-chloro-1-(2,2,2-trifluoroethyl)-1H-indazol-3-amine (**B2.4**) in $CDCl_3$

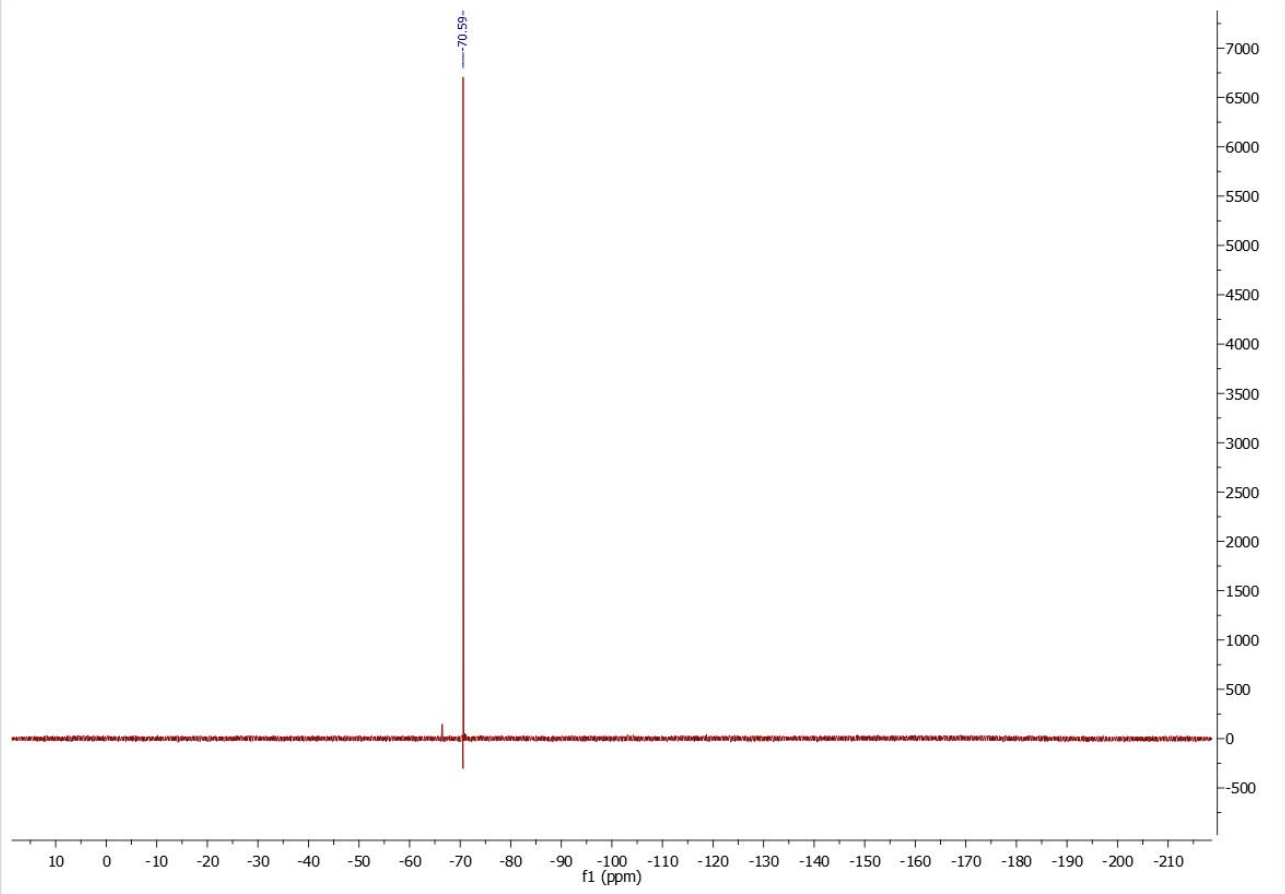


Figure 3.2.3.11 $^{19}$FNMR of 7-bromo-4-chloro-1-(2,2,2-trifluoroethyl)-1H-indazol-3-amine (**B2.4**) in $CDCl_3$

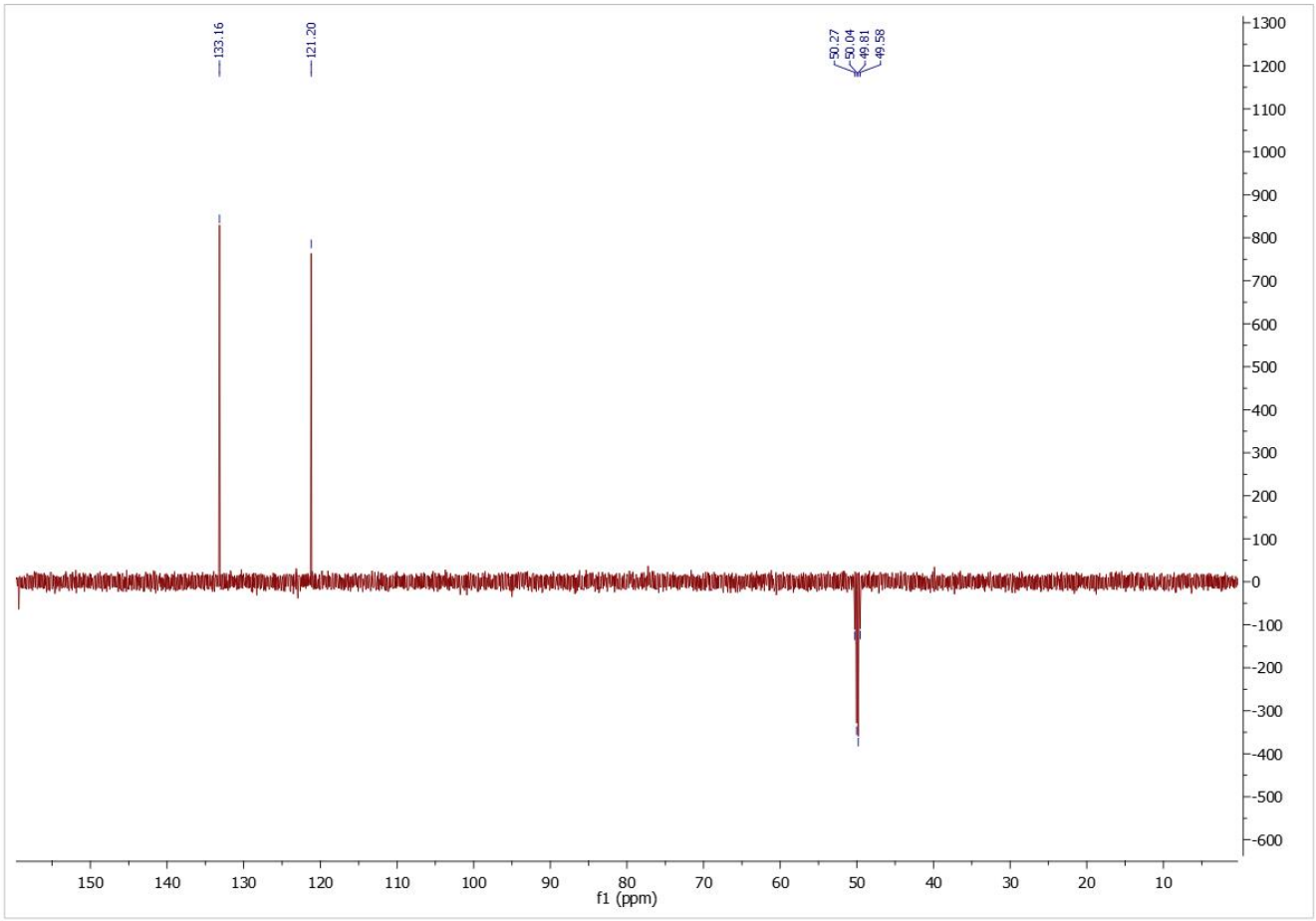


Figure 3.2.3.12 DEPT-135 of 7-bromo-4-chloro-1-(2,2,2-trifluoroethyl)-1H-indazol-3-amine (**B2.4**) in $CDCl_3$

4-chloro-7-(4,4,5,5-tetramethyl-1,3,2-dioxaborolan-2-yl)-1-(2,2,2-trifluoroethyl)-N,N-bis(trimethylsilyl)-1H-indazol-3-amine (B2.4a)

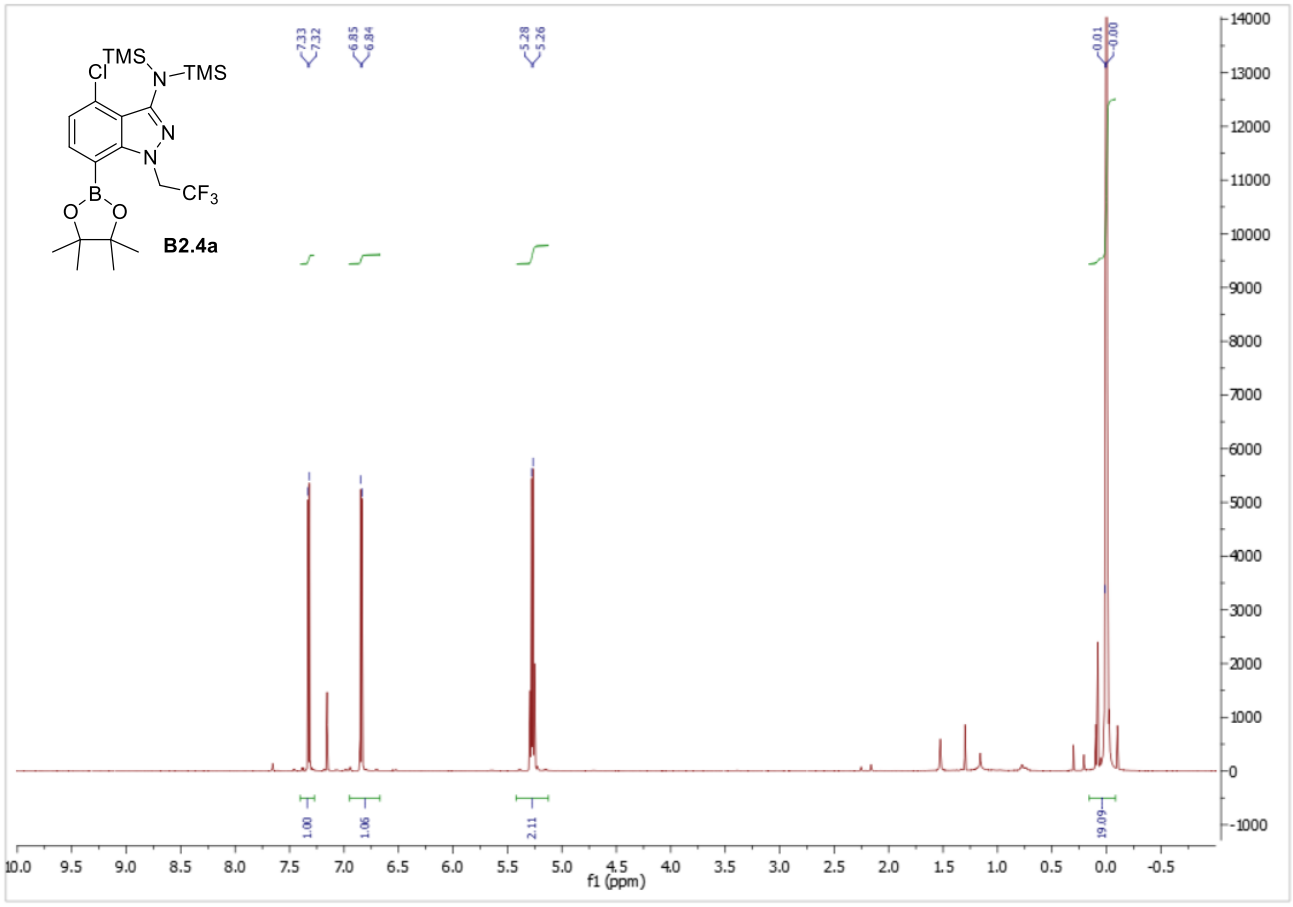


Figure 3.2.3.13 $^{1}$HNMR of 4-chloro-7-(4,4,5,5-tetramethyl-1,3,2-dioxaborolan-2-yl)-1-(2,2,2-trifluoroethyl)-N,N-bis(trimethylsilyl)-1H-indazol-3-amine (**B2.4a**) in $CDCl_3$.

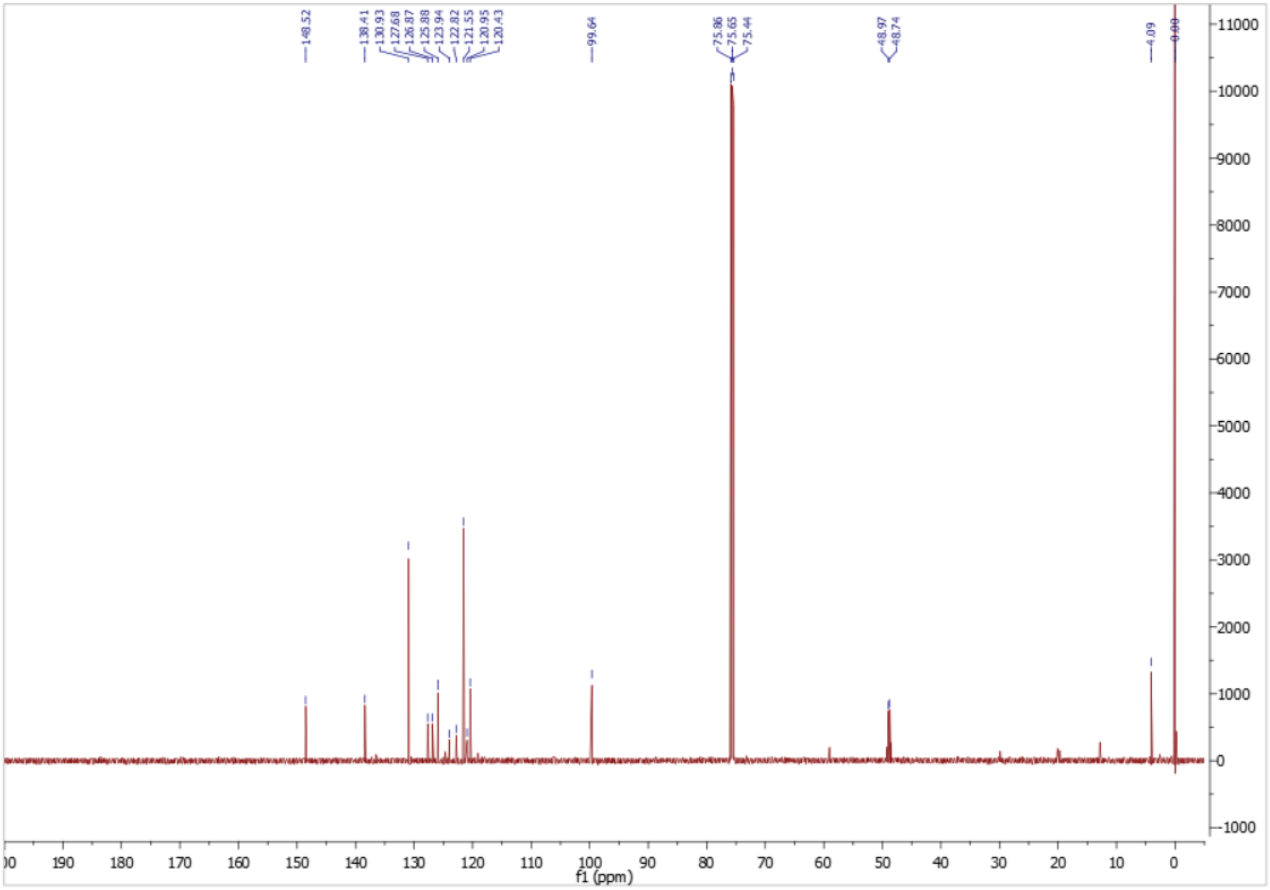


Figure 3.2.3.14 $^{13}$CNMR of 4-chloro-7-(4,4,5,5-tetramethyl-1,3,2-dioxaborolan-2-yl)-1-(2,2,2-trifluoroethyl)-N,N-bis(trimethylsilyl)-1H-indazol-3-amine (**B2.4a**) in $CDCl_3$.

4-chloro-7-(4,4,5,5-tetramethyl-1,3,2-dioxaborolan-2-yl)-1-(2,2,2-trifluoroethyl)-1H-indazol-3-amine (**Frag B**)

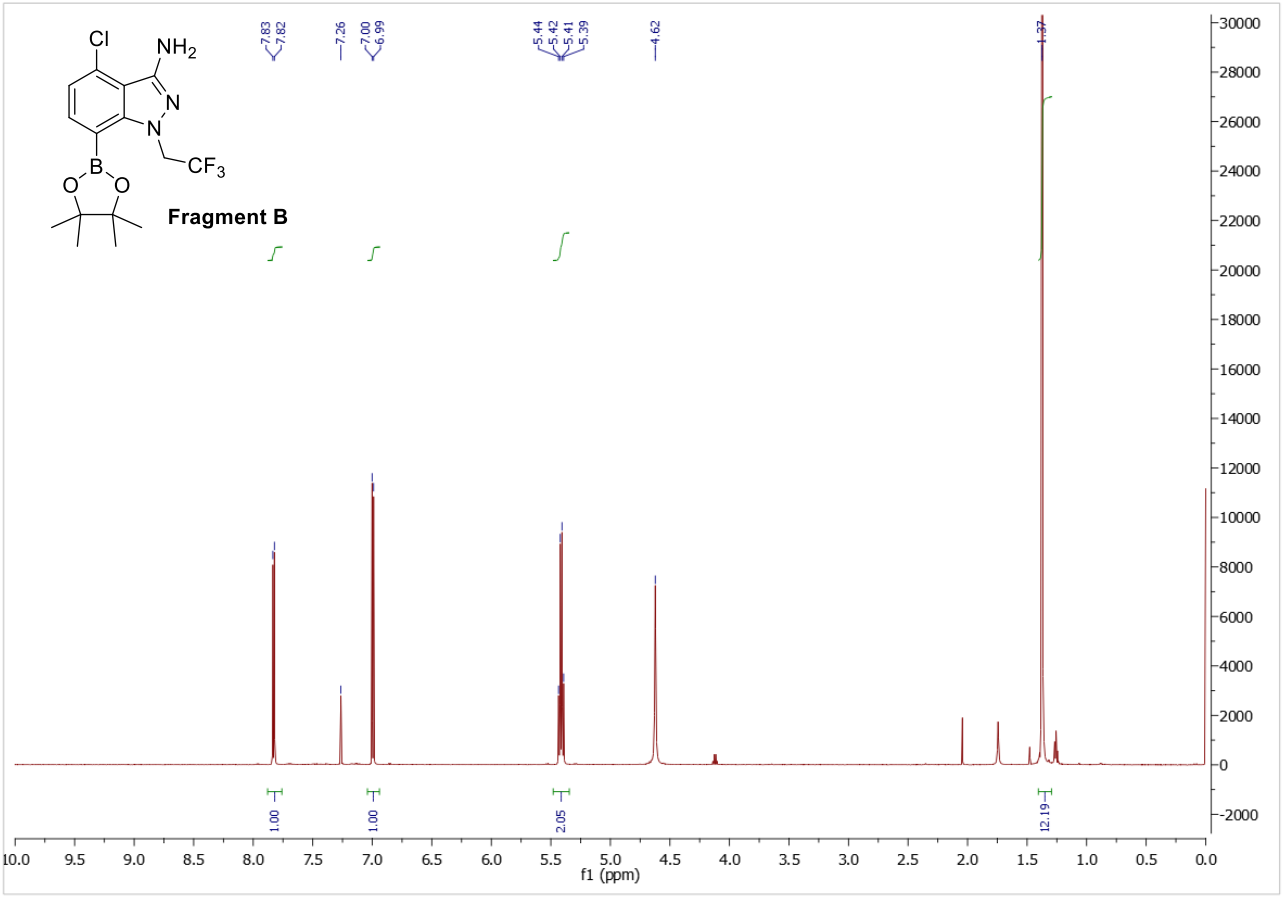


Figure 3.2.3.15 $^{1}$HNMR of 4-chloro-7-(4,4,5,5-tetramethyl-1,3,2-dioxaborolan-2-yl)-1-(2,2,2-trifluoroethyl)-1H-indazol-3-amine (**Frag B**) in $CDCl_3$.

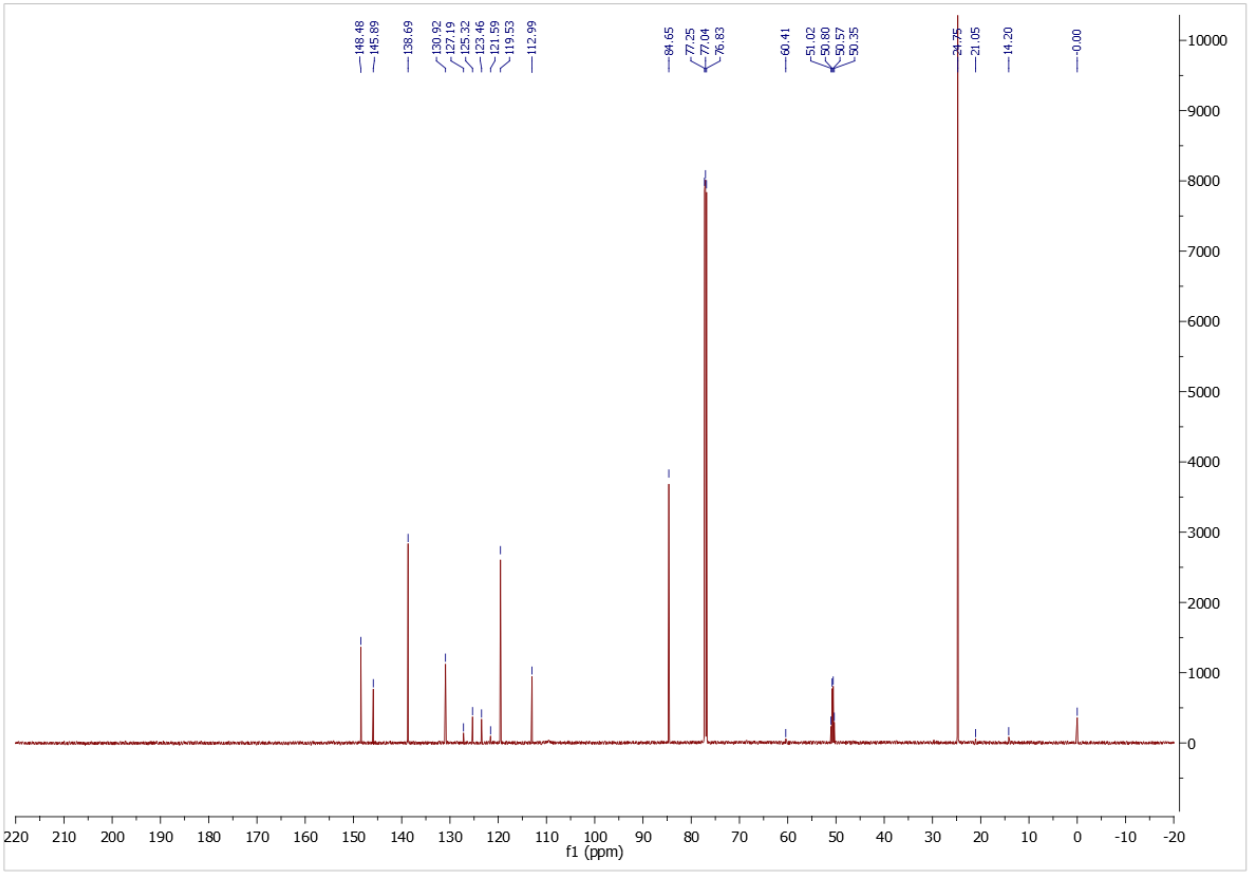


Figure 3.2.3.16 $^{13}$CNMR of 4-chloro-7-(4,4,5,5-tetramethyl-1,3,2-dioxaborolan-2-yl)-1-(2,2,2-trifluoroethyl)-1H-indazol-3-amine (**Frag B**) in $CDCl_3$.

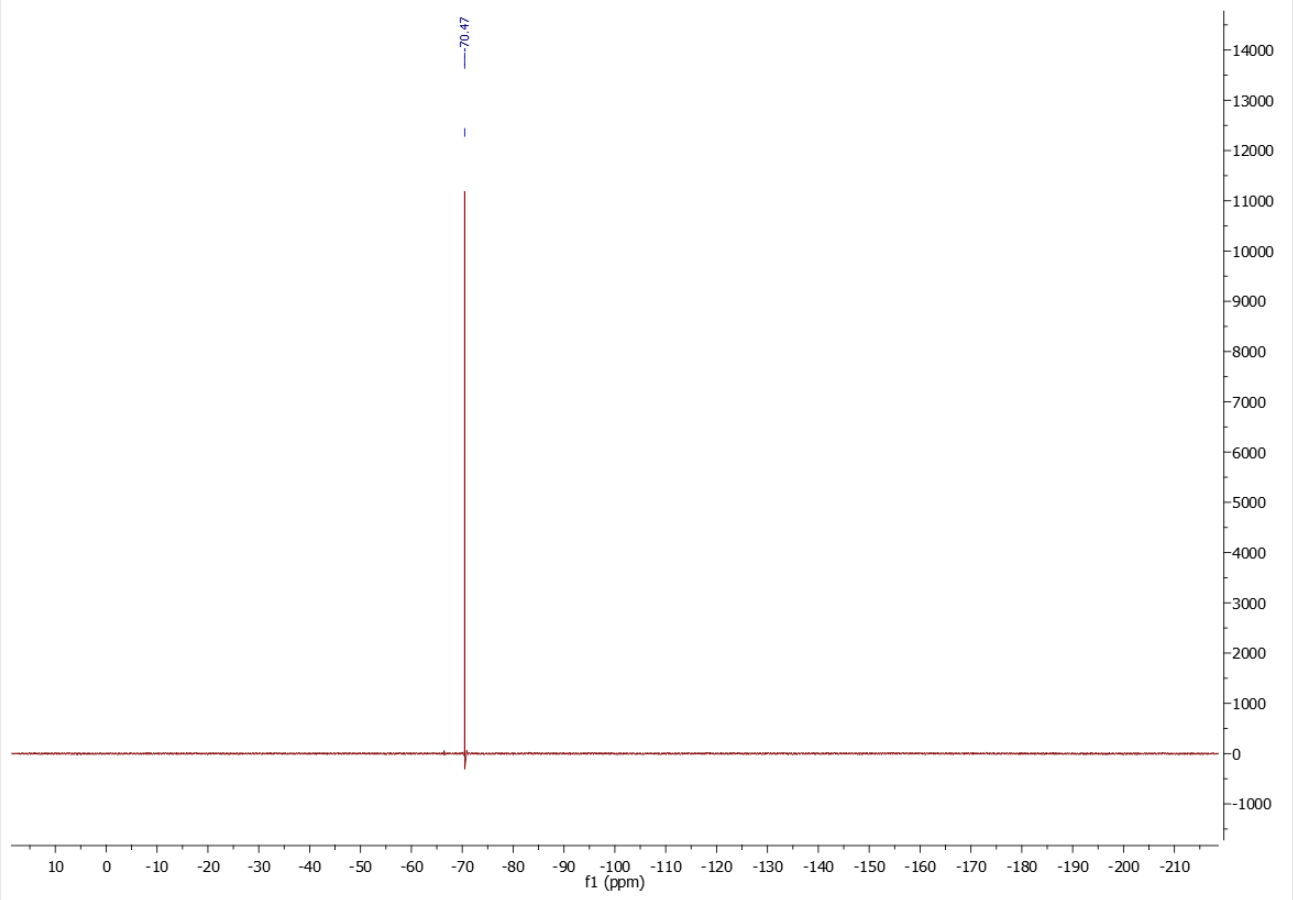


Figure 3.2.3.17 $^{19}$FNMR of 4-chloro-7-(4,4,5,5-tetramethyl-1,3,2-dioxaborolan-2-yl)-1-(2,2,2-trifluoroethyl)-1H-indazol-3-amine (**Frag B**) in $CDCl_3$.

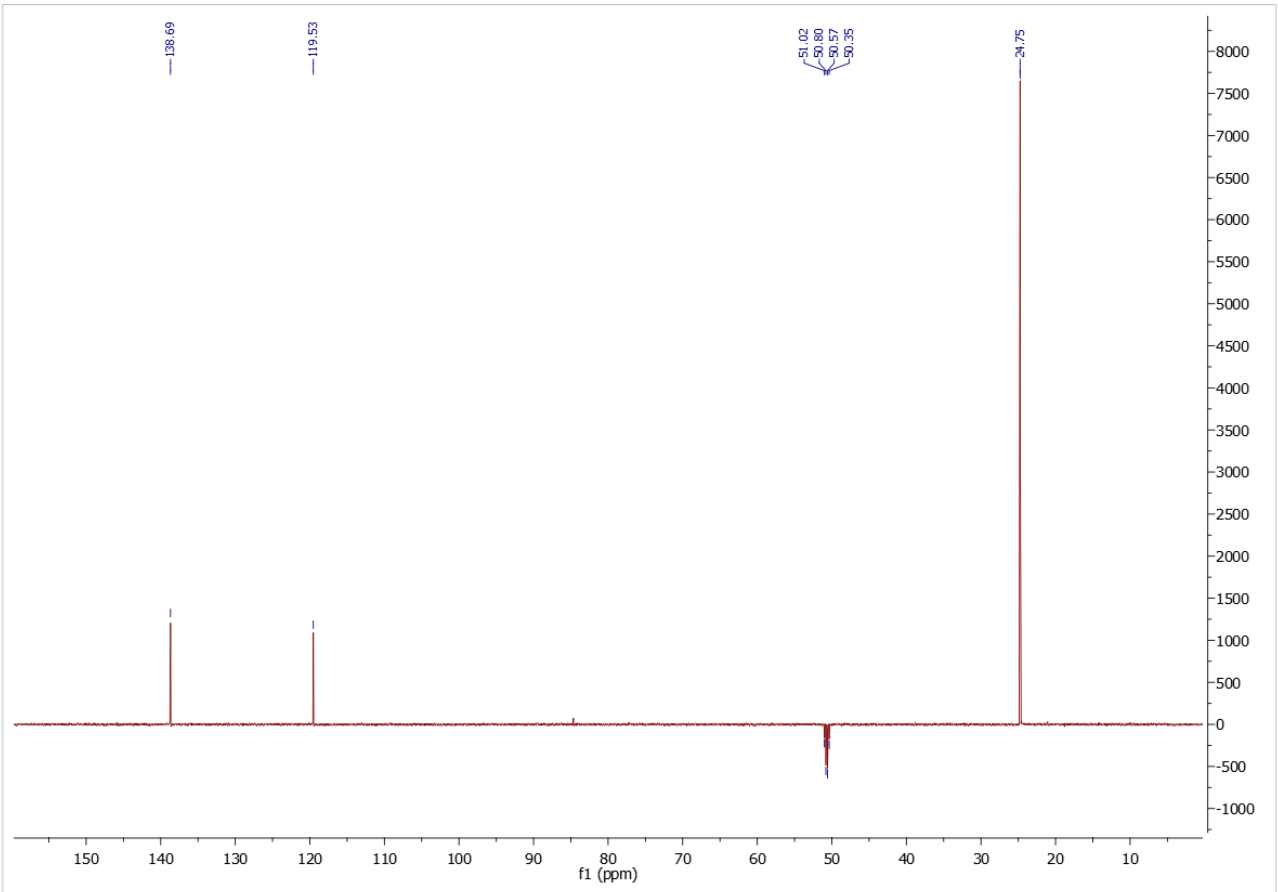


Figure 3.2.3.18 DEPT-135 of 4-chloro-7-(4,4,5,5-tetramethyl-1,3,2-dioxaborolan-2-yl)-1-(2,2,2-trifluoroethyl)-1H-indazol-3-amine (**Frag B**) in $CDCl_3$.

5-bromo-4-chloro-1H-indazol-3-amine (**B2.3a**)

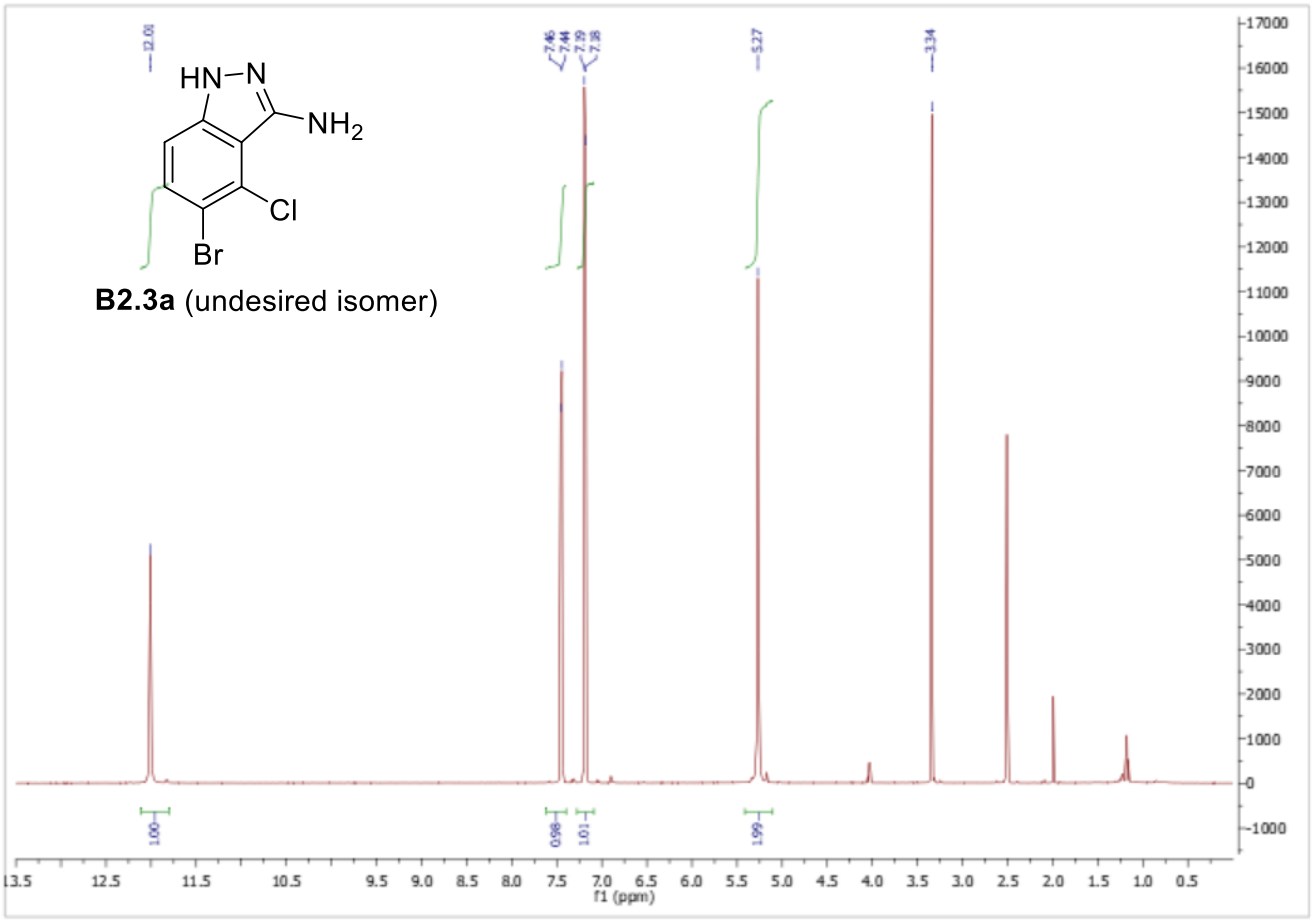


Figure 3.2.3.19 $^{1}$HNMR of 5-bromo-4-chloro-1H-indazole-3-amine (**B2.3a**) in DMSO-d6.

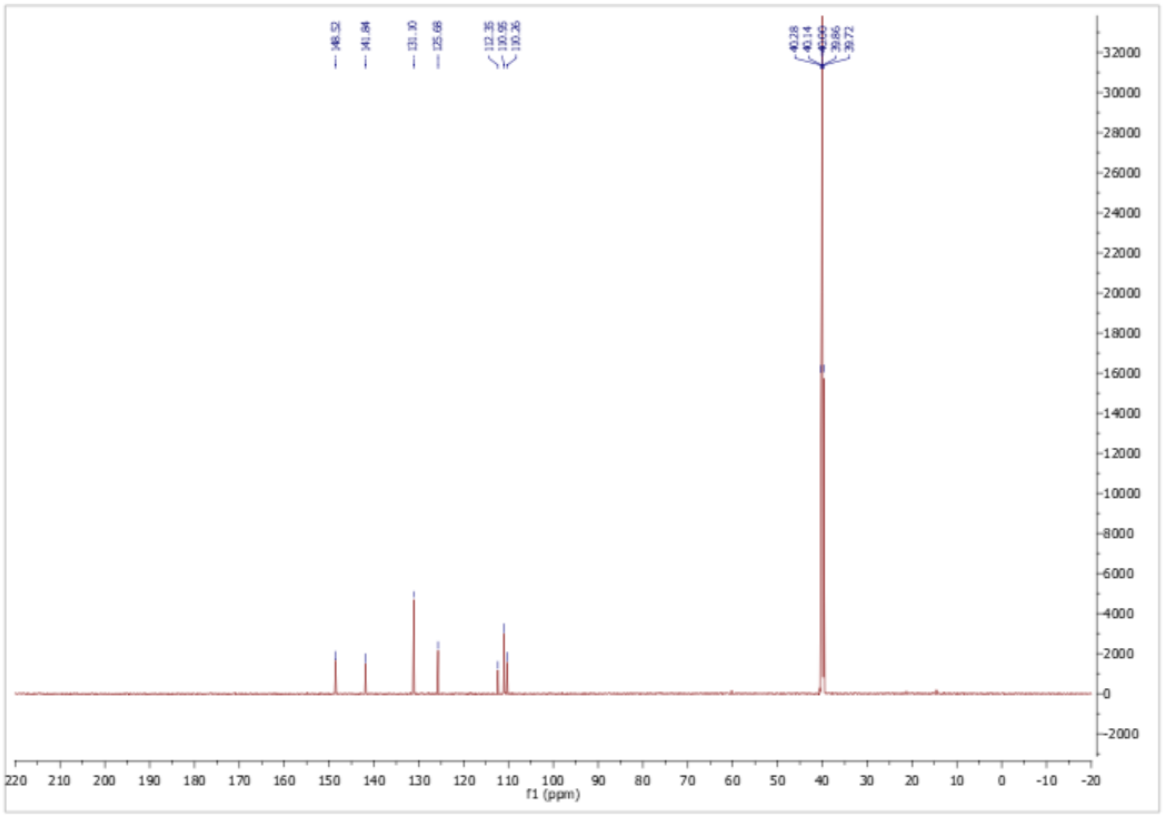


Figure 3.2.3.20 $^{13}$CNMR of 5-bromo-4-chloro-1H-indazole-3-amine (**B2.3a**) in DMSO-d6.

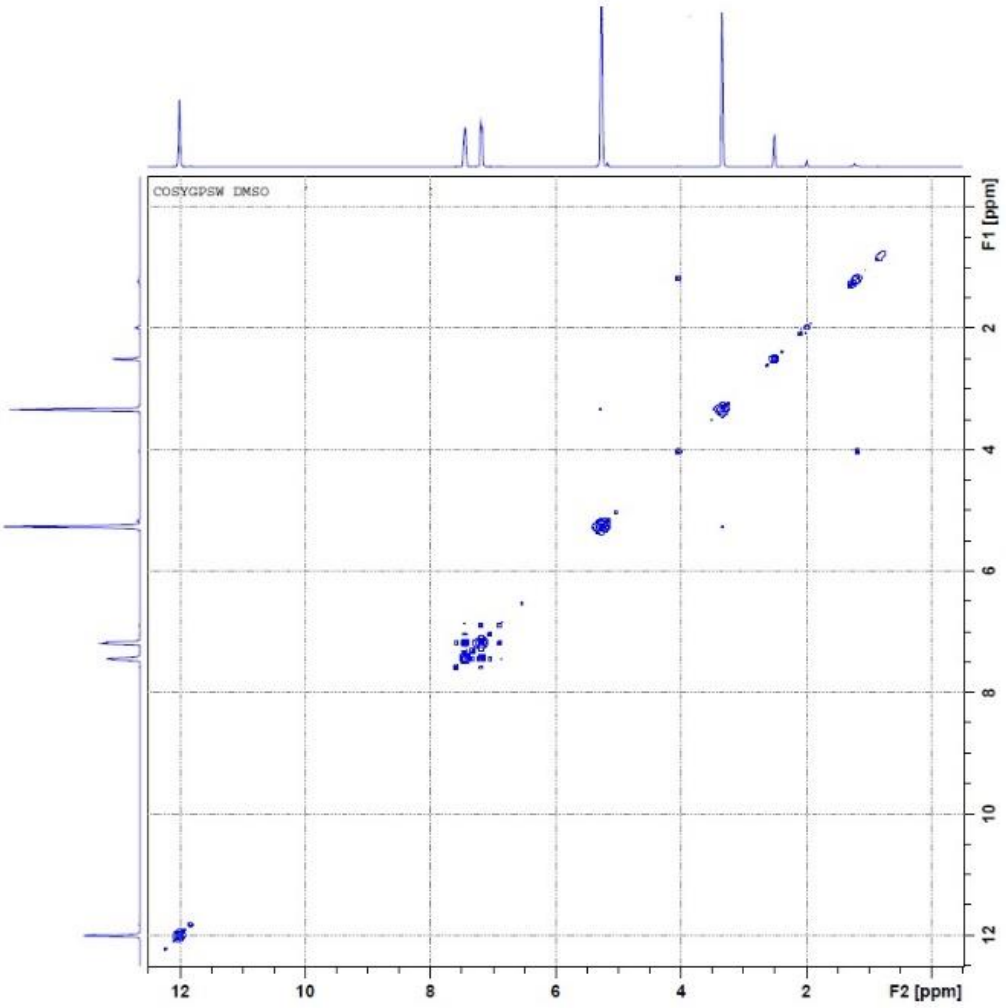


Figure 3.2.3.21 $^{1}$H-$^{1}$H COSY of 5-bromo-4-chloro-1H-indazole-3-amine (**B2.3a**) in DMSO-d6.

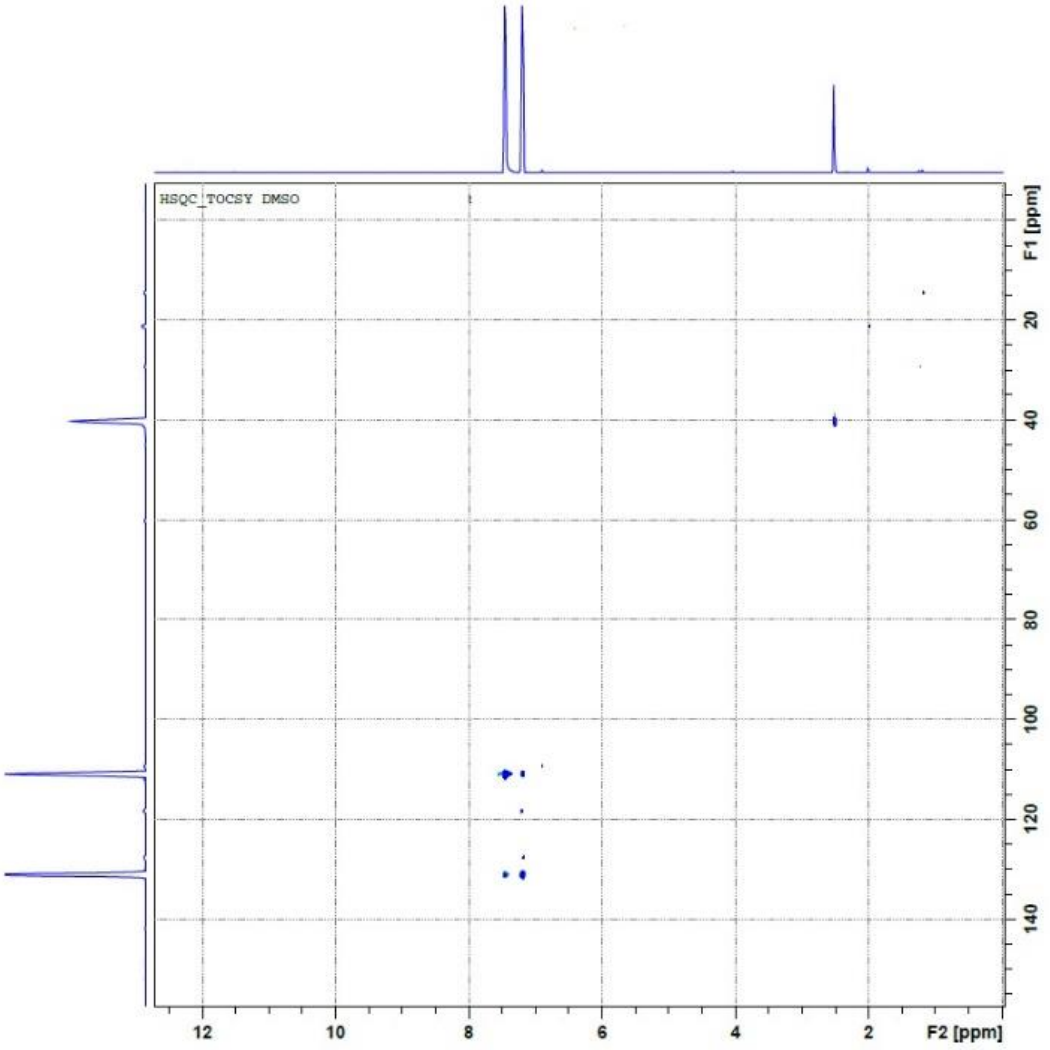


Figure 3.2.3.22 HSQC of 5-bromo-4-chloro-1H-indazole-3-amine (**B2.3a**) in DMSO-d6.

# 4. Appendix

## 4.1 Route scouting of LenB 1

LenB 1 is a three-step route and contains a late-stage C-H borylation as the key step. The proposed route as shown in Scheme 4.1.1.

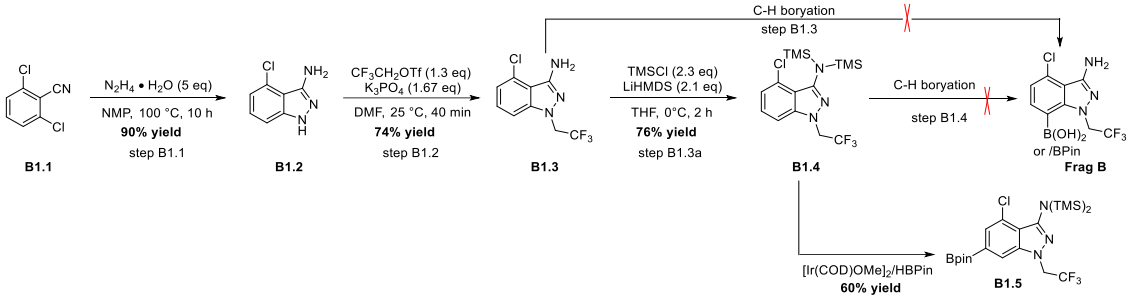


Scheme 4.1.1. Late-stage C-H borylation approach for synthesis of Frag B (LenB 1)

The key strategy of LenB 1 involved forming the 3-aminoindazole ring first and following the alkylation and a C-H borylation to afford the desired Frag B product. In accord with the literature, the 3-aminoindazole (**B1.2**) was prepared from condensation of **B1.1** with hydrazine hydrate in 90% of yield.[19] The subsequent alkylation proceeded smoothly with $CF_3CH_2OTf$ in the presence of $K_3PO_4$ and **B1.3** was obtained in 74% isolated yield. With **B1.3** in hand, direct borylation with organometallic reagents was investigated. Treating **B1.3** with different organolithium reagents, such as n-butyllithium (BuLi), lithium diisopropylamide (LDA), lithium bis(trimethylsilyl)amide (LiHMDS), TMPMgCl·LiCl or iPrMgCl·LiCl followed by treatment with $B(OMe)_3$, $B(OiPr)_3$ and iPrOBpin resulted in no desired borylation but de-fluorinated products were detected by GCMS and crude NMR. Assuming the free amino group in **B1.3** may cause issues for the C-H borylation, TMS protected amino **B1.4** was prepared by treating **B1.3** with 2.3 eq of TMSCl in the presence of 2.1 eq LiHMDS.[9] The resulting **B1.4** was then evaluated for the C-H borylation with the above-mentioned conditions. Unfortunately, all failed to yield desired product and resulted in a complex mixture of products (with organolithium reagents) or recovering the starting material (with organomagnesium reagents). Interestingly, treatment of **B1.4** with HBpin in the presence of 5 mol% $[Ir(COD)OMe]_2$ afforded a borylated product in 60% yield.[26] However, the product was the wrong regioisomer.[xv]

[xv] The structure was confirmed by $^1$HNMR and LCMS.

All the failed results indicated the challenges in the LenB 1 approach. Considering the limited timeline of the project, this approach was abandoned and our focus was shifted to LenB 2 (vide supra).

## 4.2 Acquisition Methods, Retention Times, Chromatograms, and MS Spectra

### 4.2.1 LenB 2 (GC-MS)

**Structures & IDs:**

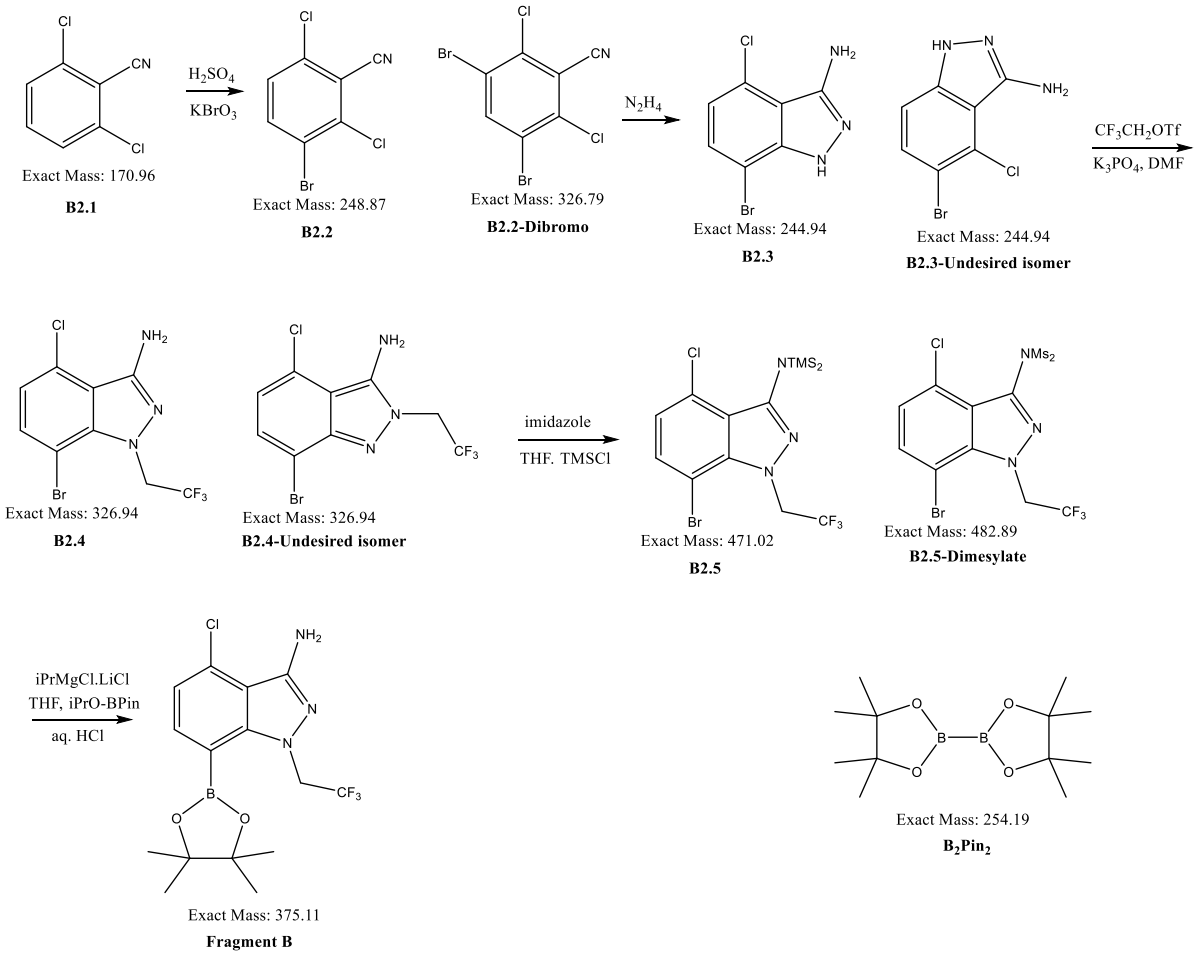


**Instrument Type:** Agilent 8890 gas chromatograph (GC) with a 5977 mass spectrometer detector (MSD)

**Conditions:**

Column: J&W HP-5ms GC Column, 30 m, 0.25 mm, 0.25 µm, 7 inch cage

Inlet Pressure: 11.747 psi | Split Ratio: 100:1 | Split Flow: 140 mL/min

Column flow: 1.4 mL/min | Injection Temp: 250ºC | Injection volume: 1 µL

Total Flow: 144.4 mL/min | Solvent Delay: 3 min | Runtime: 19 min

Temperature Program:

| Time (min) | Temp (˚C) | Ramp (˚C/min) | Hold (min) |
|---|---|---|---|
| 0 | 50 | - | 3 |
| - | 250 | 25 | 3 |
| - | 300 | 25 | 3 |

MS Parameters:

| | |
|---|---|
| Transfer Line Temp (˚C) | 250 |
| Source Temp (˚C) | 230 |
| Quad Temp (˚C) | 150 |
| Electron Energy (eV) | 70 |
| Mass Range | 40-1000 |

Sample preparation: Samples are prepared at ~1 mg/mL in acetonitrile

**Retention Times**

| **Compound** | ***m/z*** | **Time (min)** |
|---|---|---|
| B2.1 | 171 | 8.4 |
| $B_2pin_2$ | 239 | 8.7 |
| 4-Phenyl piperidine | 155 | 9.1 |
| B2.2 | 249 | 9.7 |
| B2.4 (Desired) | 327 (1 Br and 1 Cl) | 10.7 |
| Dibromo B2.2 | 327 (2 Br and 2 Cl) | 10.8 |
| B2.3 (Desired) | 245 | 11.1 |
| Undesired B2.4 | 327 (1 Br and 1 Cl) | 11.3 |
| B2.5 | 471 | 11.4 |
| Undesired B2.3 | 245 | 12.0 |
| **Frag B** | 375 | 12.9 |

| | | |
|---|---|---|
| Dimesylate B2.5 | 483 | 15.2 |

**Notes:** For any samples prepared in DMSO, increase solvent delay to 6 min as DMSO comes out around 4.5 minutes.

The B2.3 and B2.4 isomers have different solubilities between their desired and undesired forms so methanol should be avoided to prevent crashing out the undesired isomers.

**Representative Chromatograms**

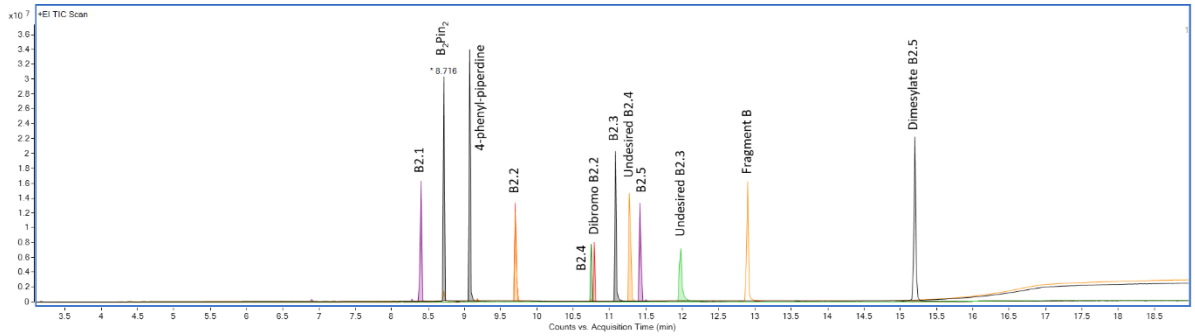


**Mass Spectra**

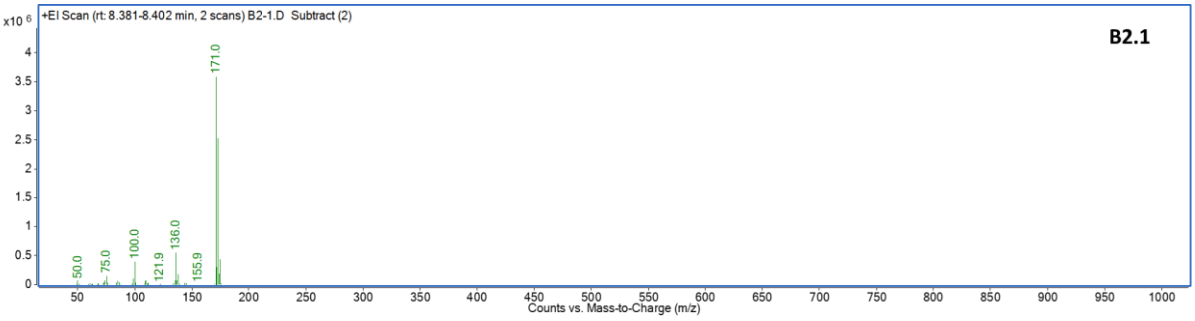


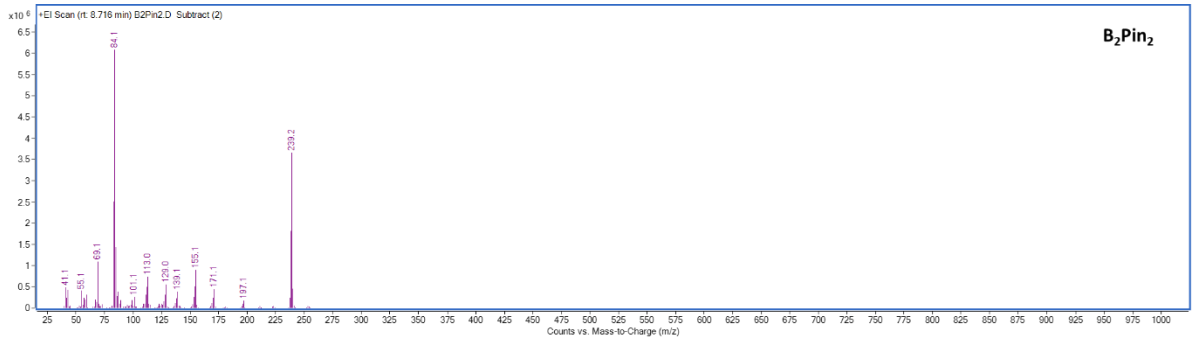

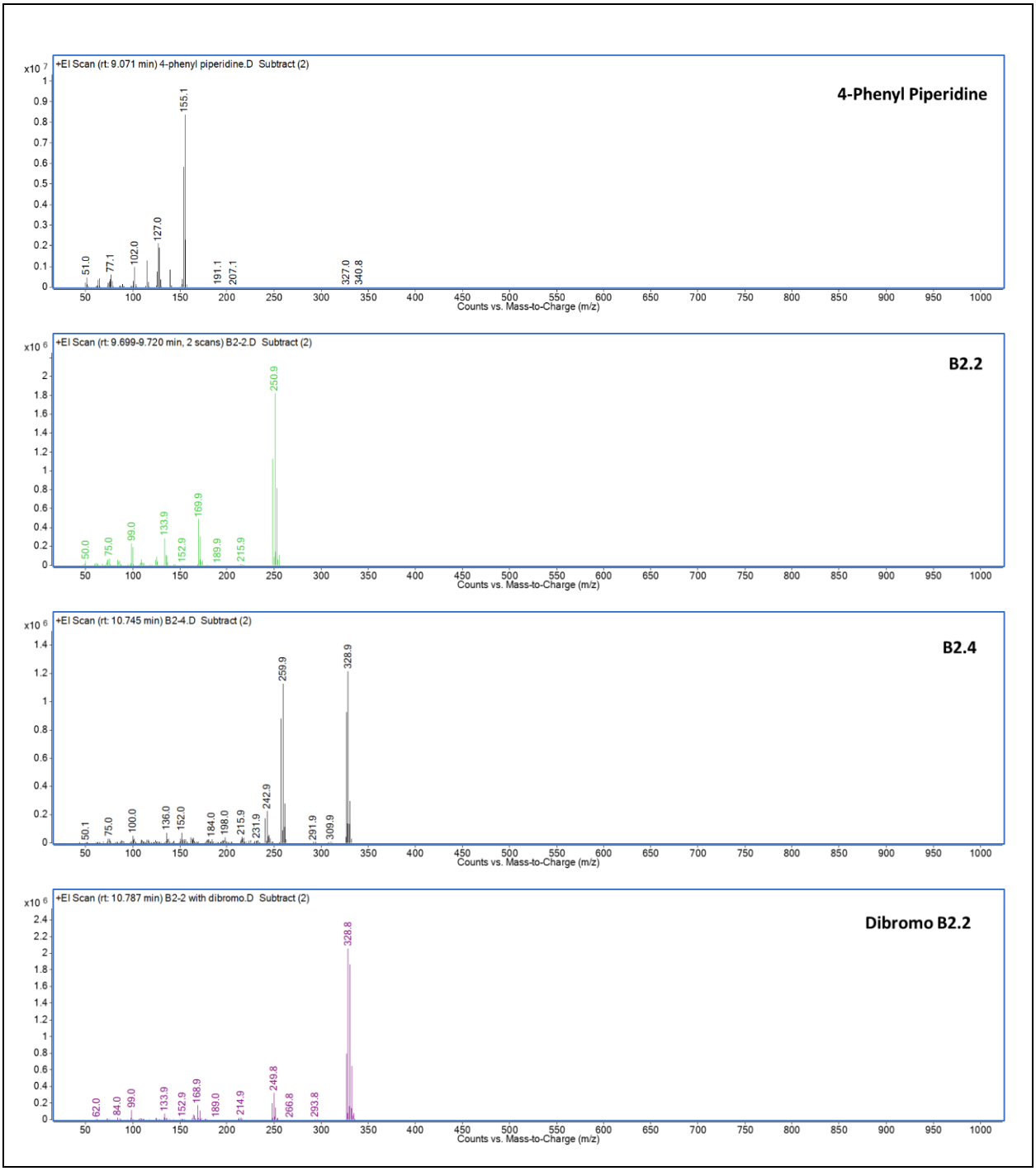
+EI Scan (rt: 9.071 min) 4-phenyl piperidine.D Subtract (2)
4-Phenyl Piperidine
+EI Scan (rt: 9.699-9.720 min, 2 scans) B2-2.D Subtract (2)
B2.2
+EI Scan (rt: 10.745 min) B2-4.D Subtract (2)
B2.4
+EI Scan (rt: 10.787 min) B2-2 with dibromo.D Subtract (2)
Dibromo B2.2
Counts vs. Mass-to-Charge (m/z)

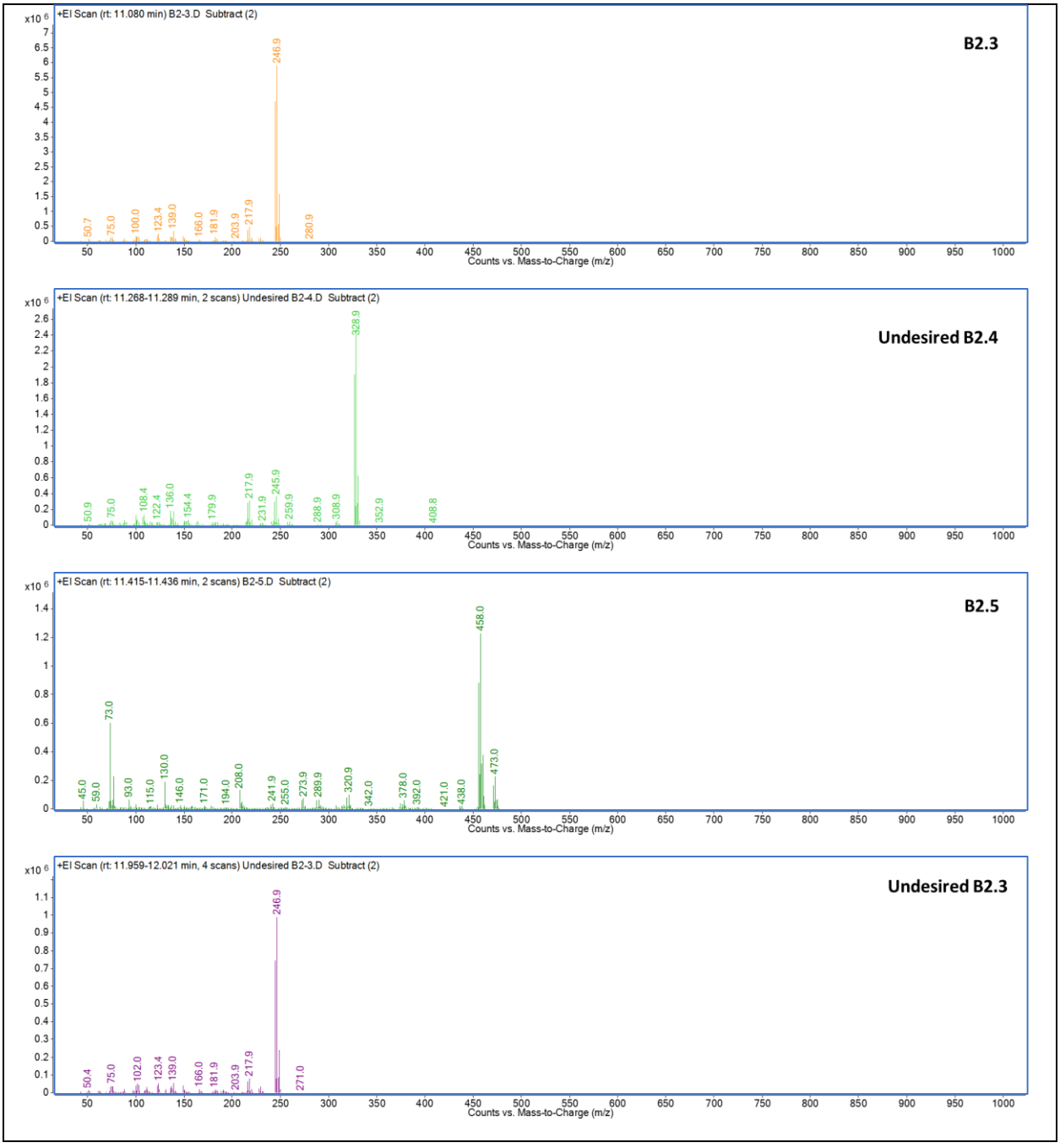
+EI Scan (rt: 11.080 min) B2-3.D Subtract (2)
B2.3
+EI Scan (rt: 11.268-11.289 min, 2 scans) Undesired B2-4.D Subtract (2)
Undesired B2.4
+EI Scan (rt: 11.415-11.436 min, 2 scans) B2-5.D Subtract (2)
B2.5
+EI Scan (rt: 11.959-12.021 min, 4 scans) Undesired B2-3.D Subtract (2)
Undesired B2.3
Counts vs. Mass-to-Charge (m/z)

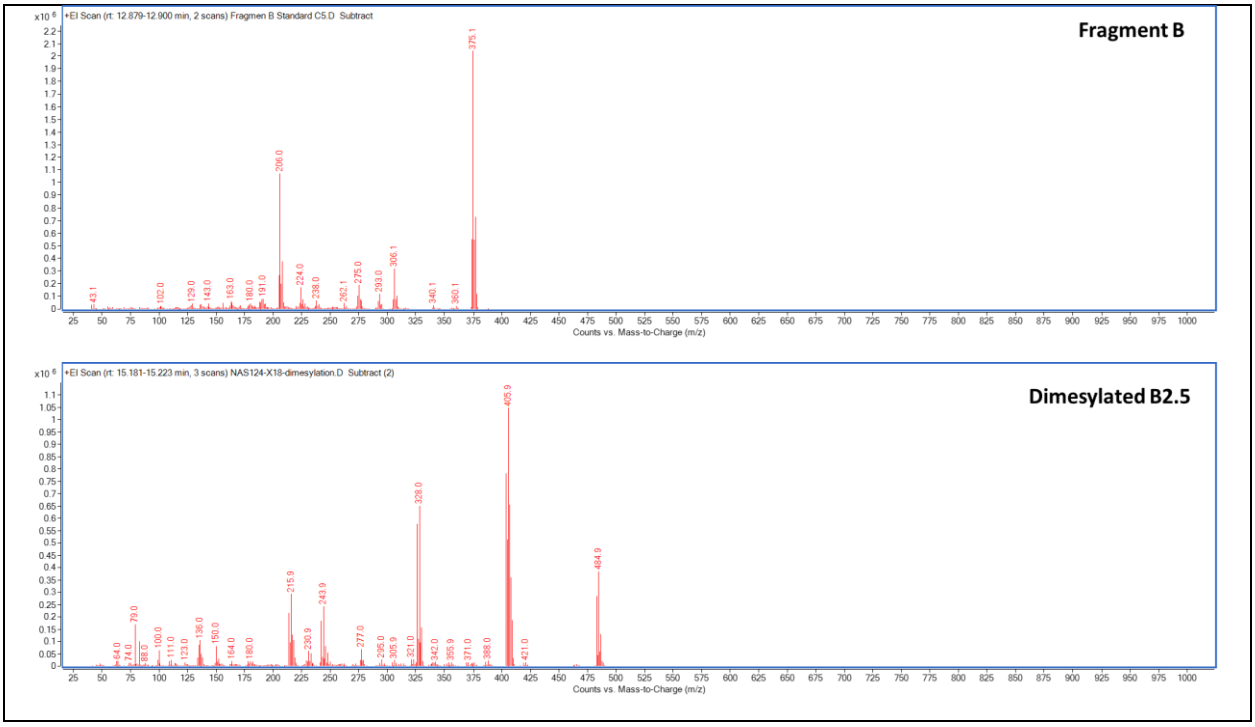


## 4.3 X-ray data of Frag B

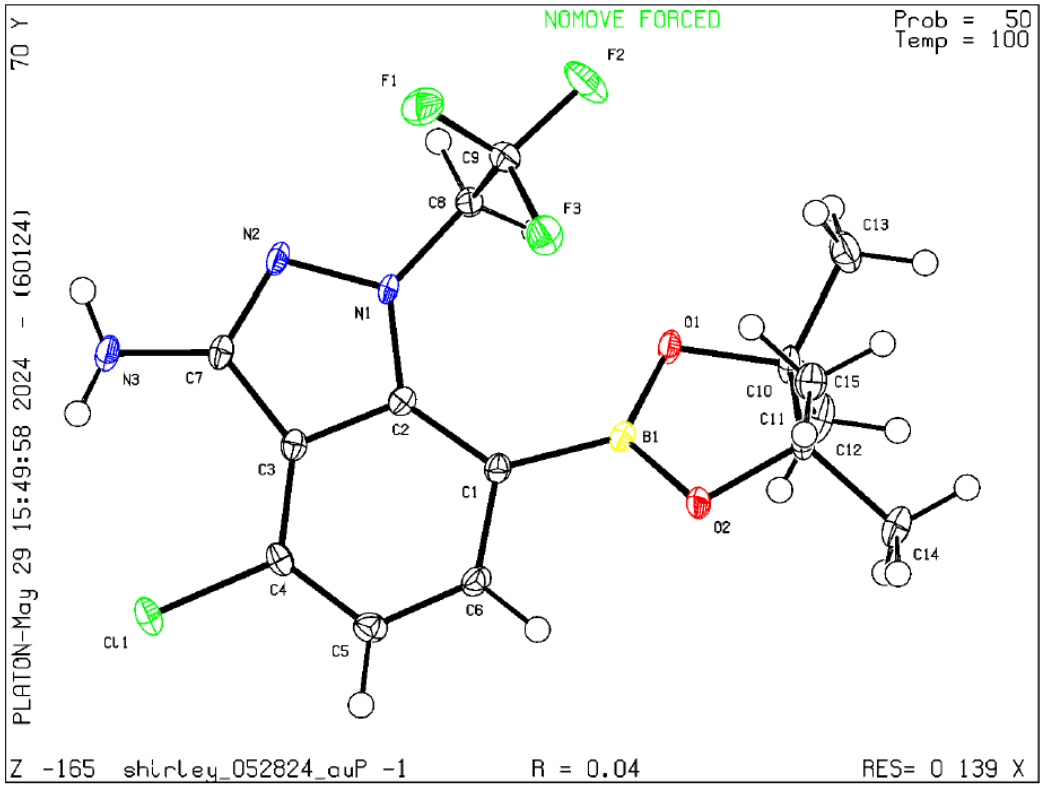


Figure 4.3.1 Single-crystal X-ray structure of **Frag B** with thermal ellipsoids drawn at 50% probability.

**Table 4.3.1** Fractional Atomic Coordinates (×10⁴) and Equivalent Isotropic Displacement Parameters (Å²×10³) for **Frag B**. $U_{eq}$ is defined as 1/3 of the trace of the orthogonalised $U_{ij}$.

| Atom | x | y | z | $U_{eq}$ |
|---|---|---|---|---|
| Cl1 | 3626.0(5) | 9142.1(5) | 1416.8(2) | 17.79(15) |
| F3 | 2888.0(14) | 11015.4(12) | -2868.3(6) | 20.9(2) |
| O2 | -603.8(16) | 6567.1(14) | -2765.1(7) | 14.5(2) |
| F1 | 4174.8(14) | 13738.4(13) | -2478.3(7) | 26.1(3) |
| F2 | 1781.0(17) | 13145.1(15) | -3531.1(6) | 29.7(3) |
| O1 | -1361.4(15) | 9331.7(14) | -2920.9(7) | 14.0(2) |
| N2 | 2872.0(18) | 13284.3(17) | -646.8(8) | 14.1(3) |
| N3 | 4250(2) | 13210.8(19) | 825.5(9) | 18.1(3) |
| N1 | 1797.9(18) | 12054.7(16) | -1290.0(8) | 12.2(3) |
| C11 | -1425(2) | 6635(2) | -3680.5(9) | 13.4(3) |

| Atom | x | y | z | $U_{eq}$ |
|---|---|---|---|---|
| C3 | 2487(2) | 10525(2) | -133.4(10) | 11.9(3) |
| C7 | 3278(2) | 12376(2) | 45.2(10) | 13.2(3) |
| C1 | 625(2) | 8700.1(19) | -1434.5(10) | 12.0(3) |
| C2 | 1544(2) | 10364.0(19) | -1008.9(10) | 11.2(3) |
| C9 | 2506(2) | 12647(2) | -2743.4(10) | 17.4(3) |
| C8 | 1141(2) | 12703.5(19) | -2121.8(10) | 14.1(3) |
| C5 | 1611(2) | 7355(2) | -44.3(10) | 15.2(3) |
| C14 | -2663(2) | 4842(2) | -3990.3(11) | 19.5(3) |
| C6 | 715(2) | 7241.6(19) | -915.3(10) | 14.1(3) |
| B1 | -453(2) | 8238(2) | -2386.2(11) | 12.2(3) |
| C4 | 2495(2) | 8993(2) | 340.5(9) | 12.6(3) |
| C10 | -2506(2) | 8218(2) | -3664.3(10) | 14.9(3) |
| C12 | -4485(2) | 7681(2) | -3442.0(12) | 23.9(4) |
| C15 | 231(2) | 7013(2) | -4172.9(10) | 17.4(3) |
| C13 | -2565(3) | 9309(2) | -4461.5(11) | 22.9(4) |

**Table 4.3.2** Anisotropic Displacement Parameters (×$10^4$) **Frag B**. The anisotropic displacement factor exponent takes the form: $-2\pi^2[h^2a^{*2} \times U_{11} + \ldots + 2hka^* \times b^* \times U_{12}]$

| Atom | $U_{11}$ | $U_{22}$ | $U_{33}$ | $U_{23}$ | $U_{13}$ | $U_{12}$ |
|---|---|---|---|---|---|---|
| Cl1 | 20.0(2) | 23.0(2) | 9.6(2) | 0.03(14) | -1.07(14) | 5.47(15) |
| F3 | 25.5(5) | 19.7(5) | 19.1(5) | -2.6(4) | 3.5(4) | 9.4(4) |
| O2 | 20.1(6) | 12.3(5) | 9.7(5) | -2.3(4) | -1.0(4) | 2.9(4) |
| F1 | 25.0(5) | 23.4(5) | 27.6(5) | 2.9(4) | 8.0(4) | -4.9(4) |
| F2 | 42.7(7) | 35.9(6) | 13.6(5) | 8.7(4) | 3.0(4) | 16.8(5) |
| O1 | 15.1(5) | 12.2(5) | 12.5(5) | -4.2(4) | -2.8(4) | 2.4(4) |
| N2 | 15.4(6) | 11.9(6) | 12.7(6) | -5.2(5) | 0.3(5) | -1.2(5) |
| N3 | 20.2(7) | 16.7(7) | 13.2(7) | -4.4(5) | -0.4(5) | -3.5(6) |
| N1 | 16.3(6) | 8.5(6) | 9.4(6) | -3.1(4) | -1.0(5) | -0.5(5) |
| C11 | 14.7(7) | 14.3(7) | 10.1(7) | -2.9(5) | -0.7(6) | 2.3(6) |
| C3 | 11.1(7) | 13.4(7) | 11.1(7) | -2.2(5) | 2.9(5) | 2.0(5) |
| C7 | 12.0(7) | 14.4(7) | 12.1(7) | -4.4(5) | 2.2(6) | 0.6(6) |
| C1 | 13.3(7) | 11.3(7) | 11.4(7) | -1.5(5) | 2.3(6) | 2.6(5) |
| C2 | 11.0(7) | 10.8(7) | 12.5(7) | -1.0(5) | 3.3(6) | 2.9(5) |
| C9 | 23.1(8) | 14.5(7) | 13.6(7) | 1.9(6) | -0.1(6) | 4.0(6) |
| C8 | 17.2(8) | 11.0(7) | 13.1(7) | -0.3(5) | -1.2(6) | 4.1(6) |
| C5 | 18.8(8) | 13.5(7) | 15.0(7) | 1.8(6) | 4.7(6) | 5.7(6) |
| C14 | 19.4(8) | 17.2(8) | 19.6(8) | -7.4(6) | 1.7(6) | -0.3(6) |
| C6 | 17.0(8) | 10.1(7) | 15.2(7) | -1.8(5) | 3.4(6) | 2.1(6) |
| B1 | 12.3(8) | 10.7(7) | 12.4(8) | -2.2(6) | 1.3(6) | 0.1(6) |

| Atom | $U_{11}$ | $U_{22}$ | $U_{33}$ | $U_{23}$ | $U_{13}$ | $U_{12}$ |
|---|---|---|---|---|---|---|
| C4 | 12.0(7) | 17.3(7) | 9.3(7) | 0.1(6) | 1.7(5) | 5.3(6) |
| C10 | 13.8(8) | 16.0(7) | 12.5(7) | -5.9(6) | -2.8(6) | 2.4(6) |
| C12 | 14.4(8) | 27.2(9) | 28.1(9) | -11.8(7) | 1.8(7) | 2.3(7) |
| C15 | 17.1(8) | 18.9(7) | 16.3(8) | -2.6(6) | 3.0(6) | 3.9(6) |
| C13 | 28.4(9) | 23.7(8) | 15.9(8) | -1.5(6) | -4.4(7) | 11.1(7) |

**Table 4.3.3** Bond Lengths in Å for **Frag B**.

| Atom | Atom | Length/Å |
|---|---|---|
| Cl1 | C4 | 1.7339(15) |
| F3 | C9 | 1.3432(18) |
| O2 | C11 | 1.4596(17) |
| O2 | B1 | 1.3745(19) |
| F1 | C9 | 1.3402(19) |
| F2 | C9 | 1.3460(18) |
| O1 | B1 | 1.370(2) |
| O1 | C10 | 1.4633(17) |
| N2 | N1 | 1.3903d(17) |
| N2 | C7 | 1.319(2) |
| N3 | C7 | 1.380(2) |
| N1 | C2 | 1.3670(19) |
| N1 | C8 | 1.4381(19) |
| C11 | C14 | 1.519(2) |
| C11 | C10 | 1.559(2) |
| C11 | C15 | 1.526(2) |
| C3 | C7 | 1.432(2) |
| C3 | C2 | 1.415(2) |
| C3 | C4 | 1.402(2) |
| C1 | C2 | 1.420(2) |
| C1 | C6 | 1.399(2) |
| C1 | B1 | 1.560(2) |
| C9 | C8 | 1.508(2) |
| C5 | C6 | 1.399(2) |
| C5 | C4 | 1.375(2) |
| C10 | C12 | 1.526(2) |
| C10 | C13 | 1.514(2) |

**Table 4.3.4** Bond Angles in ° for **Frag B**.

| Atom | Atom | Atom | Angle/° |
|---|---|---|---|
| B1 | O2 | C11 | 106.85(11) |
| B1 | O1 | C10 | 107.10(11) |
| C7 | N2 | N1 | 106.13(12) |

| Atom | Atom | Atom | Angle/° |
|---|---|---|---|
| N2 | N1 | C8 | 117.75(12) |
| C2 | N1 | N2 | 112.09(12) |
| C2 | N1 | C8 | 130.16(12) |
| O2 | C11 | C14 | 108.63(12) |
| O2 | C11 | C10 | 102.32(11) |
| O2 | C11 | C15 | 106.69(12) |
| C14 | C11 | C10 | 115.23(13) |
| C14 | C11 | C15 | 110.39(12) |
| C15 | C11 | C10 | 112.84(13) |
| C2 | C3 | C7 | 105.85(13) |
| C4 | C3 | C7 | 135.07(14) |
| C4 | C3 | C2 | 119.06(13) |
| N2 | C7 | N3 | 121.45(14) |
| N2 | C7 | C3 | 110.67(13) |
| N3 | C7 | C3 | 127.78(14) |
| C2 | C1 | B1 | 130.44(13) |
| C6 | C1 | C2 | 114.54(13) |
| C6 | C1 | B1 | 115.01(13) |
| N1 | C2 | C3 | 105.25(12) |
| N1 | C2 | C1 | 132.20(14) |
| C3 | C2 | C1 | 122.54(13) |
| F3 | C9 | F2 | 106.45(12) |
| F3 | C9 | C8 | 113.08(13) |
| F1 | C9 | F3 | 106.78(13) |
| F1 | C9 | F2 | 106.91(13) |
| F1 | C9 | C8 | 112.70(13) |
| F2 | C9 | C8 | 110.52(14) |
| N1 | C8 | C9 | 112.34(13) |
| C4 | C5 | C6 | 119.06(14) |
| C1 | C6 | C5 | 124.45(14) |
| O2 | B1 | C1 | 120.14(14) |
| O1 | B1 | O2 | 112.89(13) |
| O1 | B1 | C1 | 126.96(13) |
| C3 | C4 | Cl1 | 120.32(12) |
| C5 | C4 | Cl1 | 119.34(12) |
| C5 | C4 | C3 | 120.34(14) |
| O1 | C10 | C11 | 101.73(11) |
| O1 | C10 | C12 | 106.31(12) |
| O1 | C10 | C13 | 108.49(12) |
| C12 | C10 | C11 | 113.27(13) |
| C13 | C10 | C11 | 115.26(13) |
| C13 | C10 | C12 | 110.88(14) |

**Table 4.3.5** Torsion Angles in ° for **Frag B**.

| Atom | Atom | Atom | Atom | Angle/° |
|---|---|---|---|---|
| F3 | C9 | C8 | N1 | 56.48(17) |
| O2 | C11 | C10 | O1 | 29.54(13) |

| Atom | Atom | Atom | Atom | Angle/° |
|---|---|---|---|---|
| O2 | C11 | C10 | C12 | -84.14(14) |
| O2 | C11 | C10 | C13 | 146.68(13) |
| F1 | C9 | C8 | N1 | -64.75(16) |
| F2 | C9 | C8 | N1 | 175.69(12) |
| N2 | N1 | C2 | C3 | 0.81(16) |
| N2 | N1 | C2 | C1 | -177.47(15) |
| N2 | N1 | C8 | C9 | 91.60(15) |
| N1 | N2 | C7 | N3 | -176.30(13) |
| N1 | N2 | C7 | C3 | 0.44(16) |
| C11 | O2 | B1 | O1 | 9.66(17) |
| C11 | O2 | B1 | C1 | -171.74(13) |
| C7 | N2 | N1 | C2 | -0.80(17) |
| C7 | N2 | N1 | C8 | 179.36(13) |
| C7 | C3 | C2 | N1 | -0.51(16) |
| C7 | C3 | C2 | C1 | 177.98(13) |
| C7 | C3 | C4 | Cl1 | 1.7(2) |
| C7 | C3 | C4 | C5 | -178.11(16) |
| C2 | N1 | C8 | C9 | -88.20(19) |
| C2 | C3 | C7 | N2 | 0.04(17) |
| C2 | C3 | C7 | N3 | 176.52(15) |
| C2 | C3 | C4 | Cl1 | -179.66(11) |
| C2 | C3 | C4 | C5 | 0.6(2) |
| C2 | C1 | C6 | C5 | 0.4(2) |
| C2 | C1 | B1 | O2 | 155.01(15) |
| C2 | C1 | B1 | O1 | -26.6(3) |
| C8 | N1 | C2 | C3 | -179.37(14) |
| C8 | N1 | C2 | C1 | 2.3(3) |
| C14 | C11 | C10 | O1 | 147.21(13) |
| C14 | C11 | C10 | C12 | 33.53(18) |
| C14 | C11 | C10 | C13 | -95.65(16) |
| C6 | C1 | C2 | N1 | 178.61(15) |
| C6 | C1 | C2 | C3 | 0.6(2) |
| C6 | C1 | B1 | O2 | -24.6(2) |
| C6 | C1 | B1 | O1 | 153.81(15) |
| C6 | C5 | C4 | Cl1 | -179.45(11) |
| C6 | C5 | C4 | C3 | 0.3(2) |
| B1 | O2 | C11 | C14 | -146.58(13) |
| B1 | O2 | C11 | C10 | -24.29(14) |
| B1 | O2 | C11 | C15 | 94.41(14) |
| B1 | O1 | C10 | C11 | -24.84(14) |

| Atom | Atom | Atom | Atom | Angle/° |
|---|---|---|---|---|
| B1 | O1 | C10 | C12 | 93.92(15) |
| B1 | O1 | C10 | C13 | -146.78(13) |
| | | | | |
| B1 | C1 | C2 | N1 | -1.0(3) |
| B1 | C1 | C2 | C3 | -179.01(14) |
| | | | | |
| B1 | C1 | C6 | C5 | -179.97(14) |
| | | | | |
| C4 | C3 | C7 | N2 | 178.84(16) |
| C4 | C3 | C7 | N3 | -4.7(3) |
| C4 | C3 | C2 | N1 | -179.54(13) |
| | | | | |
| C4 | C3 | C2 | C1 | -1.0(2) |
| C4 | C5 | C6 | C1 | -0.8(2) |
| C10 | O1 | B1 | O2 | 10.80(17) |
| C10 | O1 | B1 | C1 | -167.68(14) |
| | | | | |
| C15 | C11 | C10 | O1 | -84.73(14) |
| C15 | C11 | C10 | C12 | 161.59(13) |
| C15 | C11 | C10 | C13 | 32.41(18) |

**Table 4.3.6** Hydrogen Fractional Atomic Coordinates (×10⁴) and Equivalent Isotropic Displacement Parameters (Å²×10³) for **Frag B**. $U_{eq}$ is defined as 1/3 of the trace of the orthogonalised $U_{ij}$.

| Atom | x | y | z | $U_{eq}$ |
|---|---|---|---|---|
| H3A | 4920.87 | 14175.15 | 731.26 | 27 |
| H8A | 959.89 | 13944.44 | -2038.6 | 17 |
| H8B | -105.07 | 11974.25 | -2378.88 | 17 |
| H5 | 1608.84 | 6315.14 | 276.61 | 18 |
| H14A | -1870.48 | 3927.76 | -3964.19 | 29 |
| H14B | -3303.26 | 4898.44 | -4590.89 | 29 |
| H14C | -3612.67 | 4542.66 | -3615.65 | 29 |
| H6 | 127.31 | 6096.5 | -1171.49 | 17 |
| H12A | -4410.16 | 6991.07 | -2920.56 | 36 |
| H12B | -5319.59 | 6955.05 | -3929.43 | 36 |
| H12C | -4994.71 | 8750.94 | -3333.25 | 36 |
| H15A | 1001.12 | 8182.77 | -3974.76 | 26 |
| H15B | -259.12 | 7001.52 | -4797.66 | 26 |
| H15C | 1013.92 | 6096.83 | -4062.58 | 26 |
| H13A | -3262.39 | 10271.47 | -4391.82 | 34 |
| H13B | -3202.95 | 8544.4 | -4976.94 | 34 |
| H13C | -1267.87 | 9815.97 | -4531.68 | 34 |
| H3B | 4810(30) | 12470(30) | 1177(16) | 30(6) |

| Atom | x | y | z | $U_{eq}$ |
|---|---|---|---|---|

## 4.4 Acronyms

| | |
|---|---|
| AIDS | acquired immunodeficiency syndrome |
| API | active pharmaceutical ingredient |
| ART | antiretroviral therapy |
| ARVs | antiretroviral medications |
| $B_2pin_2$ | bis(pinacolato)diboron |
| BMGF | Bill and Melinda Gates Foundation |
| $CF_3CH_2OMs$ | 2,2,2-trifluoroethyl methanesulfonate |
| $CF_3CH_2OTf$ | 2,2,2-trifluoroethyl trifluoromethanesulfonate |
| $CF_3CH_2OTs$ | 2,2,2-trifluoroethyl 4-methylbenzenesulfonate |
| DCM | dichloromethane |
| DIPEA | N,N-diisopropylethylamine |
| DMF | dimethylformamide |
| DMSO | dimethyl sulfoxide |
| EtOAc | ethyl acetate |
| EtOH | ethyl alcohol |
| FDA | United Stated Food & Drug Administration |
| Frag B | 4-chloro-7-(4,4,5,5-tetramethyl-1,3,2-dioxaborolan-2-yl)-1-(2,2,2-trifluoroethyl)-1H-indazol-3-amine |
| GC-MS TIC | gas chromatography mass spectrometry total ion chromatogram |
| HIV | human immunodeficiency virus |
| IPA | isopropyl alcohol |
| iPrMgCl·LiC | l-isopropylmagnesium chloride lithium chloride complex |
| iPrOAc | isopropyl acetate |
| iPrOBpin | 2-isopropoxy-4,4,5,5-tetramethyl-1,3,2-dioxaborolane |
| LC-DAD | liquid chromatography with a diode-array detector |
| LDA | lithium diisopropylamide |
| LiHMDS | lithium hexamethyldisilazide (lithium bis(trimethylsilyl)amide) |
| M4ALL | Medicines for All Institute |
| MDR HIV | multidrug-resistant HIV |
| 2-MeTHF | 2-methyltetrahydrofuran |
| NaOAc | sodium acetate |
| NBS | N-bromosuccinimide |

| | |
|---|---|
| NMP | N-methyl-2-pyrrolidone |
| OPT | scale-up optimization |
| PDR | process development report |
| PrEP | pre-exposure prophylaxis |
| qNMR | quantitative Nuclear Magnetic Resonance |
| RMC | raw material cost |
| $S_NAr$ | nucleophilic aromatic substitution |
| SRS | synthetic route scouting |
| TC | treatment cost |
| TE | techno-economic |
| THF | tetrahydrofuran |
| TMSCl | trimethylsilyl chloride |
| WHO | World Health Organization |

## 5. Acknowledgements

This work was supported by funding from the Bill & Melinda Gates Foundation (BMGF). The Medicines for All Institute (M4ALL) would like to express our gratitude to Dr. Trevor Laird, Dr. John Dillon, Dr. Ryan Nelson (BMGF) and Dr. Mark Krook for their helpful technical guidance throughout this project as well as Silpa Sundaram (BMGF), Dr. Susan Hershenson (BMGF), Dr. John Walker (BMGF) and Scott Rosenblum (BMGF) for the ongoing collaboration and support of the M4ALL mission. The authors are grateful to Dr. Saeed Ahmad and his team for the great efforts on TE analysis. We also would like to thank Dr. B. Frank Gupton, Dr. Douglas Klumpp, Dr. G. Michael Laidlaw, Dr. Charles Shanahan, Michael Osberg, Sarah Cox, for their inputs in this work.

## 6. References

(1) Chun, H. M.; Dirlikov, E.; Cox, M. H.; Sherlock, M. W.; Obeng-Aduasare, Y.; Sato, K.; Voetsch, A. C.; Ater, A. D.; Romano, E. R.; Tomlinson, H.; Modi, S.; Achrekar, A.; Nkengasong, J.; CDC Global HIV Working Group; CDC Global HIV Working Group; Agolory, S.; Amann, J.; Baack, B.; Behel, S.; Date, A.; Hanson, J.; Killam, W. P.; Patel, H.; Patel, S.; Pati, R.; Porter, L.; Warner, A.; Wuhib, T.; Zeh, C.; Faria E Silva Santelli, A. C.; Guevara, G.; Morales, R. E.; Ekra, A. K.; Kitenge, F.; Bonilla, L.; Mazibuko, S.; Damena, T.; Joseph, P.; Upadhyaya, S.;

Aitmagambetova, I.; Mwangi, J.; Usmanova, N.; Xaymounvong, D.; Asiimwe, M.; Alice, M.; Masamha, G. J.; Mutandi, G.; Odafe, S.; Romel, L.; Musoni, C.; Mogashoa, M.; Bolo, A.; Nabidzhonov, A.; Mgomella, G.; Lolekha, R.; Alamo-Talisuna, S.; Podolchak, N.; Nguyen, C. K.; Quaye, S.; Mwila, A.; Nyika, P. *Vital Signs* : Progress Toward Eliminating HIV as a Global Public Health Threat Through Scale-Up of Antiretroviral Therapy and Health System Strengthening Supported by the U.S. President's Emergency Plan for AIDS Relief — Worldwide, 2004–2022. *MMWR Morb. Mortal. Wkly. Rep.* **2023**, *72* (12), 317–324. https://doi.org/10.15585/mmwr.mm7212e1.

(2) Phillips, A. N.; Venter, F.; Havlir, D.; Pozniak, A.; Kuritzkes, D.; Wensing, A.; Lundgren, J. D.; De Luca, A.; Pillay, D.; Mellors, J.; Cambiano, V.; Bansi-Matharu, L.; Nakagawa, F.; Kalua, T.; Jahn, A.; Apollo, T.; Mugurungi, O.; Clayden, P.; Gupta, R. K.; Barnabas, R.; Revill, P.; Cohn, J.; Bertagnolio, S.; Calmy, A. Risks and Benefits of Dolutegravir-Based Antiretroviral Drug Regimens in Sub-Saharan Africa: A Modelling Study. *Lancet HIV* **2019**, *6* (2), e116–e127. https://doi.org/10.1016/S2352-3018(18)30317-5.

(3) Margot, N. A.; Naik, V.; VanderVeen, L.; Anoshchenko, O.; Singh, R.; Dvory-Sobol, H.; Rhee, M. S.; Callebaut, C. Resistance Analyses in Highly Treatment-Experienced People With Human Immunodeficiency Virus (HIV) Treated With the Novel Capsid HIV Inhibitor Lenacapavir. *J. Infect. Dis.* **2022**, *226* (11), 1985–1991. https://doi.org/10.1093/infdis/jiac364.

(4) Dvory-Sobol, H.; Shaik, N.; Callebaut, C.; Rhee, M. S. Lenacapavir: A First-in-Class HIV-1 Capsid Inhibitor. *Curr. Opin. HIV AIDS* **2022**, *17* (1), 15–21. https://doi.org/10.1097/COH.0000000000000713.

(5) Bester, S. M.; Wei, G.; Zhao, H.; Adu-Ampratwum, D.; Iqbal, N.; Courouble, V. V.; Francis, A. C.; Annamalai, A. S.; Singh, P. K.; Shkriabai, N.; Van Blerkom, P.; Morrison, J.; Poeschla, E. M.; Engelman, A. N.; Melikyan, G. B.; Griffin, P. R.; Fuchs, J. R.; Asturias, F. J.; Kvaratskhelia, M. Structural and Mechanistic Bases for a Potent HIV-1 Capsid Inhibitor. *Science* **2020**, *370* (6514), 360–364. https://doi.org/10.1126/science.abb4808.

(6) Zhang, J.-Y.; Wang, Y.-T.; Sun, L.; Wang, S.-Q.; Chen, Z.-S. Synthesis and Clinical Application of New Drugs Approved by FDA in 2022. *Mol. Biomed.* **2023**, *4* (1), 26. https://doi.org/10.1186/s43556-023-00138-y.

(7) Zhuang, S.; Torbett, B. E. Interactions of HIV-1 Capsid with Host Factors and Their Implications for Developing Novel Therapeutics. *Viruses* **2021**, *13* (3), 417. https://doi.org/10.3390/v13030417.

(8) Margot, N.; Ram, R.; Rhee, M.; Callebaut, C. Absence of Lenacapavir (GS-6207) Phenotypic Resistance in HIV Gag Cleavage Site Mutants and in Isolates with Resistance to Existing Drug Classes. *Antimicrob. Agents Chemother.* **2021**, *65* (3), e02057-20. https://doi.org/10.1128/AAC.02057-20.

(9) Guinle, M. I. B. A New Way to Prevent HIV Delivers Dramatic Results in Trial. *NPR*. July 3, 2024. https://www.npr.org/sections/goats-and-soda/2024/07/03/g-s1-7988/hiv-prevention-drug-clinical-trial (accessed 2024-07-23).

(10) *Gilead's Twice-Yearly Lenacapavir Demonstrated 100% Efficacy and Superiority to Daily Truvada® for HIV Prevention*. https://www.gilead.com/news-and-press/press-room/press-releases/2024/6/gileads-twiceyearly-lenacapavir-demonstrated-100-efficacy-and-superiority-to-daily-truvada-for-hiv-prevention (accessed 2024-07-23).

(11) *Gilead to Highlight Landmark Progress in Research Across HIV Prevention, Treatment and Cure Programs at AIDS 2024*. https://www.gilead.com/news-and-press/press-room/press-releases/2024/7/gilead-to-highlight-landmark-progress-in-research-across-hiv-prevention-treatment-and-cure-programs-at-aids-2024 (accessed 2024-07-23).

(12) Allan, K. M.; Batten, A. L.; Brizgys, G.; Dhar, S.; Doxsee, I. J.; Goldberg, A.; Heumann, L. V.; Huang, Z.; Kadunce, N. T.; Kazerani, S.; Lew, W.; Ngo, V. X.; O'keefe, B. M.; Rainey, T. J.; Roberts, B. J.; Shi, B.; Steinhuebel, D. P.; Tse, W. C.; Wagner, A. M.; Wang, X.; Wolckenhauer, S. A.; Wong, C. Y.; Zhang, J. R. Methods and Intermediates for Preparing a Therapeutic Compound Useful in the Treatment of Retroviridae Viral Infection. WO2019161280A1, August 22, 2019.

(13) BAUER, L. E.; GORMAN, E. M.; MULATO, A. S.; RHEE, M. S.; Rowe, C. W.; Sellers, S. P.; Stefanidis, D.; Tse, W. C.; Yant, S. R.; Chiu, A. Capsid Inhibitors for the Treatment of Hiv. WO2020018459A1, January 23, 2020. https://patents.google.com/patent/WO2020018459A1/en?oq=WO%C2%A02020018459 (accessed 2021-02-17).

(14) Graupe, M.; Henry, S. J.; Link, J. O.; Rowe, C. W.; Saito, R. D.; Schroeder, S. D.; Stefanidis, D.; Tse, W. C.; Zhang, J. R. Therapeutic Compounds Useful for the Prophylactic or Therapeutic Treatment of an Hiv Virus Infection. WO2018035359A1, February 22, 2018.

(15) Du, Z.; Farand, J.; Guney, T.; Kato, D.; Link, J. O.; Mack, J. B. C.; Mun, D.; Watkins, W. J.; Zhang, J. R. Therapeutic Compounds for HIV Infection Cross Reference to Related Applications. WO 2023/102529 A1.

(16) Link, J. O.; Rhee, M. S.; Tse, W. C.; Zheng, J.; Somoza, J. R.; Rowe, W.; Begley, R.; Chiu, A.; Mulato, A.; Hansen, D.; Singer, E.; Tsai, L. K.; Bam, R. A.; Chou, C.-H.; Canales, E.; Brizgys, G.; Zhang, J. R.; Li, J.; Graupe, M.; Morganelli, P.; Liu, Q.; Wu, Q.; Halcomb, R. L.; Saito, R. D.; Schroeder, S. D.; Lazerwith, S. E.; Bondy, S.; Jin, D.; Hung, M.; Novikov, N.; Liu, X.; Villaseñor, A. G.; Cannizzaro, C. E.; Hu, E. Y.; Anderson, R. L.; Appleby, T. C.; Lu, B.; Mwangi, J.; Liclican, A.; Niedziela-Majka, A.; Papalia, G. A.; Wong, M. H.; Leavitt, S. A.; Xu, Y.; Koditek, D.; Stepan, G. J.; Yu, H.; Pagratis, N.; Clancy, S.; Ahmadyar, S.; Cai, T. Z.; Sellers, S.; Wolckenhauer, S. A.; Ling, J.; Callebaut, C.; Margot, N.; Ram, R. R.; Liu, Y.-P.; Hyland, R.; Sinclair, G. I.; Ruane, P. J.; Crofoot, G. E.; McDonald, C. K.; Brainard, D. M.; Lad, L.; Swaminathan, S.; Sundquist, W. I.; Sakowicz, R.; Chester, A. E.; Lee, W. E.; Daar, E. S.; Yant, S. R.; Cihlar, T. Clinical Targeting of HIV Capsid Protein with a Long-Acting Small Molecule. *Nature* **2020**, *584* (7822), 614–618. https://doi.org/10.1038/s41586-020-2443-1.

(17) Gillis, E. P.; Parcella, K.; Bowsher, M.; Cook, J. H.; Iwuagwu, C.; Naidu, B. N.; Patel, M.; Peese, K.; Huang, H.; Valera, L.; Wang, C.; Kieltyka, K.; Parker, D. D.; Simmermacher, J.; Arnoult, E.; Nolte, R. T.; Wang, L.; Bender, J. A.; Frennesson, D. B.; Saulnier, M.; Wang, A. X.;

Meanwell, N. A.; Belema, M.; Hanumegowda, U.; Jenkins, S.; Krystal, M.; Kadow, J. F.; Cockett, M.; Fridell, R. Potent Long-Acting Inhibitors Targeting the HIV-1 Capsid Based on a Versatile Quinazolin-4-One Scaffold. *J. Med. Chem.* **2023**, *66* (3), 1941–1954. https://doi.org/10.1021/acs.jmedchem.2c01732.

(18) From 1Click Chemistry: 3-Bromo-6-Chloro-2-Fluorobenzonitrile: 50g/$4795.08; 2,6-Dichlorobenzonitrileprice: 1kg/$169.97.

(19) Kruger, A. W.; Rozema, M. J.; Chu-Kung, A.; Gandarilla, J.; Haight, A. R.; Kotecki, B. J.; Richter, S. M.; Schwartz, A. M.; Wang, Z. The Discovery and Development of a Safe, Practical Synthesis of ABT-869. *Org. Process Res. Dev.* **2009**, *13* (6), 1419–1425. https://doi.org/10.1021/op900208y.

(20) Song, F. B.; Zhang, Z. B.; Tang, H. Y.; Wang, Z. Q.; Song, A. R. 3-nitrile-2,4-phenylphosphinate dihalide as well as preparation method and application thereof. CN104017021A, September 3, 2014. https://patents.google.com/patent/CN104017021A/en?oq=CN104017021 (accessed 2023-02-22).

(21) Wang, Z.; Richter, S. M.; Gandarilla, J.; Kruger, A. W.; Rozema, M. J. Safe Scale-Up of a Hydrazine Condensation by the Addition of a Base. *Org. Process Res. Dev.* **2013**, *17* (12), 1603–1610. https://doi.org/10.1021/op4002577.

(22) Yoshida, T.; Ilies, L.; Nakamura, E. Iron-Catalyzed Borylation of Aryl Chlorides in the Presence of Potassium t-Butoxide. *ACS Catal.* **2017**, *7* (5), 3199–3203. https://doi.org/10.1021/acscatal.7b00310.

(23) Nagashima, Y.; Takita, R.; Yoshida, K.; Hirano, K.; Uchiyama, M. Design, Generation, and Synthetic Application of Borylzincate: Borylation of Aryl Halides and Borylzincation of Benzynes/Terminal Alkyne. *J. Am. Chem. Soc.* **2013**, *135* (50), 18730–18733. https://doi.org/10.1021/ja409748m.

(24) Molander, G. A.; Cavalcanti, L. N.; García-García, C. Nickel-Catalyzed Borylation of Halides and Pseudohalides with Tetrahydroxydiboron [B2(OH)4]. *J. Org. Chem.* **2013**, *78* (13), 6427–6439. https://doi.org/10.1021/jo401104y.

(25) Zhang, L.; Jiao, L. Pyridine-Catalyzed Radical Borylation of Aryl Halides. *J. Am. Chem. Soc.* **2017**, *139* (2), 607–610. https://doi.org/10.1021/jacs.6b11813.

(26) Hoque, M. E.; Hassan, M. M. M.; Chattopadhyay, B. Remarkably Efficient Iridium Catalysts for Directed C(Sp2)–H and C(Sp3)–H Borylation of Diverse Classes of Substrates. *J. Am. Chem. Soc.* **2021**, *143* (13), 5022–5037. https://doi.org/10.1021/jacs.0c13415.